Gesellschaft für Anlagen- und Reaktorsicherheit (GRS) mbH

Evaluation of Fire Models for Nuclear Power Plant Applications

Benchamrk Exercise No. 4: Fuel Pool Fire Inside A Compartment

International Panel Report

GRS - 213

Gesellschaft für Anlagen- und Reaktorsicherheit (GRS) mbH

Evaluation of Fire Models for Nuclear Power Plant Applications

Benchmark Exercise No. 4: Fuel Pool Fire Inside A Compartment

International Panel Report

Compiled by:
Walter Klein-Heßling (GRS)
Marina Roewekamp (GRS)
Olaf Riese (iBMB)

November 2006

Remark:

This report was prepared under contract No. 02 SR 2491 “Übergreifende Bewertung des Brandschutzes bei Kernkraftwerken - Auswertung von spezifischen Brandereignissen, Mitarbeit in internationalen Gremien, Entscheidungshilfe bei der Verwendung von Brandsimulationsprogrammen“ with the German Bundesminsterium für Umwelt, Naturschutz und Reaktorsicherheit (BMU) durchgeführt.

The work was conducted by the Gesellschaft für Anlagen- und Reaktorsicherheit (GRS) mbH together with the Institut für Baustoffe, Massivbau und Brandschutz (iBMB).

The authors are responsible for the content of this report.

GRS - 213
ISBN 978-3-931995-80-5

Deskriptoren:
Ausbreitung, Auswirkung, Brand, Brandgefährdung, Brandschutz, Brandverhalten, Druck, Gas, Kohlendioxid, Öl, Reaktor, Rechenverfahren, Sauerstoff, Simulation, Temperatur, Verbrennung

Abstract

Fire simulations as well as their analytical validation procedures have gained more and more significance, particularly in the context of the fire safety analysis for operating nuclear power plants. Meanwhile, fire simulation models have been adapted as analytical tools for a risk oriented fire safety assessment.

Calculated predictions can be used, on the one hand, for the improvements and upgrades of fire protection in nuclear power plants by the licensees and, on the other hand, as a tool for reproducible and clearly understandable estimations in assessing the available and/or foreseen fire protection measures by the authorities and their experts. For consideration of such aspects in the context of implementing new nuclear fire protection standards or of updating existing ones, an “International Collaborative Project to Evaluate Fire Models for Nuclear Power Plant Applications” also known as the “International Collaborative Fire Model Project” (ICFMP) was started in 1999. It has made use of the experience and knowledge of a variety of worldwide expert institutions in this field to assess and improve, if necessary, the state-of-the-art with respect to modeling fires in nuclear power plants and other nuclear installations.

This document contains the results of the ICFMP Benchmark Exercise No. 4, where two fuel pool fire experiments in an enclosure with two different natural vent sizes have been considered. Analyzing the results of different fire simulation codes and code types provides some indications with respect to the uncertainty of the results. This information is especially important in setting uncertainty parameters in probabilistic risk studies and to provide general insights concerning the applicability and limitations in the application of different types of fire simulation codes for this type of fire scenario and boundary conditions.

During the benchmark procedure the participants performed different types of calculations. These included totally blind simulations without knowledge of the pyrolysis rate, semi-blind calculations with knowledge of this rate only, and completely open post-calculations with knowledge of all experimental measurements. It has been demonstrated, as expected, that the pyrolysis rate has a strong influence on the calculation results. This could be derived from the large differences in the quality of results between the few blind and ‘semi-blind’ or open calculations. The range of the results is much larger for the blind simulations compared to the semi-blind ones. This reduces

the reliability of the results in the event of fire simulation codes being applied e.g. in the frame of probabilistic risk analyses.

The Benchmark Exercise has furthermore shown that the simulation of under-ventilated fires is more difficult for the fire simulation codes and that a highly transient fire behavior leads to a wider range of the code simulation results. Compared to typical fire scenarios analyzed in the fire PSA the considered Benchmark Exercise is extreme in terms of thermal loads. This has to be considered for the assessment of the deviations between the simulation results and the experimental data.

Kurzfassung

Brandsimulationen sowie deren analytische Validierung erhalten mehr und mehr Bedeutung im Rahmen von Brandsicherheitsanalysen in Betrieb befindlicher Kernkraftwerke. Mittlerweile sind Brandsimulationsmodelle als analytische Werkzeuge, welche sich insbesondere für risikoorientierte Brandsicherheitsbewertungen eignen, anerkannt.

Die Verwendung rechnerischer Vorhersagen kann zum einen die Verbesserungen und Nachrüstungen des Brandschutzes durch die Betreiber aufzeigen, zum anderen aber auch als ein Hilfsmittel für reproduzierbare und klar verständliche Abschätzungen im Rahmen der Bewertung vorhandener bzw. geplanter Brandschutzmaßnahmen seitens der Genehmigungs- und Aufsichtsbehörden und deren Gutachter genutzt werden. Zur Berücksichtigung derartiger Aspekte auch bei der Umsetzung neuer oder der Erweiterung kerntechnischer Brandschutzregelwerke wurde ein so genanntes 'International Collaborative Project to Evaluate Fire Models for Nuclear Power Plant Applications auch bekannt unter 'International Collaborative Fire Model Project (ICFMP)' im Jahr 1999 initiiert, in welchem Erfahrungen und Kenntnisse einer Vielzahl von Experteninstitutionen auf diesem Fachgebiet dazu genutzt werden sollen, den Stand von Wissenschaft und Technik auf dem Gebiet der Modellierung von Bränden für Anwendungen in Kernkraftwerken und anderen kerntechnischen Einrichtungen zu bewerten und, falls erforderlich, zu verbessern.

Der nachfolgende Bericht beinhaltet die Ergebnisse des ICFMP Benchmark Exercise Nr. 4, bei welchem zwei Versuche zum Treibstofflachenbrand in einem Brandraum mit unterschiedlicher natürlicher Ventilation betrachtet werden. Die Analyse der Ergebnisse von Simulationsrechnungen mit unterschiedlichen Brandsimulationscodes und -codearten gibt Hinweise in Bezug auf die Unsicherheiten der Resultate. Dies ist zum einen von Bedeutung für die Auswahl von Unsicherheitsparametern in probabilistischen Sicherheitsanalysen. Zum anderen ergeben sich daraus Erkenntnisse hinsichtlich der Anwendbarkeit und Anwendungsgrenzen verschiedener Arten von Brandsimulationscodes für solche Brandszenarien und die entsprechenden Randbedingungen.

Im Verlauf des Benchmarks werden von den Teilnehmern unterschiedliche Arten von Simulationsrechnungen durchgeführt. Dabei handelt es sich um so genannte 'blinde' Vorausrechnungen ohne Kenntnis der Pyrolyserate, um 'semi-blinde' Rechnungen, bei welchen nur die Pyrolyserate bekannt ist, und um vollständig offene Nachrechnungen unter Kenntnis der Versuchsdaten. Wie erwartet, zeigte sich, dass die Pyrolyserate

einen erheblichen Einfluss auf die rechnerischen Ergebnisse hat. Dies zeigte sich insbesondere an den doch erheblichen Qualitätsunterschieden der Rechenergebnisse von den wenigen blinden im Vergleich zu den ‚semi-blinden' bzw. offenen Rechnungen. Die Bandbreite der Ergebnisse ist bei den blinden Vorausrechnungen erheblich größer als bei den semi-blinden, was zu höheren Ergebnisunsicherheiten bei Nutzung von Brandsimulationsrechnungen bei z.B. probabilistischen Analysen führt. Es zeigt sich weiterhin, dass die Simulation unterventilierter Brände für die Brandsimulationscodes erheblich schwieriger ist. Ein sehr instationäres Brandverhalten führt zu einer größeren Bandbreite der Ergebnisse. Die betrachtete Benchmarkaufgabe ist in Bezug auf die thermischen Belastungen extrem im Vergleich zu den in Rahmen von Brand PSA betrachteten Szenarien. Dies ist bei der Betrachtung der Abweichungen der Simulationsergebnisse von den experimentellen Werten zu berücksichtigen.

Table of Contents

1 Introduction

Fire simulations as well as analytical validation procedures have gained more and more significance, particularly in the context of fire safety analysis for operating nuclear power plants (NPPs). Fire simulation models have been developed as analytical tools for a risk oriented fire safety assessment.

The use of calculated predictions could be considered, on the one hand, for improvements and upgrades of the fire protection by the licensees and, on the other hand as a tool for reproducible and clearly understandable estimations in assessing the available and/or foreseen fire protection measures by the authorities and their experts. For consideration of such aspects even in the frame of implementing new nuclear fire protection standards or upgrading existing ones, an “International Collaborative Project to Evaluate Fire Models for Nuclear Power Plant Applications” also known as the “International Collaborative Fire Model Project” (ICFMP)” was started in 1999, to make use of the experience and knowledge of a variety of expert institutions in this field worldwide to assess and improve, where necessary, the state-of-the-art with respect to modeling fires for application to nuclear installations/plants.

Within the ICFMP project the following Benchmark Exercises have been performed:

- Benchmark Exercise No. 1: Cable fire and thermal load on cables in a cable spreading room (theoretical) /DEY 02/;
- Benchmark Exercise No. 2: Heptane pool fire in a large hall (experiment) and large oil fire in a turbine hall with 2 floor levels and horizontal openings /MIL 04/;
- Benchmark Exercise No. 3: Heptane spray fire in a cable room to investigate thermal loads on cables and cable trays (experiments) /MCG 06/;
- Benchmark Exercise No. 4: Relatively large fuel pool fire with two variations of the door cross section area (experiments);
- Benchmark Exercise No. 5: Fire spreading on vertical cable trays with variations on the pre-heating and cable material (experiments) /RIE 06/.

In this Panel Report, Benchmark Exercise No. 4 will be discussed and the results of the different participants will be evaluated. The individual reports of the participants are presented as attachments.

The main objective of the experiments for Benchmark Exercise No. 4 was to analyze the thermal load on the structures surrounding a fire relatively large compared to the floor area and volume of the fire compartment. In several experiments the natural and forced ventilation has been changed to investigate the influence of oxygen depleted conditions on the fire. Both the thermal loads and the oxygen depleted conditions are somewhat difficult aspects to calculate. Therefore these experiments can contribute to the further improvement of fire codes. Additionally, the results give some insight concerning the uncertainties of fire simulations of pool fires in an enclosure under the given boundary conditions. This information is important for the definition of uncertainty input parameters for PSA studies.

2 Specification of Benchmark Exercise No. 4

At iBMB (Institut für Baustoffe, Massivbau und Brandschutz) of Braunschweig University of Technology, a set of nine real scale fuel pool fire experiments has been performed. The objective of these experiments was to systematically vary the major influencing parameters on the burning behavior to derive standard fire curves (time dependence of temperatures and heat flow densities at different distances from the fire source, burning rates, energy release rates and temperature loads) and to examine the dependence on the pool surface area, the fuel filling level and the ventilation conditions.

The fire compartment OSKAR of iBMB, an enclosure with a compartment floor size of 3.6 m x 3.6 m = 12.96 m^2 and a height of 5.7 m, was used for the pool fire test series. This facility has 3 possible openings for the natural ventilation of the fire compartment. At the ceiling, the hot gases and smoke can be extracted and cleaned by a fan system with filters. During the experiments gas and surface temperatures, gas composition, velocities and heat flux densities were measured.

2.1 Review of Previous Related Work within the ICFMP Project

In this section, the relation of Benchmark Exercise No. 4 to the previous Benchmark Exercises is discussed.

Looking to Benchmark Exercise No. 1, one result was the strong influence of the assumed lower oxygen limit (LOL) on the calculated results /DEY 02/. Fig. 2-1 presents the calculated oxygen concentrations for the Benchmark Exercise No. 1, Part II base case. The results depend on the assumed parameter of LOL. The range of this parameter varied between 0 and 10 Vol.-%. The difference between calculations with the zone model MAGIC by different users, MAGIC-EDF (with 10 Vol.-%) and MAGIC-CTICM (with 0 Vol.-%) are of special interest. The consequences of this parameter on the hot gas layer temperature (HGL) are shown in Fig. 2-2**.** In particular, the fire duration is predicted quite differently.

The main difference between Test 1 and Test 3 in Benchmark Exercise No. 4 is the ventilation opening at the front wall, leading to oxygen depleted conditions in Test 3.

Therefore, this Benchmark Exercise gives some indications for the appropriate estimation of the LOL value as well as for the simulation of oxygen depleted conditions.

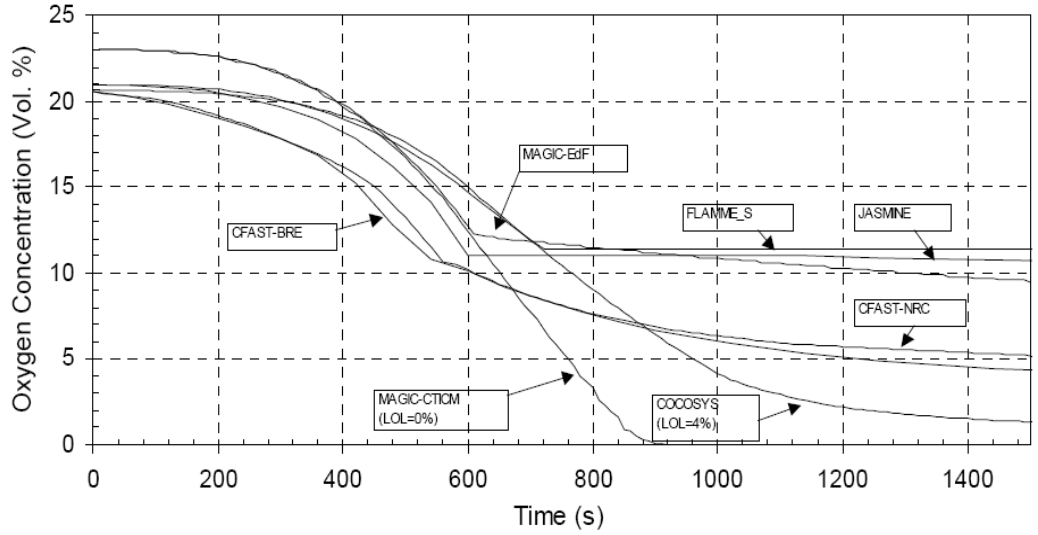

Fig. 2-1 Benchmark Exercise No.1, Part II base case - calculated oxygen concentrations

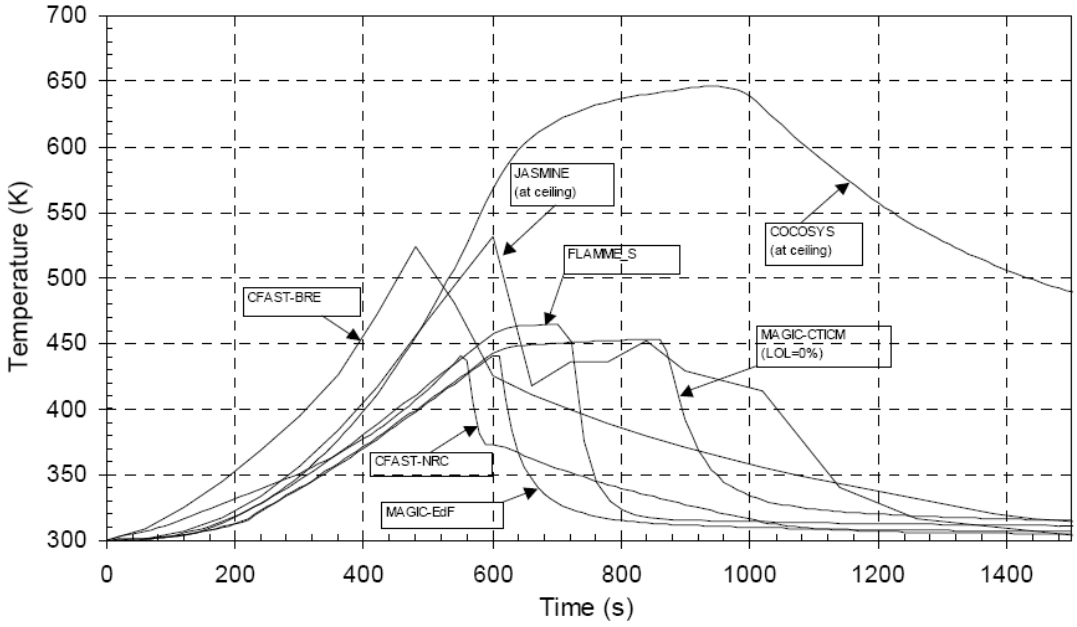

Fig. 2-2 Benchmark Exercise No. 1, Part II base case - calculated HGL temperatures

One of the main tasks of fire simulation codes applied within the ICFMP is the calculation of thermal loads to safety significant targets. These include electrical components, cable trays and wall structures. Benchmark Exercise No. 3 shows, that this topic should be further improved /MCG 06/.

In Benchmark Exercise No. 4 the relation between fire load and compartment floor area (267 MJ/m^2) is quite high. This leads to some extent to a rather high thermal load on the wall structures. Different material types (concrete, aerated concrete and steel) have been investigated in these experiments. In addition, a barrel type waste container with a rather complex material composition has been positioned close to the fire source. Therefore, the Benchmark Exercise No. 4 results can be used to evaluate the simulation of the target by the fire codes.

2.2 Specification of the Experiments

This section contains the specification of the experiments delivered to the participants.

2.2.1 Description of the Test Facility

In the following, the OSKAR test facility of iBMB is described in detail.

Geometry

Fig. 2-3 to Fig. 2-6 show the test facility. It has a floor area of 3.6 m x 3.6 m = 12.96 m^2 and a height of 5.7 m. At the ceiling, there are two ventilation ducts with a width of 0.42 m and a height of 1.03 m. The length of both ducts is approximately 3.625 m and leads to the fan system.

In the center of the floor area a steel pan with a size of 4 m^2 has been installed on a weight scale. The lower level of this pan has an elevation of about 0.36 m. The side walls are approx. 0.3 m high (Fig. 2-7). The weight loss of the liquid fuel was measured by the scale. To protect this measurement aerated concrete had been added to the fire compartment around this pan on the complete floor area up to an elevation of 0.6 m. The inner side of the large pan had been covered by a 0.05 m thick light concrete plate for protection. In the center of the large pan, a smaller pan of 1 m^2 was placed. The bottom of this pan has an elevation of approx. 0.51 m. The height of the side walls is

0.2 m. For stability, a 0.03 m wide steel plate had been fixed around the upper edge of the pan side wall.

Ventilation

In the experiments considered only the front vent (door) was opened. The door is located at the center of the front wall (x = 1.8; y = 0.). In Test 1, the door was completely open with a free cross section of 0.7 m x 3.0 m. The lower edge of the door is just above the aerated concrete at z = 0.6 m. In the Test 3, the opening was partly restricted. The open (free) cross section was reduced to 0.7 m x 1.0 m and the opening started at an elevation of 1.6 m (1 m above the aerated concrete bottom surface).

Although the FUCHS fan system extracting air from the top of the fire compartment was not in use, some velocity flow (measurements V11 and V12) could be measured, because the valves were not leak-tight. The values are specified below (Table 2-7 and Table 2-8).

A hood had been installed above the open front door (Fig. 2-10). Using the oxygen consumption method the energy release could be estimated. The volume flow rates are given in Table 2-9 and Table 2-10.

Infiltration

All other vents were closed. However, some leakage area can be assumed in the lower part of the fire compartment. Due to the construction kit technique used, it is difficult to measure the leakage. A rough estimation of the leakage is about 0.05 m^2 in the lower region of the facility.

Wall Structures and Properties

The following Table 2-1 gives information on the composition of the fire compartment wall structures.

Table 2-1 Composition of the wall structures

Position	Material	Thickness [m]
Floor	Concrete	0.30
	Aerated concrete	0.60 (see Fig. 2-5)
Side walls	Light concrete	0.25
	Insulation	0.05
Ceiling	Concrete	0.25
	Insulation	0.05
Side walls channel	Light concrete	0.125
	Insulation	0.06
Ceiling channel	Concrete	0.13
	Insulation	0.07

The properties of the different materials are:

Table 2-2 Properties of the fire compartment materials

Material	Heat conductivity λ [W/mK]	Heat capacity c_p [kJ/kgK]	Density ρ [kg/m^3]
Concrete	2.10	880	2400
Light concrete	0.75	840	1500
Aerated concrete (bottom)	0.11	1350	420
Insulation	0.05	1500	100

Targets

Behind the large pan, a barrel type waste container typically used in nuclear facilities was installed. The center of the bottom of the barrel was located at (x = 1.8m, y = 3.2 m, z = 0.6 m). This container had a diameter of 0.64 m and a height of 0.96 m. It was a double vessel container. The diameter of the inner barrel is 0.515 m (Fig. 2-12, Fig. 2-13) consisting of tinplate and is filled with styrene divinylbenzene copolymer with sul-

fur acid groups. The gap between the inner and outer steel barrel was filled with concrete (Table 2-3) and equipped with six (2 at each of three levels) thermocouples for measurements.

Three different types of material probes were positioned on the right side of the fire compartment (x = 0 m). The materials are "aerated concrete", concrete and steel. The size of these elements is 0.3 m x 0.3 m (Fig. 2-11). For the concrete probes, the thickness is 0.1 m, for the steel plate it is 0.02 m. The properties of the materials used are given in Table 2-3. The location of the center surface is given in Table 2-4.

Table 2-3 Properties of the target materials

Material	Heat conductivity λ [W/mK]	Heat capacity c_p [J/kgK]	Density ρ [kg/m^3]
Granulate (styrene)	0.233	1600	1000
Tin plate	63	230	7280
Concrete (between barrels)	2.1	880	2400
Steel	44.5	480	7743
Concrete (probe)	2.1	880	2400
Aerated concrete	0.11	1350	420

Table 2-4 Location of the material probes

Material probe	x [cm]	y [cm]	z [cm]
Aerated concrete	8	65	170
Concrete	8	190	170
Steel	2	280	170

Hood

To measure the oxygen consumption of the fire, a hood in front of the front door was installed. The cross section of the hood is 2.9 m $\times$ 2.9 m = 8.41 m^2 and the hood was positioned at the center of the front door just at the upper edge (at z = 3.6 m). A flexible soot apron of 1 m height was fixed at the hood inlet. Therefore, the lower edge of the hood apron is at z = 2.6 m. The scheme of the hood is shown in Fig. 2-9.

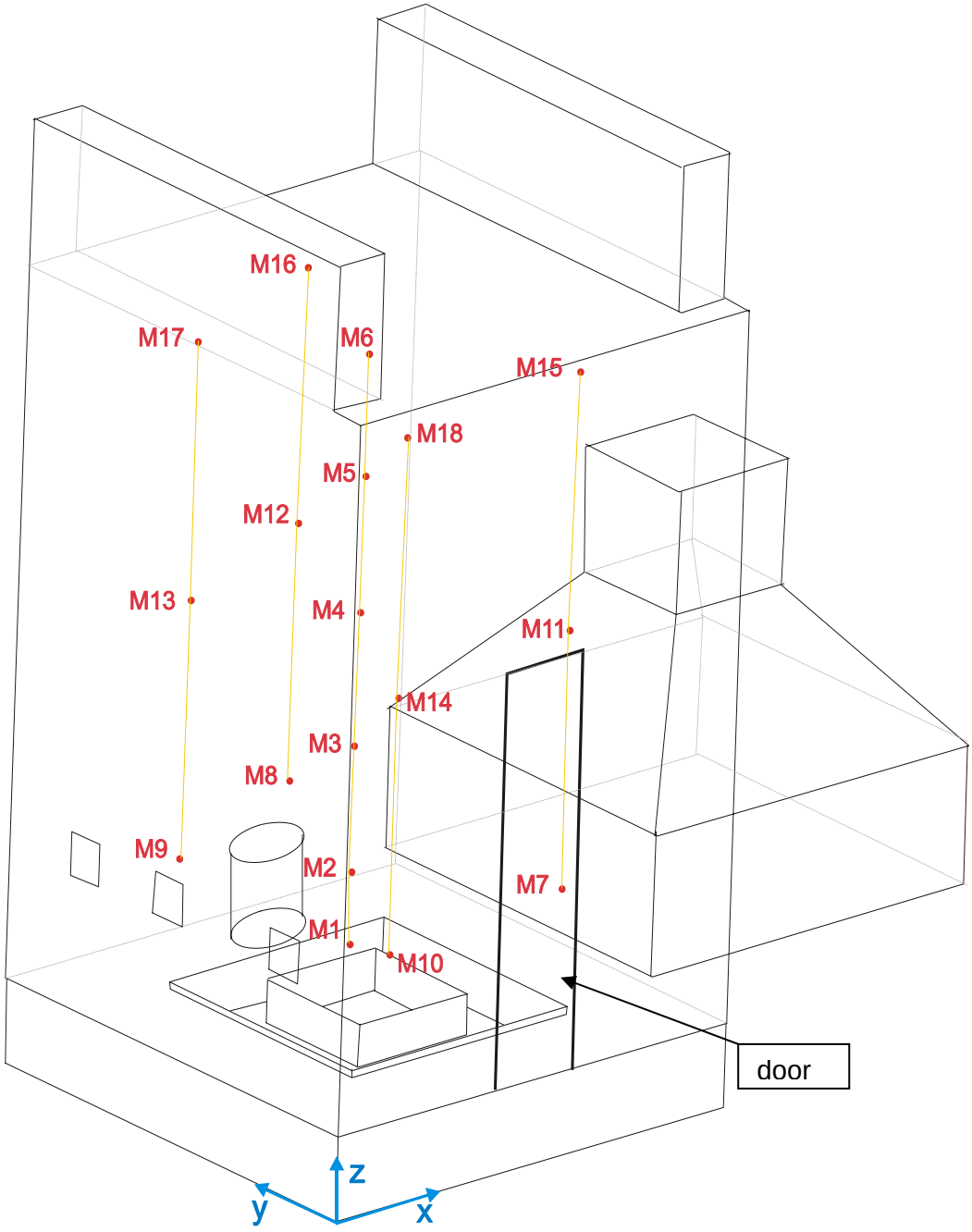

Fig. 2-3 3D view of the OSKAR fire compartment

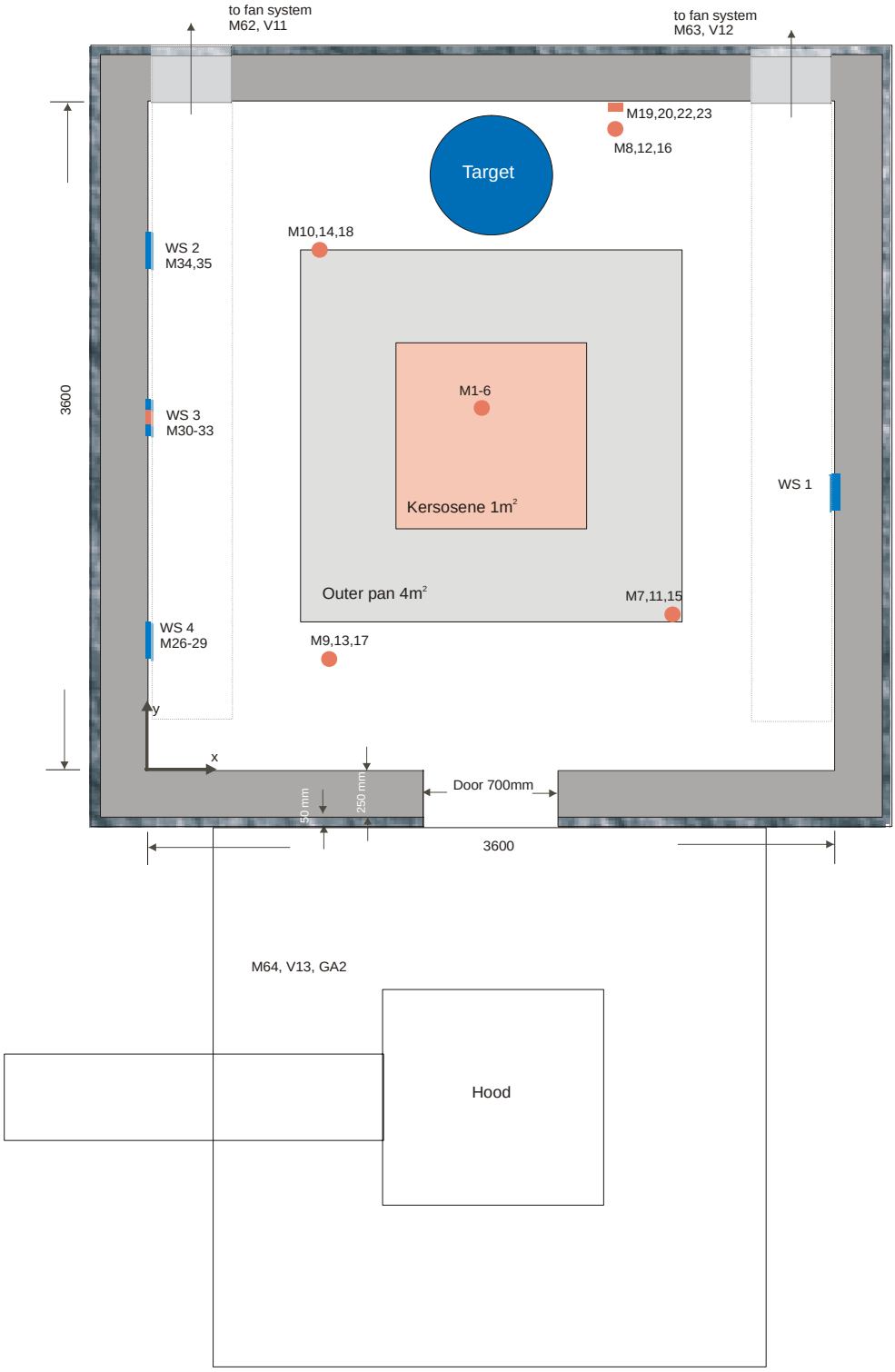

Fig. 2-4 Top view of the OSKAR fire compartment

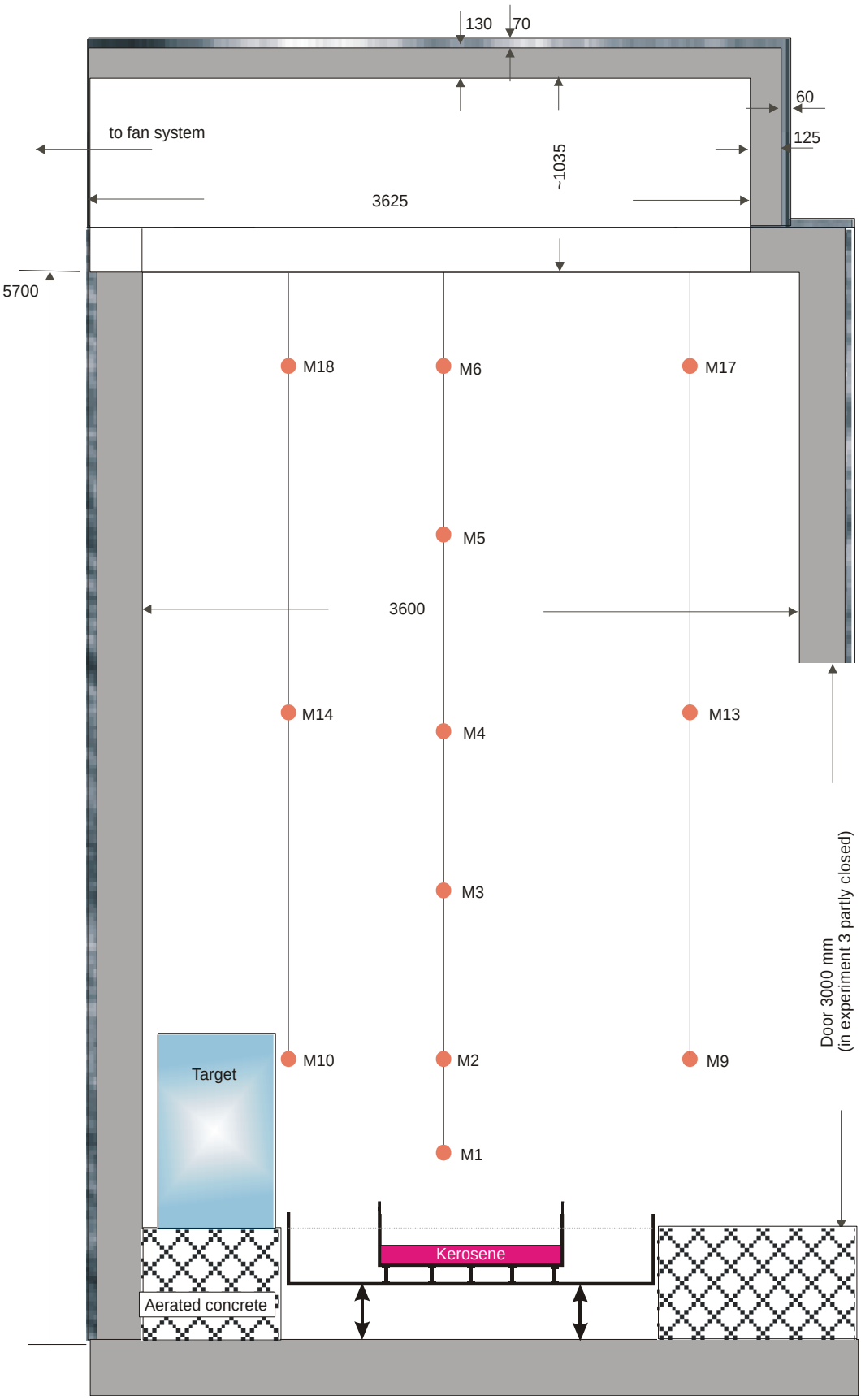

Fig. 2-5 Side view of the OSKAR fire compartment (in + y direction)

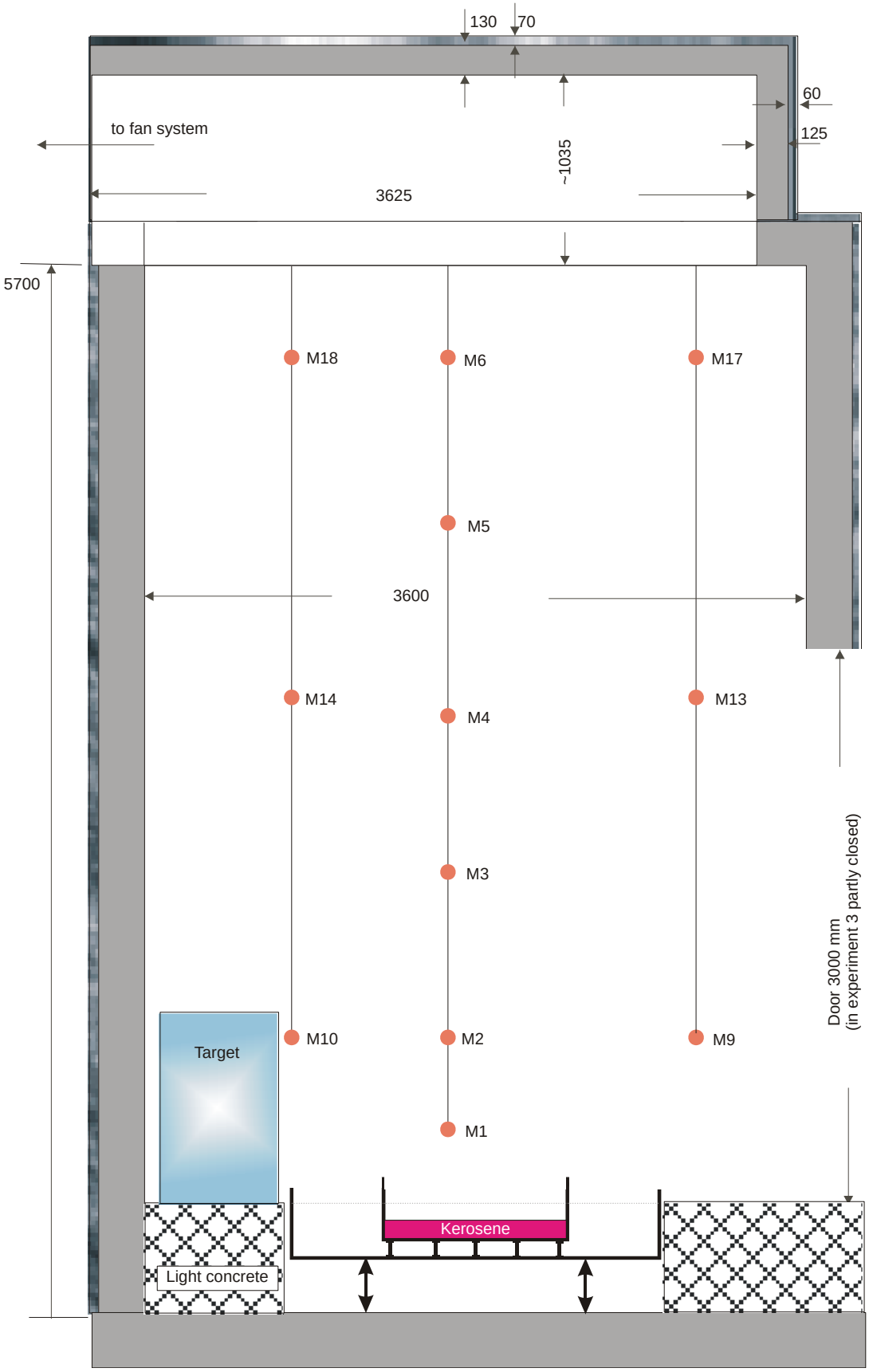

Fig. 2-6 Side view of the OSKAR fire compartment (in + x direction)

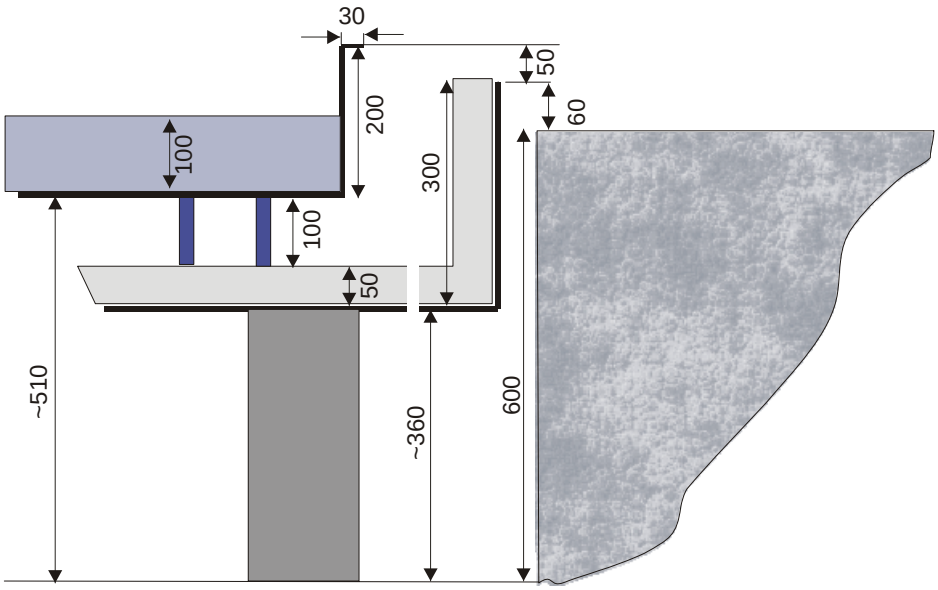

Fig. 2-7 Height of the fuel pan side walls and its elevations

Fig. 2-8 View of the fire compartment through the front door

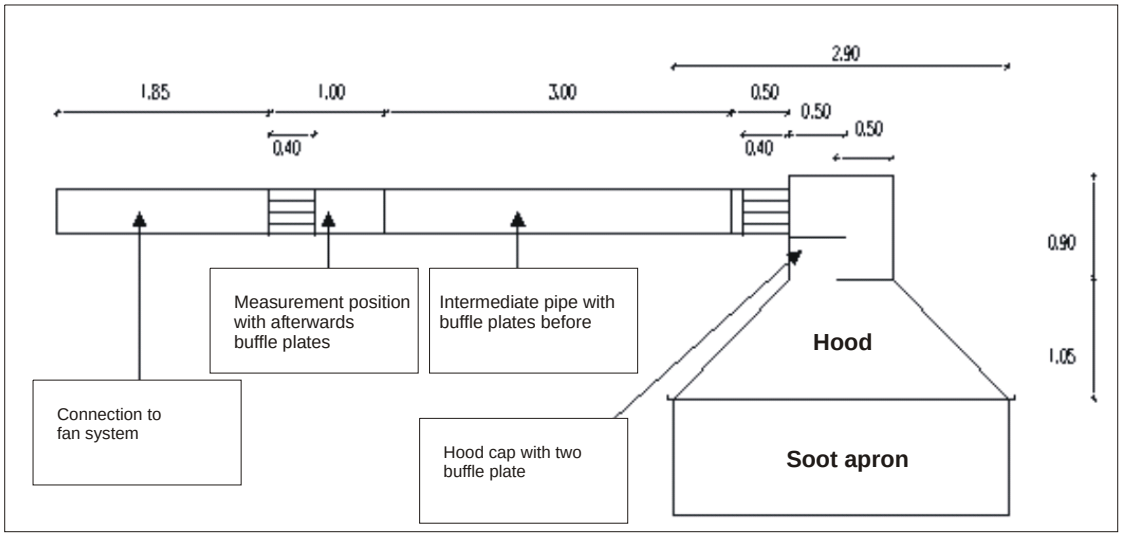

Fig. 2-9 Scheme of the hood above the front door

Fig. 2-10 View onto the hood installed above the front door

2.2.2 Measurements Performed

For measuring the temperatures inside the fire compartment, 3 mm-thick thermocouples were used. These were not protected against flame radiation. The position of the thermocouples was fixed on a grid.

To measure the surface temperatures, the measuring point was fixed with a 5 mm thick thermo-wire. In parallel, “coated thermocouples” with a diameter of 3 mm were used.

To measure the temperatures of typical materials used at NPPs, three different types of material probes (concrete, aerated concrete, steel) were inserted into the fire compartment (Fig. 2-11). The convective and radiative heat flow into the material probes were measured by water cooled heat transfer blocks. The coolant temperature was approximately 10 °C.

Along three lines, the temperatures inside the barrel container were measured (M36 to M53). The location of these measurements is shown in Fig. 2-13.

The velocity inside the plume, at the door and inside the fan systems were measured using bi-directional probes. The cross section area at the measurement positions V11 and V12 is 0.4 m x 0.8 m, and at the velocity measurement position V13 inside the hood the diameter of the pipe was 0.4 m.

To measure the gas concentrations and pressure, open pipes were routed to the outside of the fire compartment and connected to the measurement systems. The positions and nomenclature of the different measurements are shown in Fig. 2-3 to Fig. 2-6 and in Table 2-5.

Table 2-5 List of measurements performed

Nomenclature WS = Heat flow density measurement M = Temperature measurement GA = Measurement of gas composition V = Gas velocity measurement P = Measurement of total pressure GV = Measurement of weight loss		
Measurement position	**Comment for Test 1**	**Comment for Test 3**
Plume-temperature (x = 175, y = 195)**:**		
M 1 (z = 100 cm)		
M 2 (z = 150 cm)		
M 3 (z = 240 cm)		
M 4 (z = 335 cm)		
M 5 (z = 430 cm)		
M 6 (z = 520 cm)		
Temperature inside fire compartment:		
Level 1: (z = 150 cm)		
M 7 (x = 275; y = 85)		
M 8 (x = 245; y = 345)		
M 9 (x = 95; y = 60)		
M 10 (x = 90; y = 280)		
Level 2: (z = 335 cm)		
M 11 (x = 275; y = 85)		
M 12 (x = 245; y = 345)		
M 13 (x = 95; y = 60)		
M 14 (x = 90; y = 280)		
Level 3: (z = 520 cm)		
M 15 (x = 275; y = 85)		
M 16 (x = 245; y = 345)		
M 17 (x = 95; y = 60)		
M 18 (x = 90; y = 280)		
Surface temperature		
Plates on the surface		
M 19 (x = 245; y = 360; z = 150)		
M 20 (x = 245; y = 360; z = 335)		

M 21 (x = 0; y = 190; z = 170)		
"Coated thermocouples" on the surface:		
M 22 (x = 245; y = 360; z = 150)		
M 23 (x = 245; y = 360; z = 335)		
M 24 (x = 0; y = 190; z = 170)		
Fuel temperature:		
M25 (x = 175; y = 195; z = 33)		
Material probes:		
“Aerated concrete” (plate 10 cm thickness)		
M26 (x = 2; y = 65; z =.170) *)		
M27 (x = 5; y = 65; z = 170)		
M28 (x = 8; y = 65; z = 170) *)		
M29 (x = 10; y = 65; z = 170)		
Concrete (plate 10 cm thickness)		
M30 (x = 2; y = 190; z = 170) *)		
M31 (x = 5; y = 190; z = 170)		
M32 (x = 8; y = 190; z = 170) *)		
M33 (x = 10; y = 190; z = 170)		
Steel (plate 2 cm thickness)		
M34 (x = 2; y = 280; z = 170)		
M35 (x = 0; y = 280; z = 170)		
Barrel type target (waste package):		
Upper level (z = 140)		
M36 (x = 180; y = 288; z = 140)		
M37 (x = 180; y = 292; z = 140)		
M38 (x = 180; y = 294.5; z = 140)		
M39 (x = 180; y = 299; z = 140)		
M40 (x = 180; y = 310; z = 140)		
M41 (x = 180; y = 320; z = 140)		
Center level (z = 110)		
M42 (x = 180; y = 288; z = 110)		
M43 (x = 180; y = 292; z = 110)		
M44 (x = 180; y = 294.5; z = 110)		
M45 (x = 180; y = 299; z = 110)		

M46 (x = 180; y = 310; z = 110)		
M47 (x = 180; y = 320; z = 110)		
Lower level (z = 85)		
M48 (x = 180; y = 288; z = 85)		
M49 (x = 180; y = 292; z = 85)		
M50 (x = 180; y = 294.5; z = 85)		
M51 (x = 180; y = 299; z = 85)		
M52 (x = 180; y = 310; z = 85)		
M53 (x = 180; y = 320; z = 85)		
<u>Temperature measurement at velocity probe positions</u>:		
Front door		
M54 (x = 180; y = 0; z = 80)		not used
M55 (x = 180; y = 0; z = 140)		not used
M56 (x = 180; y = 0; z = 180)		
M57 (x = 180; y = 0; z = 240)		
M58 (x = 180; y = 0; z = 280)		not used
M59 (x = 180; y = 0; z = 340)		not used
Door, right side	not used	
M60 (x = 360; y = 210; z = 100)		
Door, left side	not used	
M61 (x = 0; y = 335; z = 140)		
Fan system FUCHS (at ceiling)	although valves are closed some flow has occurred	
M62 (outside fire compartment)		
M63 (outside fire compartment)		
Hood above open front door		
M64 (outside fire compartment)		
<u>Heat flow density</u>:		
WS 1 (x = 360; y = 150; z = 180)		
WS 2 (x = 0; y = 280; z = 170)		
WS 3 (x = 0; y = 190; z = 170)		
WS 4 (x = 0; y = 70; z = 170)		
<u>Weight loss of kerosene</u>:		
GV 1 (x = 180; y = 180; z = 0)		
<u>Gas velocities</u>:		
Centerline Plume		
V1 (x = 175; y = 195; z = 150)		

V2 (x = 175; y = 195; z = 335)		
Door		
V3 (x = 180; y = 0; z = 80)		
V4 (x = 180; y = 0; z = 140)		
V5 (x = 180; y = 0; z = 180)		
V6 (x = 180; y = 0; z = 240)		
V7 (x = 180; y = 0; z = 280)		
V8 (x = 180; y = 0; z = 340)		
Door, right side	not used, door closed	
V9 (x = 360; y = 210; z = 100)		
Door, left side	not used, door closed	
V10 (x = 0; y = 335; z = 140)		
Fan system FUCHS		
V11 (outside fire compartment)		
V12 (outside fire compartment)		
Hood above open front door		
V13 (outside fire compartment)		
Gas composition:		
Fire compartment		
GA1 (x = 10; y = 190; z = 380)		
Hood above front door		
GA2 (outside fire compartment)		
Fan system FUCHS	not used	
GA3 (outside fire compartment)		
Pressure:		
P1 (x = 110; y = 240; z = 540)		
P2 (x = 30; y = 200; z = 280)		

*) corrected after performance of calculations and documentation

Fig. 2-11 View of the three material probes

Fig. 2-12 View from top into the open barrel container

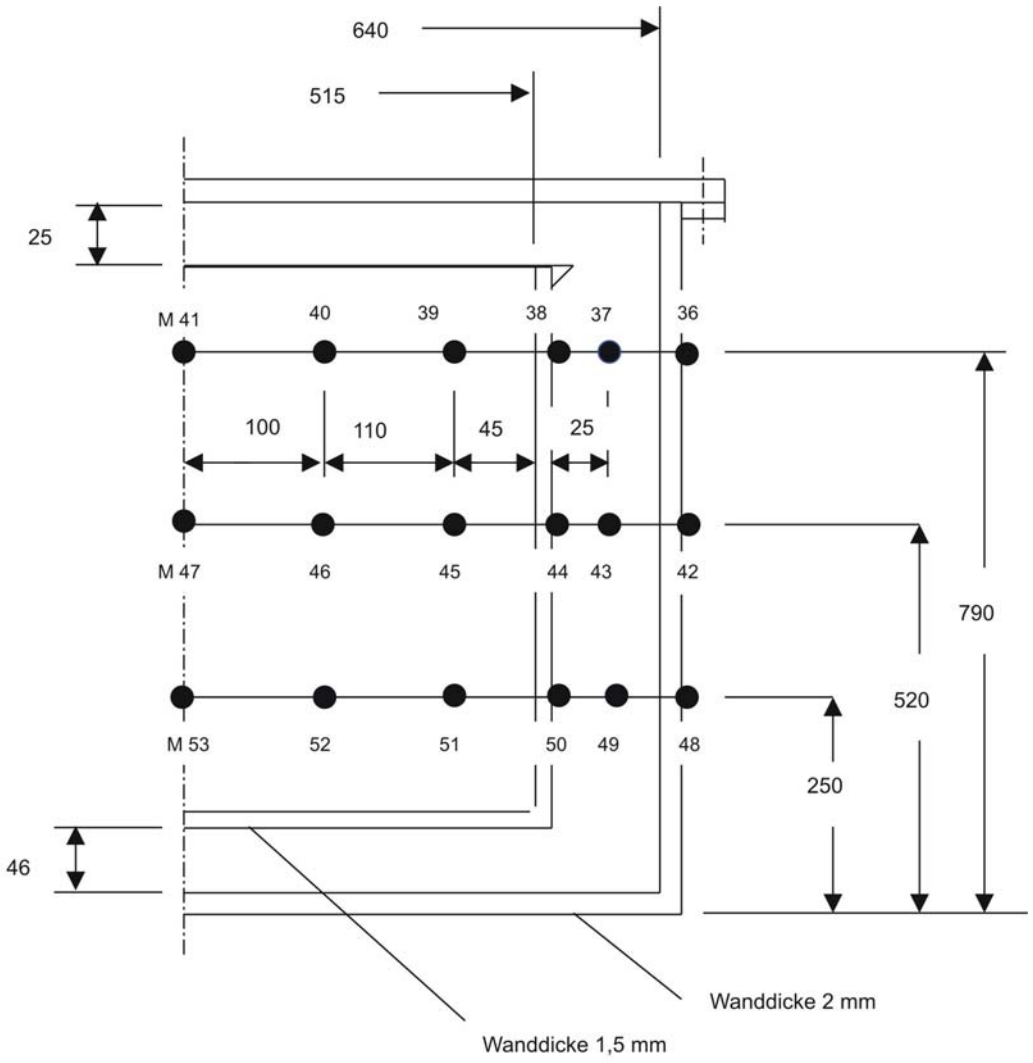

Fig. 2-13 Measurement positions inside barrel

2.2.3 Experimental Procedure

Procedure

At the beginning of the experiments the pan was filled with fuel. In all experiments the fuel level was 0.1 m. Fig. 2-14 shows a typical composition of the fuel used with the chemical summary formula $C_{11.64}H_{25.29}$. Other fuel characteristics are outlined in Table 2-6.

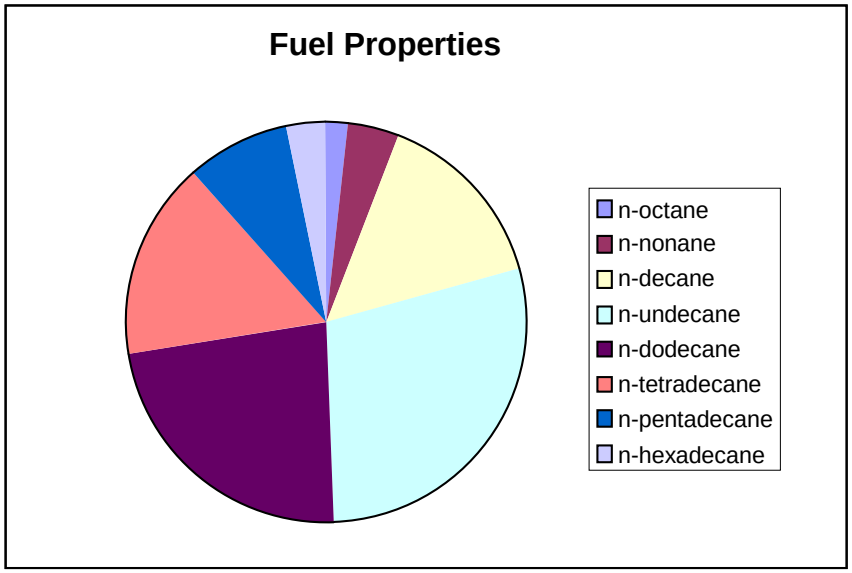

Fig. 2-14 Typical chemical composition of fuel

Table 2-6 Fuel material properties

Density [kg/m^3]	810
Heat capacity [J/kgK]	2400 *)
Heat conductivity [W/mK]	0.109 *)
Heat release [MJ/kg]	42.8

*): values for dodecane taken

To ignite the fuel pool, a cleaning rag soaked with liquid fuel was put at the corner of the pan. Then the outer end was ignited, so that the pool was then ignited. The duration of this process was approx. 30 to 60 s. The experiments ran until the fuel was burned down. In the Test 3, the cool-down behavior was measured for a time period of approx. 16 h.

Ventilation

In those tests considered for Benchmark exercise No. 4 the fan system was running. Although the valves on the top of the fire compartment should have been closed, some velocity (measurements V11 and V12) was measured. Due to these measurements some leakages from the ceiling of the fire compartment have to be assumed. Because

negative values were measured part of the time, the resulting volume flow through fan system is assumed to be

$$\dot{V} = 0.4 \cdot 0.8 \cdot \max\left[0., \left(v_{V11} + v_{V12}\right)\right]. \qquad (3\text{-}1)$$

Table 2-7 and Table 2-8 contain the smoothed volume flow and velocity values for each experiment.

Table 2-7 Smoothed values for the total volume flow and velocity through the FUCHS fan system (measurements V11 and V12) for Test 1

Test 1 (V11 and V12)		
Time [s]	**Velocity v [m/s]**	**Volume flow $\dot{V}$ [m³/s]**
0.00	0.00	0.00
150.00	0.00	0.00
165.00	0.26	0.08
180.00	1.38	0.44
195.00	2.59	0.83
210.00	4.12	1.32
225.00	4.41	1.41
551.00	6.82	2.18
615.00	6.78	2.17
666.00	6.64	2.13
720.00	7.03	2.25
859.00	6.01	1.92
1011.00	4.92	1.57
1245.00	3.41	1.09
1405.00	1.36	0.43
1650.00	0.45	0.14
1800.00	0.19	0.06

Table 2-8 Smoothed values for the total volume flow and velocity through the FUCHS fan system (measurements V11 and V12) for Test 3

Test 3 (V11 and V12)		
Time [s]	**Velocity v [m/s]**	**Volume flow $\dot{V}$ [m³/s]**
0.00	1.22	0.39
37.00	1.22	0.39
61.00	2.21	0.71
88.00	2.33	0.74
120.00	4.65	1.49
195.00	5.06	1.62
255.00	5.75	1.84
1324.00	6.43	2.06
1400.00	5.52	1.77
1500.00	3.93	1.26
1714.00	3.20	1.02

To calculate the gas concentrations inside the hood above the open door, one has to know the velocity. Table 2-9 and Table 2-10 show the smoothed table values for the volume flow rate and the velocity (measurement V13).

Table 2-9 Smoothed values for the total volume flow and velocity through the hood (measurement V13) for Test 1

Test 1 (V13)		
Time [s]	**Velocity v [m/s]**	**Volume flow $\dot{V}$ [m³/s]**
0.00	0.37	2.12
15.00	0.39	2.24
30.00	0.42	2.41
45.00	0.39	2.26
195.00	0.44	2.55
210.00	0.55	3.20
225.00	0.53	3.08
240.00	0.55	3.20
255.00	0.56	3.26
405.00	0.57	3.30
886.00	0.61	3.51
1449.00	0.63	3.66
1711.00	0.46	2.65
1755.00	0.52	3.03
1770.00	0.46	2.68
1785.00	0.49	2.86
1800.00	0.49	2.82

Table 2-10 Smoothed table values for the total volume flow and velocity through the hood (measurement V13) for Test 3

Test 3 (V13)		
Time [s]	**Velocity v [m/s]**	**Volume flow $\dot{V}$ [m³/s]**
0.00	0.50	2.90
37.00	0.52	3.00
61.00	0.52	3.00
211.00	0.53	3.06
504.00	0.52	2.99
1102.00	0.56	3.22
1177.00	0.62	3.60
1280.00	0.65	3.77
1400.00	0.56	3.25
1591.00	0.56	3.22
1748.00	0.58	3.37

Initial and Ambient Conditions

The initial and ambient conditions are given in Table 2-11.

Table 2-11 Initial and ambient conditions

Description	Name(s)	Unit	Test 1	Test 3
Temperature in fire compartment	M1 - M24	°C	18.9	24.7
Temperature outside fire compartment		°C	18.9	18.9
Fuel temperature	M25	°C	18.3	19.0
Material probe: gas-concrete	M26 - M29	°C	17.2	25.6
Material probe: concrete	M30 - M33	°C	18.8	26.3
Material probe: steel	M34 - M35	°C	19.5	24.1

Description	Name(s)	Unit	Test 1	Test 3
Barrel Target	M36, M42, M48	°C	18.8	32.3
	M37, M43, M49	°C	18.8	30.2
	M38, M44, M50	°C	18.8	31.1
	M39, M45, M51	°C	18.8	36.4
	M40, M46, M52	°C	18.8	43.3
	M41, M47, M53	°C	18.8	45.0
Time of ignition		S	165	15

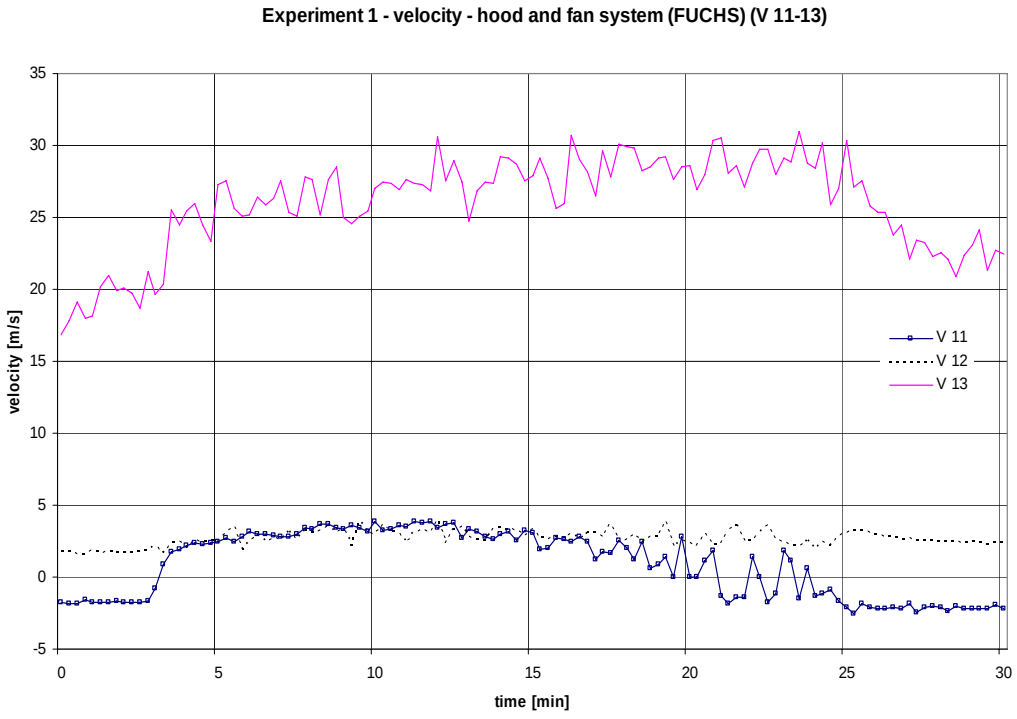

Fig. 2-15 Test 1 - Measured velocities (V11 - V13)

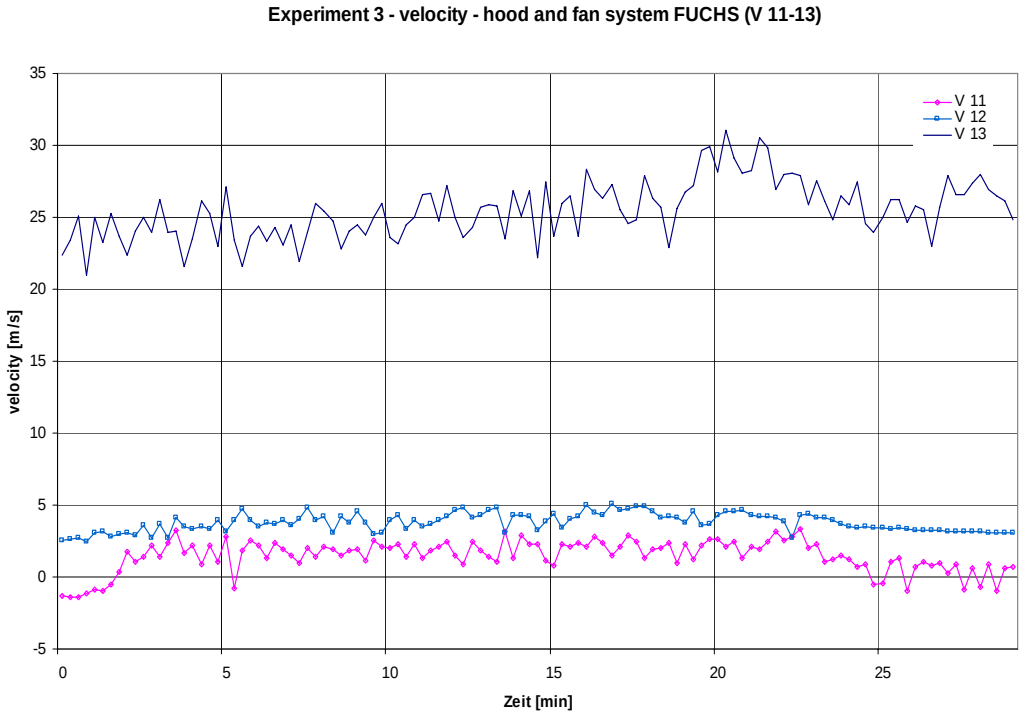

Fig. 2-16 Test 3 - Measured velocities (V11 - V13)

3 Experimental Results

The following section provides data and results from both experiments of the ICFMP Benchmark Exercise No. 4. The results have been made available to the participants of ICFMP in two steps. In April 2004, the pyrolysis rates of the fuel pool fires were released. Most of the results were delivered in May 2004. These results were presented during the 8th ICFMP Meeting at VTT in Finland /KLE 04/.

The tests 1 and 3 are part of a total of 9 fuel pool fire tests at iBMB. Table 3-1 shows the test matrix. In the frame of these tests, the influence of openings as well as of the forced ventilation and the pool size on the thermal load has been investigated. In some tests large pool sizes compared to the fire compartment volume were used, leading to rather high temperature loads.

Table 3-1 Test matrix of the iBMB fuel pool fire tests

Test	Pool area [m^2]	Openings [m^2]	Ventilation
1	1	door: 3 x 0.7	no
2	1	door: 2 x 0.7	no
3	1	door: 1 x 0.7 (1 m above floor)	no
4	1	door: 1 x 0.7 (2 m above floor)	no
5	1	door: 2 x 0.7 (1 m above floor) sides: 0.6 x 0.7 and 0.6 x 1.2	yes
6	1	door: 2 x 0.3 (1 m above floor) sides: 0.3 x 0.7 and 0.4 x 1.2	yes
7	2	door: 3 x 0.7 sides: 0.6* x 0.7 and 0.6 x 1.2	yes
8	2	door: 2 x 0.7 (1 m above floor)	yes
9	4	door: 2 x 0.7 (1 m above floor)	yes

3.1 Summary of Test 1

The fire compartment had a 3 m high opening at the front wall. The smoke was extracted via the ventilation in a natural way. The pool size was 1 m^2 filled with 100 litres of fuel. To ignite the fuel pool, a cleaning rag steeped with fuel was placed on the edge of the pan. It took approx. 15 s until the whole surface area was burning. The duration of the fire was about 20 min. Fig. 3-1 shows the fully developed fire phase during the experiment.

In Fig. 3-2, a thermo-graphic view of the temperature distribution inside the fire is presented. This has been recorded via the infrared camera at a 10 m distance from the front door.

The measurements of the weight loss show a continuous decrease (Fig. 3-3). At about half-way through the test the measurement was defective. Until this time, the measured data may be used. From the pyrolysis rate, the energy release was estimated. The temperature distribution inside the fire compartment was relatively constant. The maximum temperature was about 800 °C (Fig. 3-4). The temperatures increased due to the heating of the compartment structure. The measurements of the heat flux into the walls are rather unsteady. But according to the temperature the heat flux increased with time. The evaluated heat flux is approx. 10 to 30 kW/m^2 (Fig. 3-5). Heat fluxes in this range may lead to an ignition of cellulose products and PVC insulated cables. The temperatures inside the fuel are presented in Fig. 3-6. The measuring point was located approx. 3 cm above the bottom of the pan.

Fig. 3-1 Fire development inside the fire compartment - Test 1, view through front door

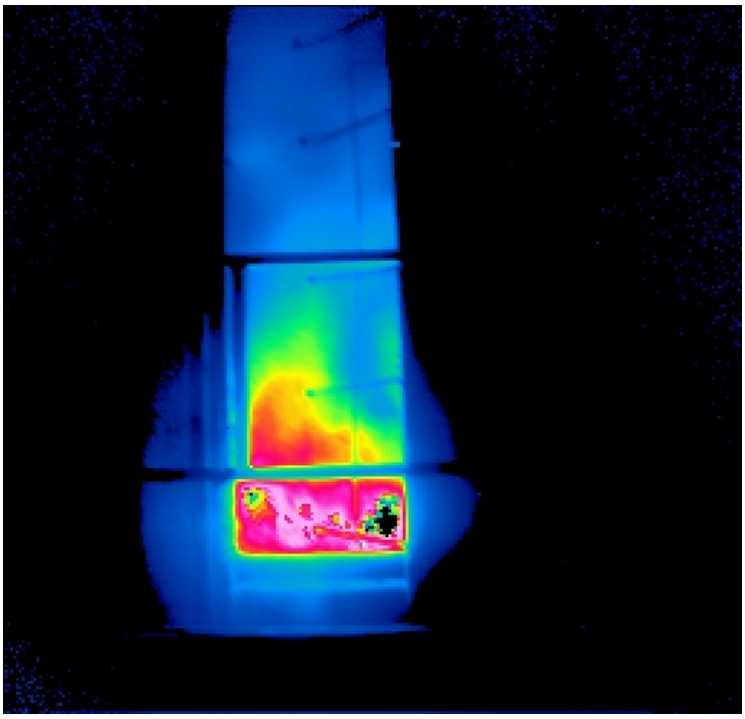

Fig. 3-2 Temperature distribution during the fully developed fire phase - Test 1, view through front door

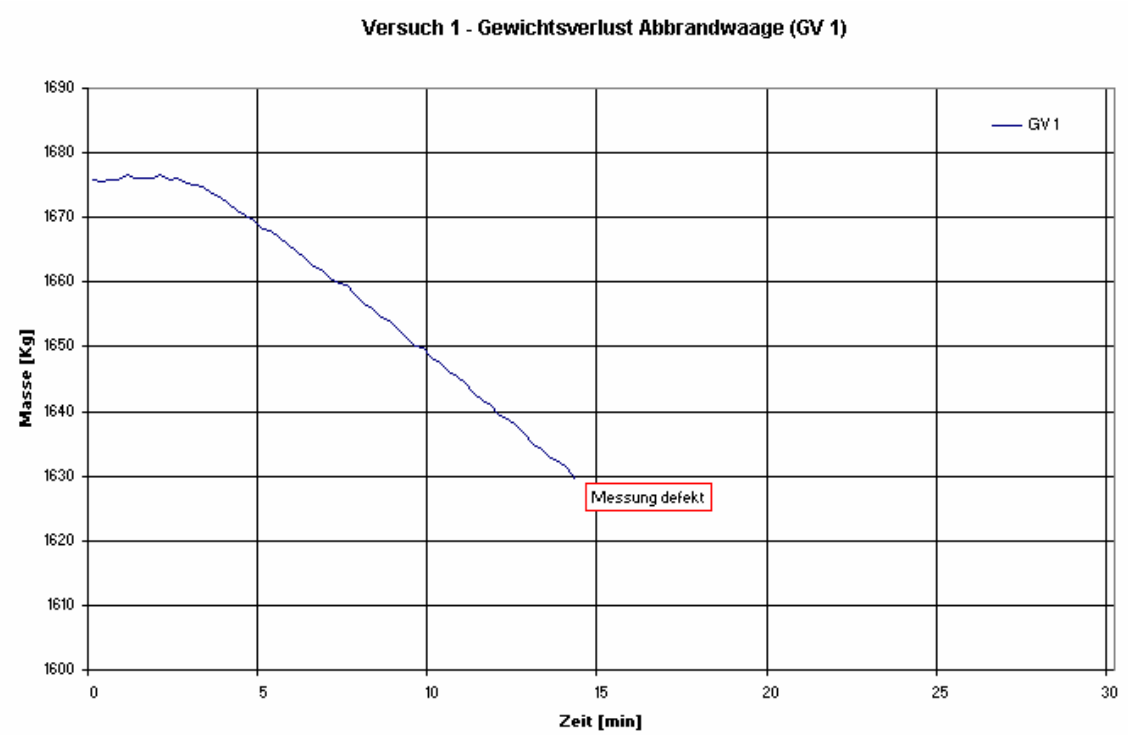

Fig. 3-3 Weight loss - Test 1

Fig. 3-4 Temperature distribution in measurement level 1 - Test 1

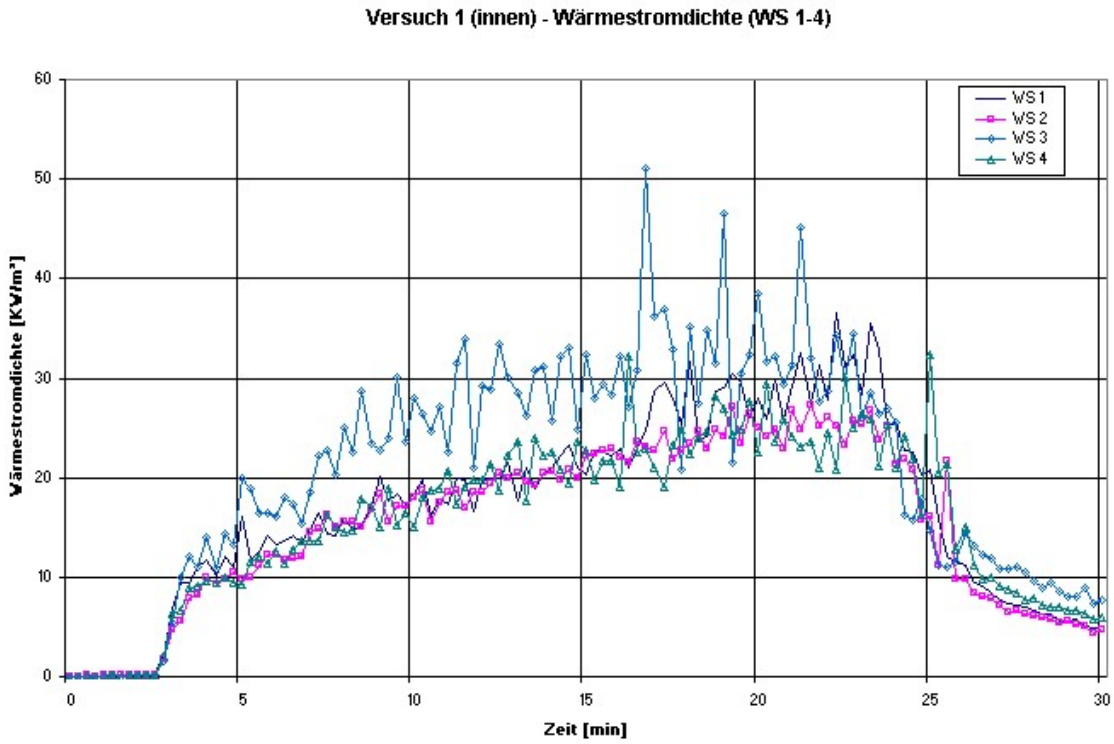

Fig. 3-5 Heat flux into material probes - Test 1

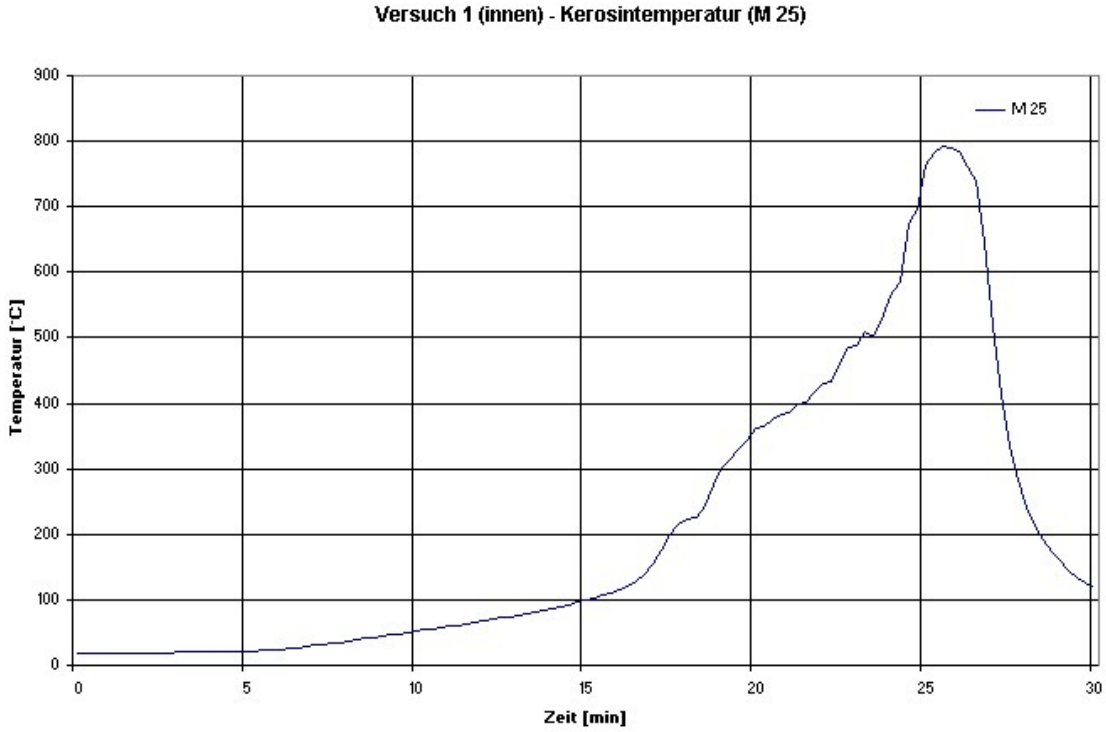

Fig. 3-6 Measured fuel temperature 3 cm above pan bottom - Test 1

3.2 Summary of Test 3

In comparison to Test 1, the opening at the front wall of the compartment was only one third of the size and started at 1 m above the floor of the fire compartment. All other conditions were quite similar to those of Test 1.

The duration of the fire was about 22 min. Fig. 3-7 shows the temperature distribution inside the fire plume during the fully developed fire phase. The measurement of the weight loss shows a constant decrease in the initial phase (Fig. 3-8). During the last third of the test the fire changed from a fuel controlled state to a ventilation controlled one (Fig. 3-9), due to the increased pyrolysis rate and complete consumption of the oxygen available. In this phase of the test some erratic weight loss measurements occurred with deviations of more than 80 kg. After the test, the measurement device was checked and found to work properly. Maximum temperatures of approx. 1000 °C were reached during ventilation controlled conditions (Fig. 3-10). The measured heat fluxes were between 10 and 60 kW/m^2 with peaks up to 100 kW/m^2 (see Fig. 3-11).

The heating curves inside the inner barrel of the barrel type target are comparable for all tests. Fig. 3-12 illustrates the temperature progression at the medium level of the target. The temperature decrease over several hours is presented in Fig. 3-13.

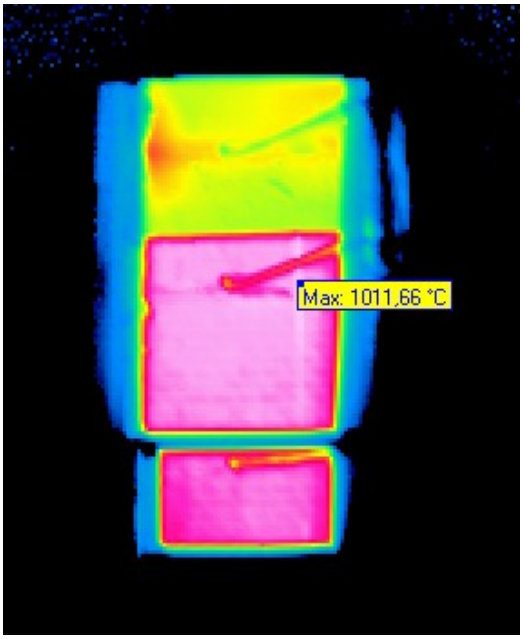

Fig. 3-7 Temperature distribution inside the fire - Test 3

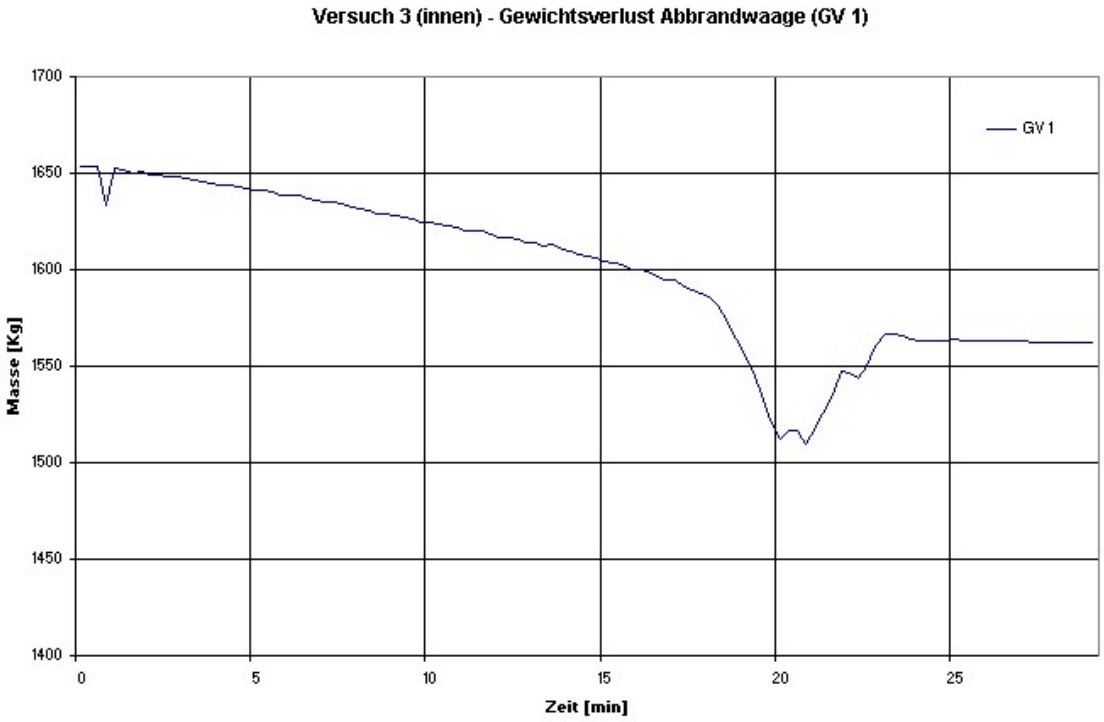

Fig. 3-8 Weight loss - Test 3

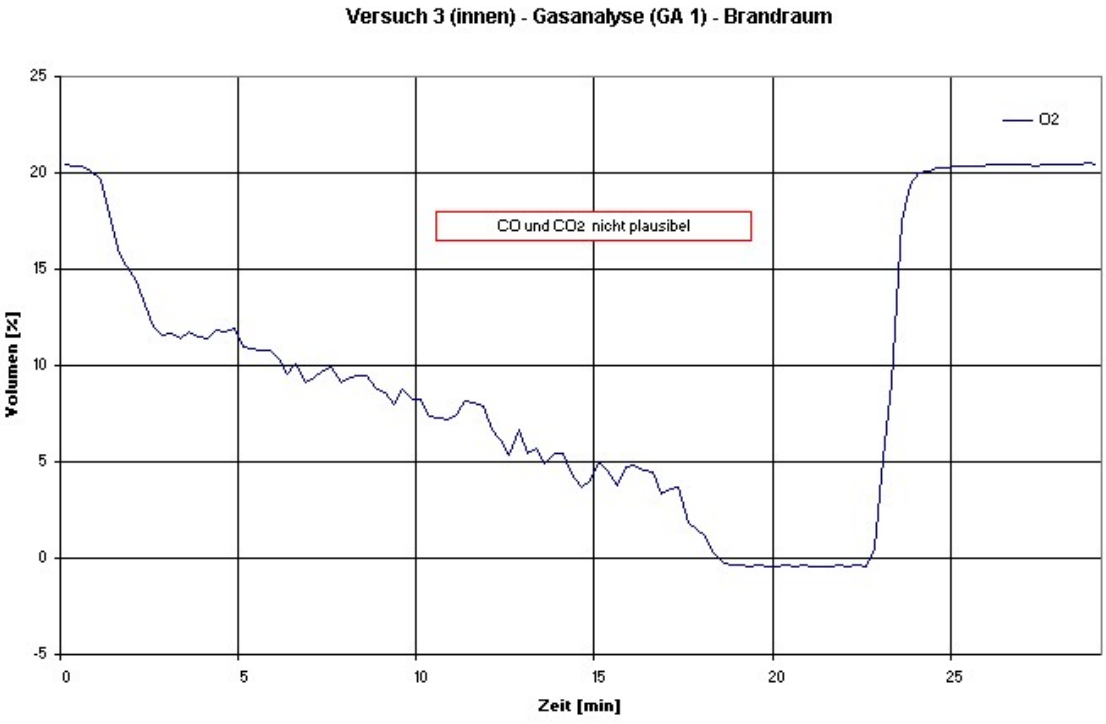

Fig. 3-9 Oxygen concentration in the fire compartment - Test 3

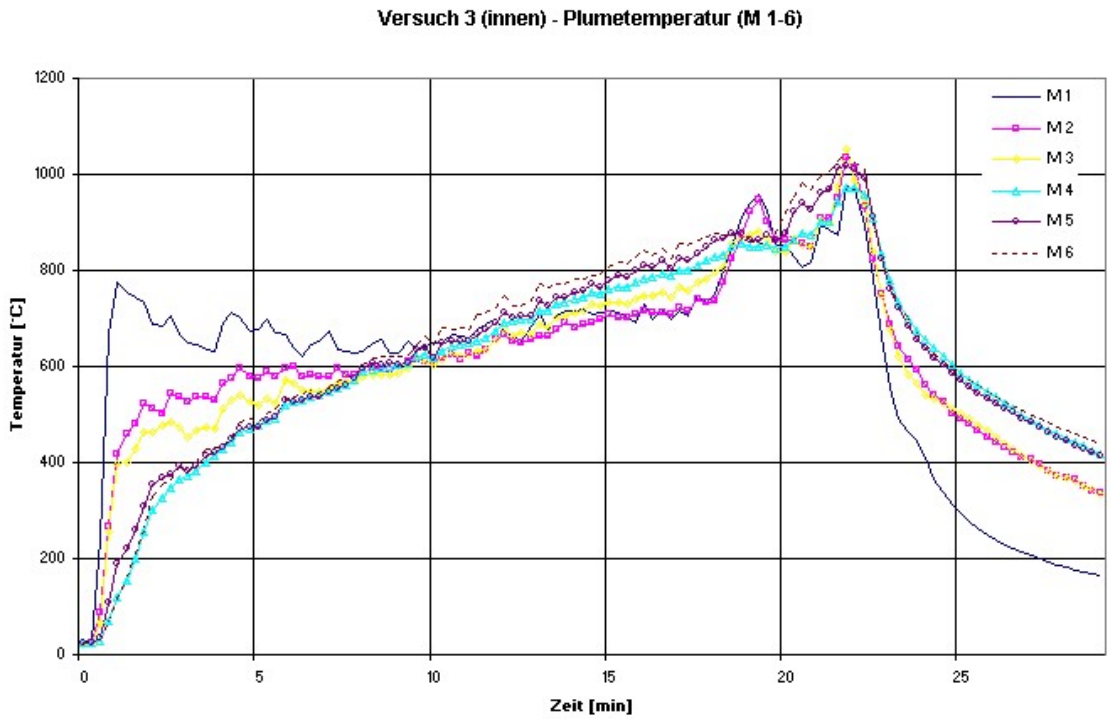

Fig. 3-10 Plume temperatures - Test 3

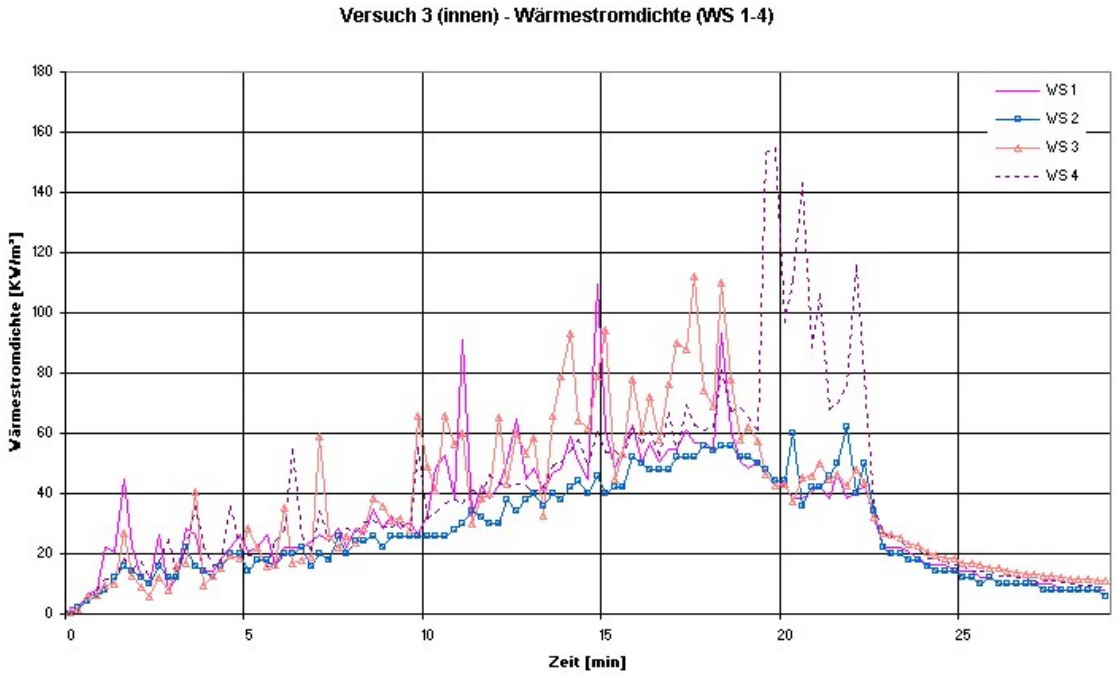

Fig. 3-11 Heat flux into the test probe structures - Test 3

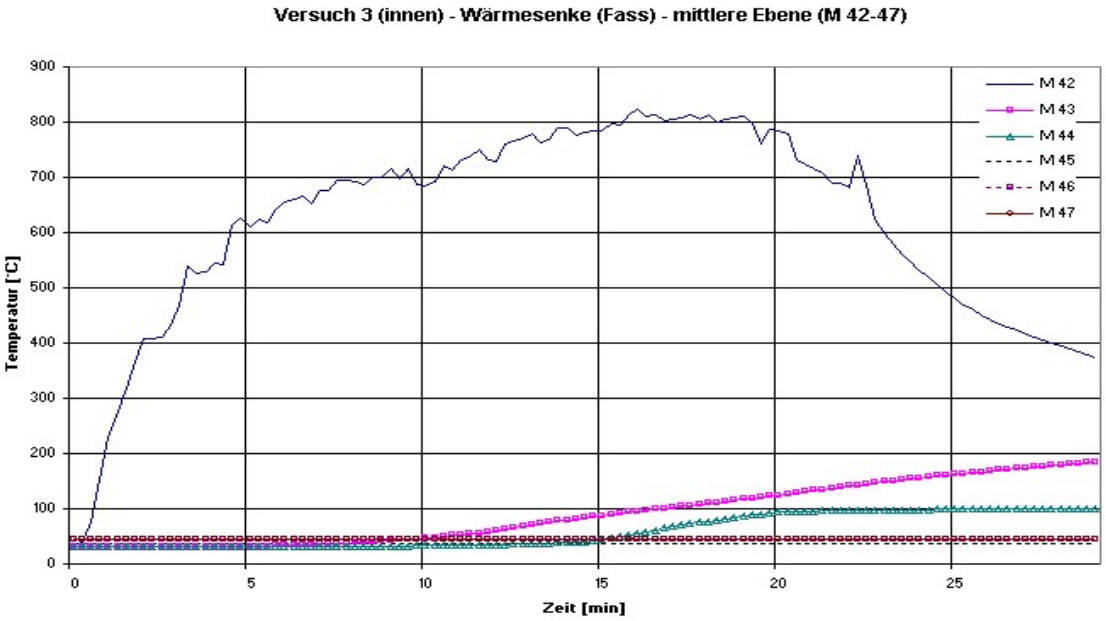

Fig. 3-12 Temperature distribution inside the barrel during Test 3

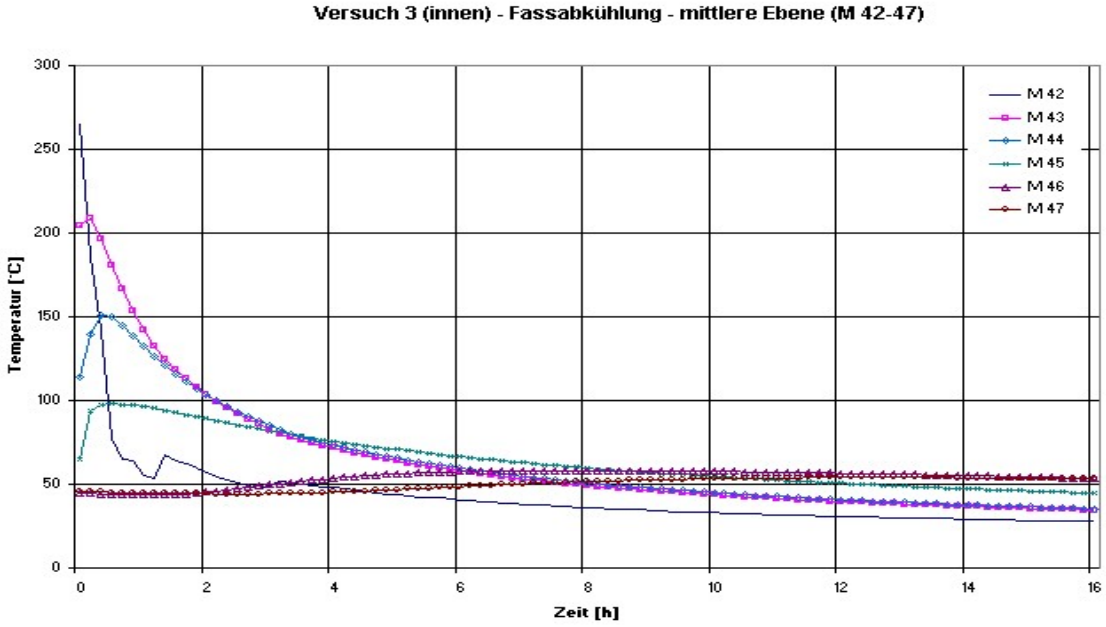

Fig. 3-13 Temperature decrease after Test 3

3.3 Conclusions

In this section, some conclusions are drawn, partly regarding the results from the other tests listed in Table 3-1.

Ventilation

In both tests, the smoke was extracted through the door vent. But as the measurements show, some flow occurs also through the FUCHS fan system installed on top of the fire compartment. This volume flow has to be considered in the evaluation of energy balance. In the case of the natural (door) ventilation, the velocity through the door is between 2 and 6 m/s. This flow leads to some leaning of the plume towards the rear of the fire compartment. Larger openings lead to a higher convection heat loss through the openings. Regarding all experiments of this series, the largest temperatures occur in case of an optimum size of openings with minimum heat loss and enough oxygen being available, just before changing to ventilation controlled phases.

Temperatures

A pool fire with an area of 1 m^2 did not completely fill the fire compartment which had a floor area of approx. 13 m^2 and a volume of 76 m^2 and an opening to the environment of area of 2.1 m^2. Therefore, in Test 1 temperature variation with height could be observed. In case of the smaller opening (Test 3) the temperature inside the fire compartment was much more homogenous.

Heat Flux Density

Four heat flux measurements were implemented at a height of about 1.7 m on opposite walls. They measured the total heat flux including convection and radiation. In all tests, the heat flux density increased due to the heating of the surrounding compartment structures leading to a higher reflection of heat. Due to the intensity of the pool fires a strong pulsation occurred in temperature of the burned gases. In addition, this was influenced by the entrance of fresh air leading to a relatively high oscillation in the measured heat flux densities.

Oxygen Concentration

The oxygen concentration inside the fire compartment was measured at an elevation of 3 m above the floor. In the tests the concentration decreased to practically zero, indicating the presence of ventilation controlled conditions.

4 Input Parameters and Assumptions

For the Benchmark Exercise No. 4, it was intended to perform blind calculations without knowing the pyrolysis rate or the other experimental results, semi-blind calculations (knowing only the pyrolysis rate) and open calculations with all data being available to the modelers. From the beginning, it was clear that performing blind calculations is a challenging task. But, on the other hand, this is a typical situation for real applications in nuclear power plants and installations. The deviations of the calculated results from the measured data provides some insights into the uncertainties of the results for such (somewhat extreme) situations, particularly due to the high heat release rate compared to the volume of the fire compartment.

In the following section the major assumptions employed in performing the calculations are listed and discussed:

Heat Release Rate

The specified pyrolysis rate (used in the semi-blind and open calculations) is based on the measurement of the weight loss, which had some problems for Test 1 (weight loss data available until 850 s only) and Test 3 (containing positive gradients leading to negative pyrolysis rates). Therefore, some approximations and assumptions have been made influencing the results to some extent. Fig. 4-1 and Fig. 4-2 show the proposed smoothed pyrolysis rates compared to the raw measured data.

LOL Value

Main difference between the two tests is the cross section of the door opening. This leads to under-ventilated conditions in Test 3. Some codes have to specify the LOL value or it is fixed inside the program. A too high value for LOL reduces the accuracy of the predictions for Test 3. In case of high temperatures the entrained oxygen seems to be completely consumed by the combustion process.

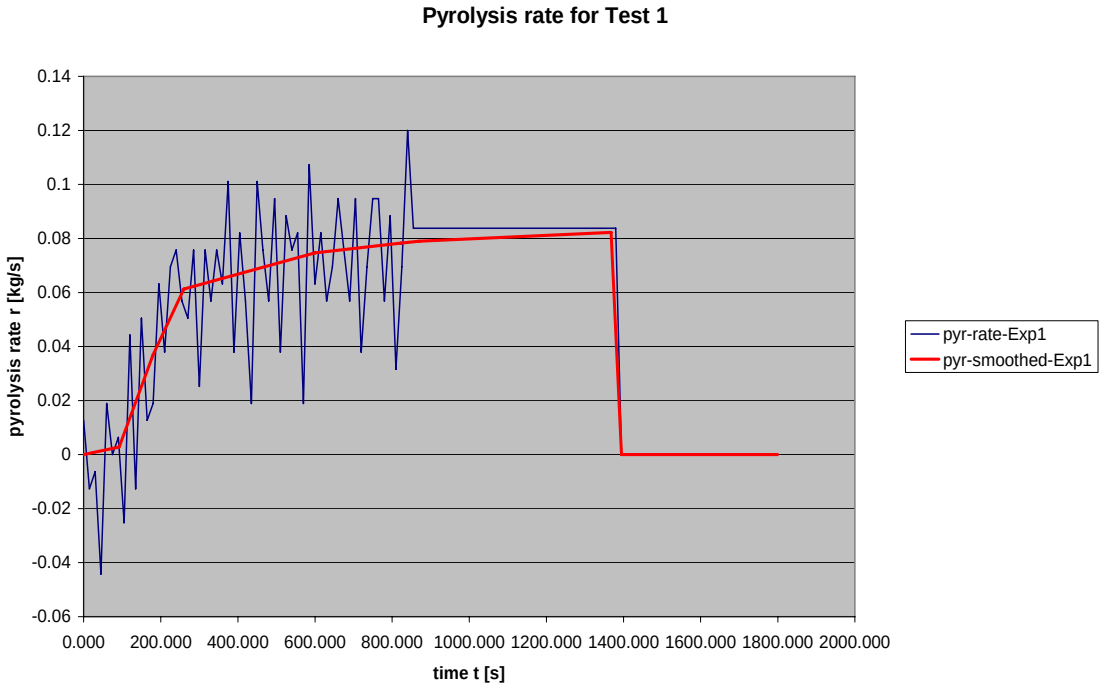

Fig. 4-1 Smoothed pyrolysis rate for Test 1

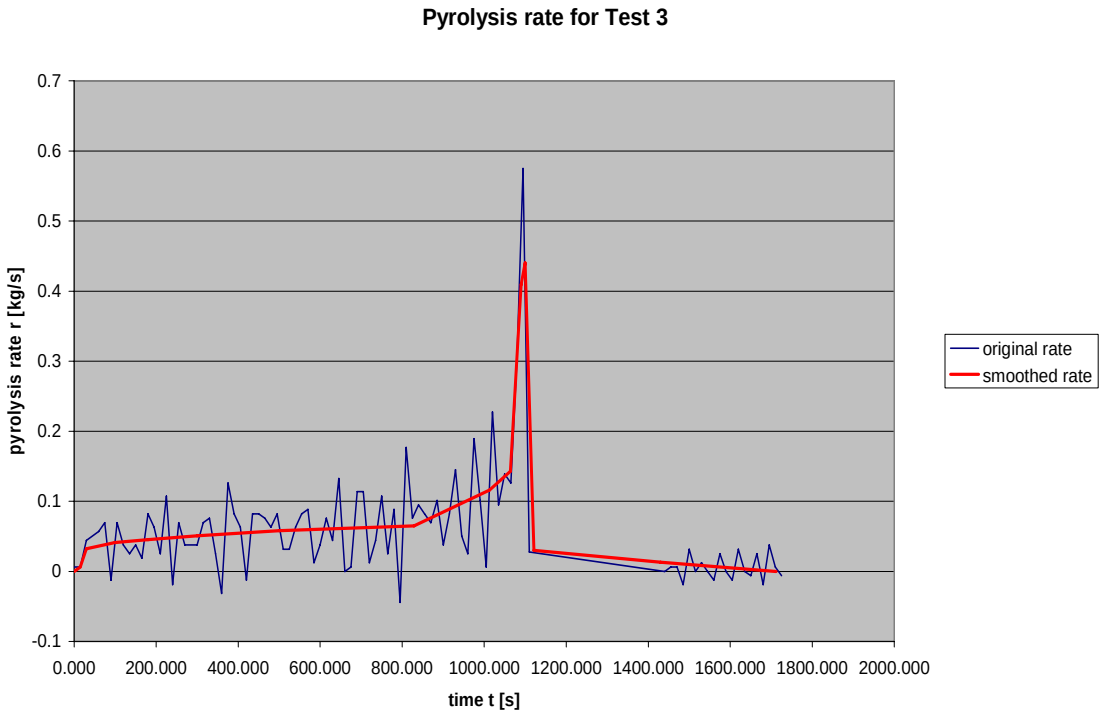

Fig. 4-2 Smoothed pyrolysis rate for Test 3

Ventilation

In most cases, the ventilation was defined as it was described in the specification. Some participants decided not to simulate the ventilation system and the hood.

Radiation Fraction

The radiation fraction has to be defined by the user. Values about 40% have been used. In some calculations the radiation fraction is assumed to be released from the pan, possibly leading to different temperature loads on the targets.

Targets

The targets (three material probes) and the barrel type container are not always considered in the calculations. For the material probes (particularly for steel) one problem was the thickness. Furthermore, a backward heating was possible, which was not (and could not be) considered in any of the calculations. With respect to the barrel, the cylindrical shape could not be modeled with some of the codes. In addition, the multi-layer material composition could not be considered in all codes.

Combustion Scheme and Yields

The composition of the fuel was specified, but not the chemical reaction itself. Therefore, the user had to specify the yields and to decide if the combustion is complete or not. In particular for Test 3, the input may have an impact on the results, due to the under-ventilated condition and production of CO and soot.

Grid Size

For CFD (*c*omputational *f*luid *d*ynamics) codes the user has to specify the grid size. The cell size used in FDS /MCG 04/ with a width of approx. 10 cm is somewhat larger than the cell size used in CFX-5.7 /CFX 04/. The choice of suitable grid size will depend on the type of CFD model (e.g. RANS of LES) and the numerical schemes employed.

Air Entrainment

For zone models, the simulation of the air entrainment (the plume mode) seems to be a key parameter, as this effects the available oxygen for the combustion.

5 Comparison of Code Simulations and Experimental Results

For Benchmark Exercise No. 4 full blind calculations (without knowing the pyrolysis rate), semi-blind calculations (knowing pyrolysis rate) and full open calculations have been performed. Table 5-1 lists the participants for this Benchmark Exercise, the fire codes used, type of analysis and the reference to the Appendix provided by the participant. A summary of the performed calculations is provided below.

Table 5-1 List of fire simulations performed within Benchmark Exercise No. 4

Participant	Fire Code	Code Type	Tests	Type of Analysis	Appendix
K. McGrattan, NIST	FDS	zone	1 & 3	blind, semi-blind	A
S. Miles, BRE	JASMINE	CFD	1 & 3	blind, semi-blind, open (3 only)	B
	CFAST	zone	1 & 3	semi-blind	B
M. Dey, USNRC	FDS	CFD	1 & 3	semi-blind	C
	CFAST	zone	1 & 3	semi-blind	C
T. Elicson (Fauske)	FATE	zone	1 & 3	open	D
L. Rigollet (IRSN)	FLAMME-S	zone	1 & 3	open	E
M. Heitsch (GRS)	CFX	CFD	1 & 3	open	F
W. Brücher (GRS)	FDS	CFD	3	open	G
B. Schramm (GRS)	COCOSYS	LP	1 & 3	open	H
V. Nicolette (SNL)	VULCAN	CFD	3	open	I
B. Gautier (EdF)	MAGIC	zone	1 & 3	open	J

5.1 Blind Calculations

5.1.1 FDS (CFD Code) Applied by K. McGrattan (NIST, USA)

FDS Code Description and Input

In cooperation with the fire protection engineering community, a computational fire model, Fire Dynamics Simulator (FDS) /MCG 04/, has been developed at the National Institute of Standards and Technology (NIST) in the USA to study fire behavior and to evaluate the performance of fire protection systems in buildings. The software was released into the public domain in 2000, and since then has been used for a wide variety of analyses by fire protection engineers. Briefly, FDS is a computational fluid dynamics code that solves the Navier-Stokes equations in low Mach number, or thermally expandable, form. The transport algorithm is based on large eddy simulation techniques, radiation is modeled using a gray gas approximation and a finite-volume method is used to solve the radiation transport equation. Combustion is modeled using a mixture fraction approach, in which a single transport equation is solved for a scalar variable representing the fraction of gas originating in the fuel stream.

The dimensions of the grid were 36 by 72 by 56, and the cells were exactly 10 cm in size throughout. All objects within the computational domain were approximated to the nearest 10 cm. The decision to use a 10 cm grid was based on the observation that the ratio of the fire's characteristic diameter D* to the size of the grid cell *dx* is an indicator of the degree of resolution achieved by the simulation. D* is given by the expression $(\dot{Q}/\rho_\infty c_p T_\infty \sqrt{g})^{2/5}$, and was about 1 m for this series of fires. Past experience has shown that a ratio of 10 produces favorable results at a moderate computational cost.

FDS performs a one-dimensional heat transfer calculation into an assumed homogenous material of given thickness and (temperature-dependent) thermal properties. The compartment walls and ceiling were made of various types of concrete, the thermal properties of which were input directly into the model. It was assumed that the target slabs of concrete, aerated concrete, and steel were only exposed at the front surface, although the internal temperature measurements suggested otherwise. No attempt was made to model the barrel container at the rear of the compartment, due to its cylinder geometry and composition of different materials.

Some of the properties of the liquid fuel used in the tests were provided. For kerosene, the fuel properties of “dodecane” ($C_{11.64}H_{25.29}$) were input into the model with assumed soot and CO yields of 0.042 and 0.012, respectively. The current version of FDS did not adjust the soot or CO yield as a consequence of reduced compartment ventilation or combustion efficiency. The assumed heat of vaporization and boiling temperature: 256 kJ/kg and 216 °C, respectively, were important input values for the simulation. For the blind calculations the fire was simulated by including in the simulation a small, hot block that heated up the surface of the pool until the fire was self-sustaining, after which the block literally disappeared from the calculation. FDS predicted the radiative and convective heat flux from the fire to the fuel surface, and the evaporation of the fuel according to the Clausius-Clapeyron equilibrium pressure of the fuel vapors above the pan.

FDS uses a finite volume method to solve the radiation transport equation in the gray gas limit. By default, the radiation from the fire and hot gases is tracked in 100 directions, which is adequate to predict the radiation heat flux to nearby targets.

The ventilation rates for all the compartment fans and hood were input directly into the model.

Code Results

For blind calculations only the heat release has been discussed. For Test 1, the predicted heat release rate (HRR) rose very quickly to about 3 MW following ignition, followed by a gradual rise over 15 min as the compartment heated up and the increased thermal radiation from the hot upper layer led to an increased burning rate (Fig. 5-1). The measured HRR did not exhibit the rapid rise, taking several minutes to grow to 3 MW and then gradually increasing at a rate comparable to the prediction. The reason for the discrepancy is that FDS uses a mixture fraction model of combustion. Briefly, the evaporated fuel burns readily with oxygen when mixed to the appropriate ratio, regardless of temperature. Thus, FDS did not simulate properly the spreading of the fire across the pan; rather it predicted an almost instantaneous involvement of the entire fuel surface.

In Test 3, FDS over-emphasized the effect of the small compartment opening (Fig. 5-1). Initially, it predicted the same rapid growth as it had in Test 1, but then the fire consumed the available oxygen, and the fire died down, decreasing the burning rate.

As air began to re-enter the compartment, the burning rate increased again, and the oscillatory pattern emerged. FDS never predicted the large spike in HRR that was measured at 15 min, most likely because the model was predicting a substantial amount of burning outside the compartment, even though this was not observed in the experiment.

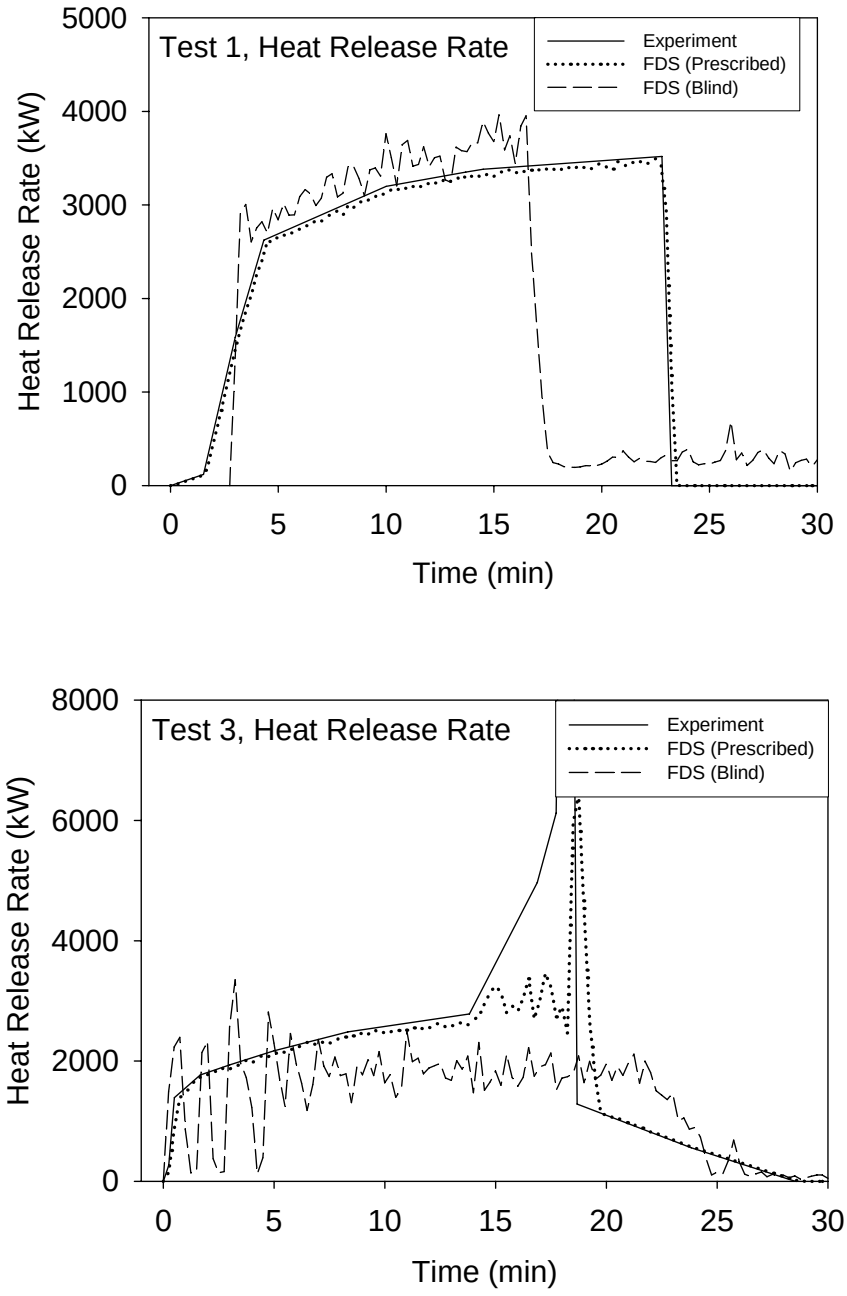

Fig. 5-1 Measured and predicted (blind) heat release rates for Tests 1 and 3 (from Appendix A)

5.1.2 JASMINE (CFD Code) Applied by S. Miles (BRE, UK)

Blind calculations (prior to the dissemination of the experimentally measured fuel mass release rate) were conducted for Tests 1 and 3 with JASMINE Version 3.2.3 /COX 87/. One important purpose of these blind simulations was to examine how realistic predictions could be made for gas temperatures, fluxes etc using a simple, empirical expression for fuel pyrolysis rate.

JASMINE Code Description and Input Assumptions

JASMINE solves the Reynolds-Averaged Navier Stokes (RANS) equations of fluid flow on a single-block Cartesian grid. The coupled set of equations for each of the three Cartesian velocity components, enthalpy (heat) and other scalars required by the various sub-models (e.g. fuel mass and mixture fractions for combustion) is approximated as a system of algebraic equations that are solved numerically on a discrete grid. This generates a solution value for each variable at each grid location. JASMINE uses the finite volume method, where the differential equations are first transformed into an integral form and then discreticizsed on the control volumes (or cells) defined by the numerical grid. This solution procedure is coupled with a variant of the SIMPLE pressure-correction scheme. Transient solutions are generated by a first-order, fully-implicit scheme. A standard κ-ε turbulence model with additional buoyancy source terms was used. Standard wall functions for enthalpy and momentum describe the turbulent boundary layer adjacent to solid surfaces.

In the benchmark exercise combustion was modeled using the eddy break-up sub-model in which the fuel pyrolysis rate is specified as an input boundary condition. Reaction (oxidation) is calculated at all control volumes as a function of fuel concentration, oxygen concentration and the local turbulent time-scale. A simple one-step, infinitely fast chemical reaction is assumed. Complete oxidation of the fuel is assumed where sufficient oxygen is available. The effect of oxygen concentration on the local rate of burning may be incorporated by setting oxygen and temperature limits which define 'burn' and 'no burn' regions. For the blind simulations no oxygen concentration limit was specified, i.e. there was only a 'burn' region.

A fuel source area of 1 m^2 and a heat of combustion of 4.28×10^7 J kg^{-1} were used in all calculations. For the blind calculations a fixed fuel pyrolysis rate was assumed from 60 s after ignition (increasing linearly to this value over the first 60 s). A value of

0.039 kg s^{-1} was chosen, based upon published engineering information. The sensitivity to reducing this value to 0.0234 kg s^{-1} was investigated.

Radiant heat transfer is modeled with either the six-flux model, which assumes that radiant transfer is normal to the co-ordinate directions, or the potentially more accurate discrete transfer method. All blind calculations were performed using the six-flux radiation model. Local absorption-emission properties are computed using a mixed grey-gas model, which calculates the local absorption coefficient as a function of temperature and gas species concentrations. As soot was not modeled in this benchmark exercise, only CO_2 and H_2O acted as participating media in the radiation calculations.

Where soot is not explicitly modeled, its influence on the overall energy budget may be incorporated, somewhat crudely, by reducing the heat release rate of the fire, i.e. either the pyrolysis rate or the effective heat of combustion, by a fixed fraction. This is akin to the radiative fraction employed in zone models such as CFAST. The amount of heat then removed represents what could be expected to be 'lost' by radiation from the sooty flame region above the fuel source. The remainder of this heat is assumed to be convected into the rest of the compartment or, as a relatively small fraction, by radiation from the plume region due to CO_2 and H_2O. Note also that of the heat convected into the compartment (from the fire source), some of this is subsequently radiated from the ‘smoke gases’ (due to CO_2 and H_2O).

Thermal conduction into solid boundaries may be included by means of a quasi-steady, semi-infinite, one-dimensional assumption, which is appropriate for many smoke movement applications. Alternatively, the solution of the one-dimensional heat conduction equation into the solid is also available. The quasi-steady, one-dimensional assumption was employed in the blind calculations. The thermal properties of the concrete walls, floor and ceiling were included as specified.

The dimensions of the compartment, doorway opening and exhaust ventilation duct were modeled exactly as in the problem specification. Only half the compartment was modeled, imposing symmetry at the x = 1.8 m plane, and using a numerical mesh of approximately 80,000 cells. A fixed numerical time-step of 2.5 s was employed in all simulations.

Ventilation through the fan system was modeled as a time-dependent mass sink, set to a value corresponding to the experimentally measured volumetric flow rate.

The thermal response of the material probe targets and the heat flow densities (WS2, WS3 & WS4) was included in the JASMINE calculations. Furthermore, the wall surface temperatures at the locations of the plates/thermocouples (M19 etc) were calculated. While the blockage due to the barrel target was included, its thermal response was not modeled and so no comparisons were made with the barrel temperature measurements.

Further general information on JASMINE is provided in the Appendix B to this report.

JASMINE Code Results

Two sets of blind predictions were made for each of Test 1 and Test 3, one using a fixed fuel pyrolysis rate of 0.039 kg s^{-1} and the other a rate of 0.0234 kg s^{-1}. These calculations were performed only for the first ten minutes of the experiments.

Comparisons between prediction and measurement were made for gas temperatures, oxygen concentration, door/wall vent velocities and compartment surface temperatures. The blind predictions made with the higher value of the pyrolysis rate were closer to the experimental measurements than those made with the lower pyrolysis rate.

Fig. **5-2** and Fig. 5-3 (from the Appendix B) show the gas phase and wall surface temperature calculations for Test 3 using the two fuel pyrolysis specifications.

The blind calculations using the higher fuel pyrolysis rate of 0.039 kg s^{-1} were quite encouraging considering the complexity of the physics involved. A simple engineering estimate of the pyrolysis rate was in this case sufficient to capture the main gas phase properties of the experiments. It was noted, however, that the transient effects due to changes in the pyrolysis rate due to the development of conditions inside the enclosure were not captured. Effects due to the feedback of radiation from soot particulates and the compartment walls are likely to be highly transient.

A main discrepancy between the blind calculations and the measurements was in the doorway vent flow in Test 3, where in contrast to the flow being predominantly into the compartment as indicated in the predictions, the measurements suggest a more distinct two-way flow at the wall vent. This discrepancy may be due, in part at least, to the imposed exhaust flow at the mechanical ventilation duct in the JASMINE calculations forcing a significant amount of air into the compartment through the wall vent.

Pyrolysis rate = 0.039 kg s^{-1}

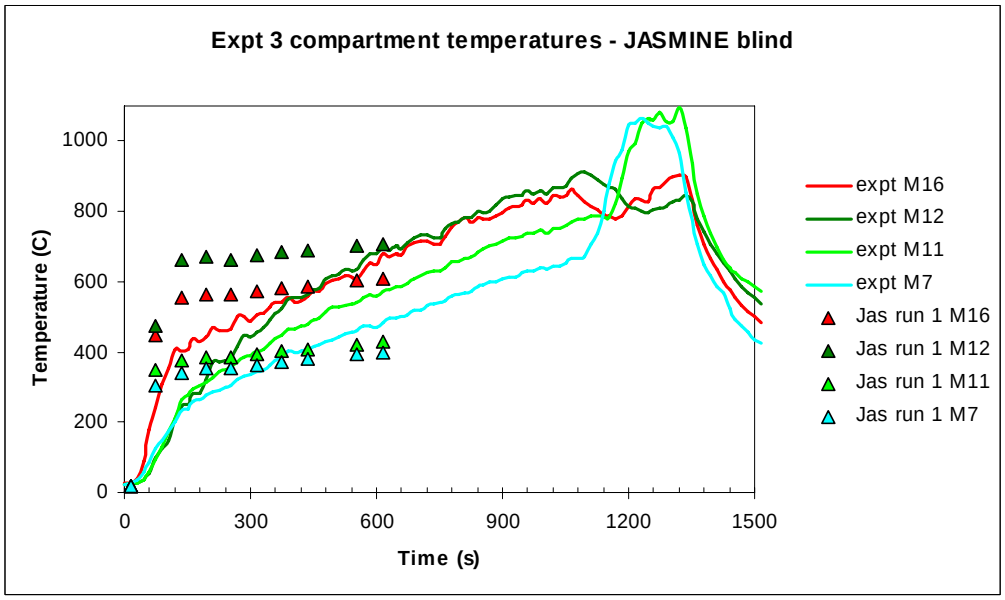

Pyrolysis rate = 0.0234 kg s^{-1}

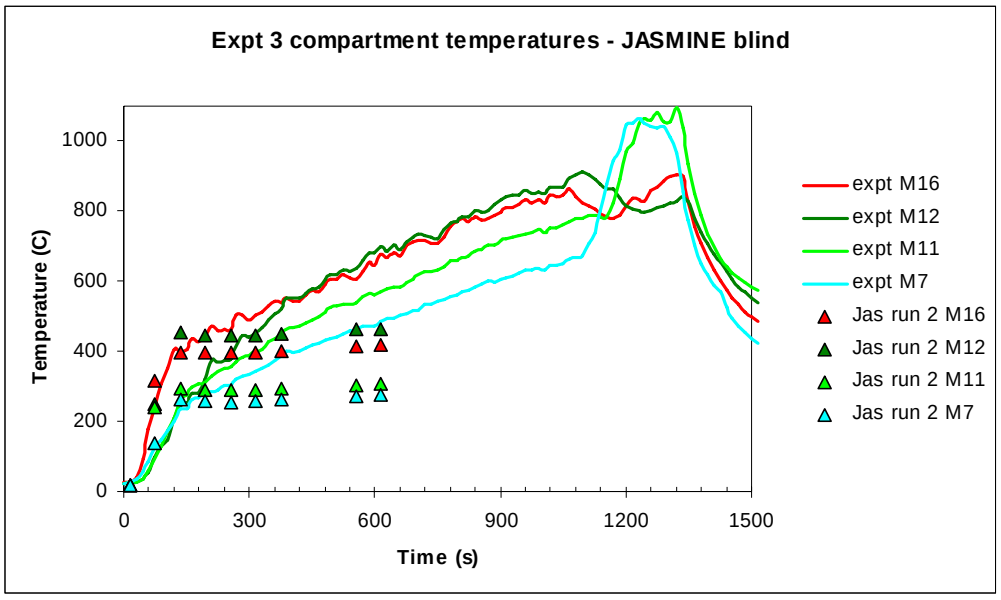

Fig. 5-2 Measured and predicted (blind) gas temperatures for Test 3 (from Appendix B)

Pyrolysis rate = 0.039 kg s^{-1}

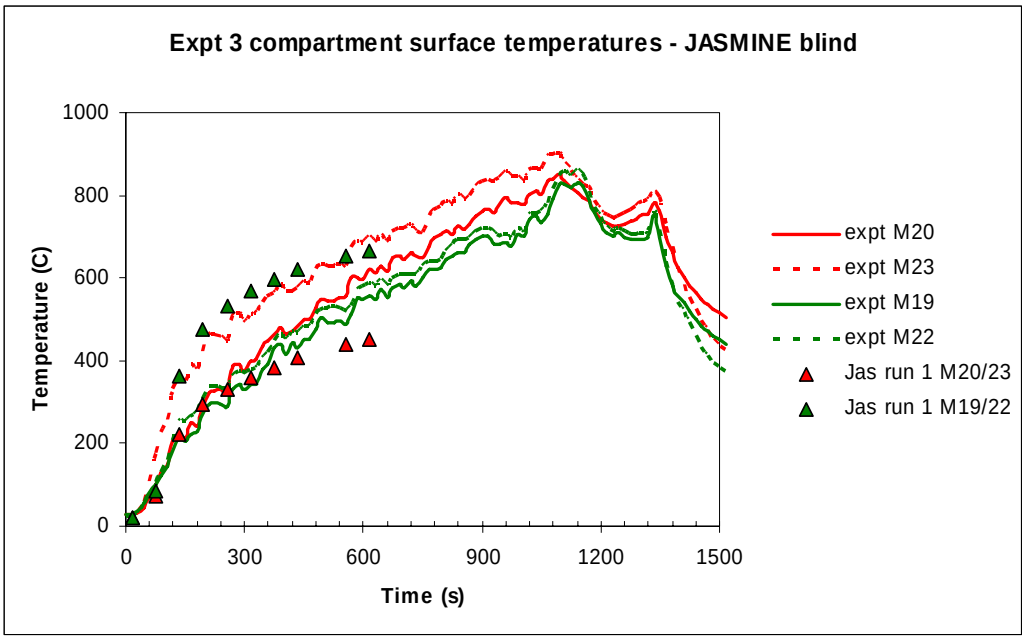

Pyrolysis rate = 0.0234 kg s^{-1}

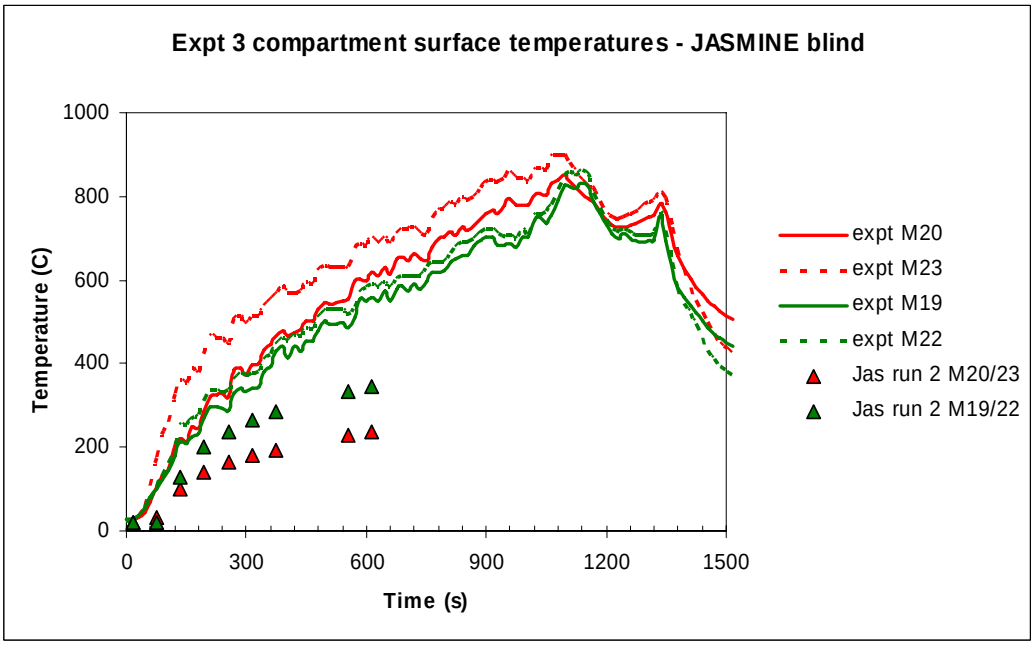

Fig. 5-3 Measured and predicted (blind) wall surface temperatures for Test 3 (from Appendix B)

5.2 Semi-blind Calculations

5.2.1 FDS (CFD Code) Applied by K. McGrattan (NIST, USA)

FDS Code Description and Input

(See paragraph 5.1.1)

Code Results

Assuming an uncertainty of 15 % for the heat release rate (HRR) an uncertainty of temperatures about 10 % can be concluded. In general, the difference between measured and predicted compartment temperatures in Tests 1 and 3 was within the uncertainty bounds established by the prescribed HRR, but there were some exceptions, especially in Test 3. In making comparisons between model and experiment, the temperatures were compared from 10 min onwards. Earlier in the tests, the measured temperatures exhibited a delay relative to the predictions, probably due to the thermal inertia of the thermocouples.

Three plates were positioned on the side wall of the compartment, about 1.7 m above the floor. FDS did compute the inner temperatures of the slabs, and the temperatures decreased monotonically with depth since FDS considered the slab to back up to an ambient temperature environment. However, the measured temperatures did not decrease monotonically, either because of a measurement error or the slab might have been heated from behind. Sometimes the comparison of surface temperatures and heat flux with the experimental data was somewhat inconsistent. In some situations, the predicted surface temperature was more accurate than the predicted heat flux, suggesting either that the heat flux measurement was inaccurate, or that the model benefited from “two wrongs making a right”; that is, an under- or over-prediction in the heat flux was compensated by a comparable error in the surface properties or solid phase heat transfer calculation.

FDS uses a mixture fraction combustion model, meaning that all gas species within the compartment are assumed to be functions of a single scalar variable. For the major species, like carbon dioxide and oxygen, the predictions are essentially an indicator of how well FDS is predicting the bulk transport of combustion products throughout the

space. For minor species, like carbon monoxide, FDS at the present time did not account for changes in combustion efficiency, relying only on a fixed yield of CO from the combustion product. In reality, the generation rate of CO changes depending on the ventilation conditions in the compartment.

The quality of the calculated velocity depends strongly on the grid resolution at the door opening. The model used 10 cm grid cells, fine enough to compute the bulk temperatures and flows within the compartment, but not fine enough to capture the steep gradient in horizontal velocity over the height of the doorway, especially in Test 3 where the door was resolved by just a few cells spanning the vertical dimension.

Sensitivity studies have been performed using a double grid size. In general, there were no significant degradations of the results using the 20 cm grid. Indeed, it appeared that the heat fluxes and surfaces temperatures were predicted more accurately with the coarse grid. The coarse grid tends to “smooth out” the temperature and heat flux fields, sometimes resulting in lower predicted values that are closer to the measured values. However, this “smoothing” of the temperature field more often leads to less accurate predictions. For example, consider the plume temperature predictions. The upper layer temperature predictions (M-3 and M-6) were not degraded on the 20 cm grid, but the lower level prediction (M-1) was significantly degraded due to the “smoothing” of high temperatures near the base of the fire.

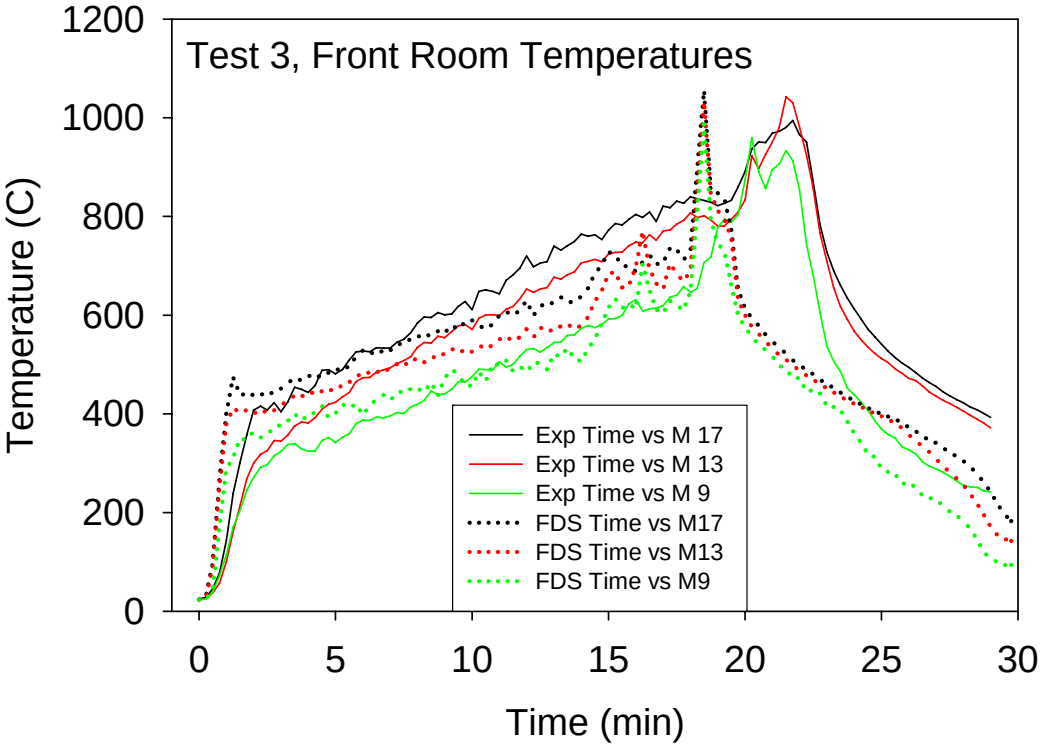

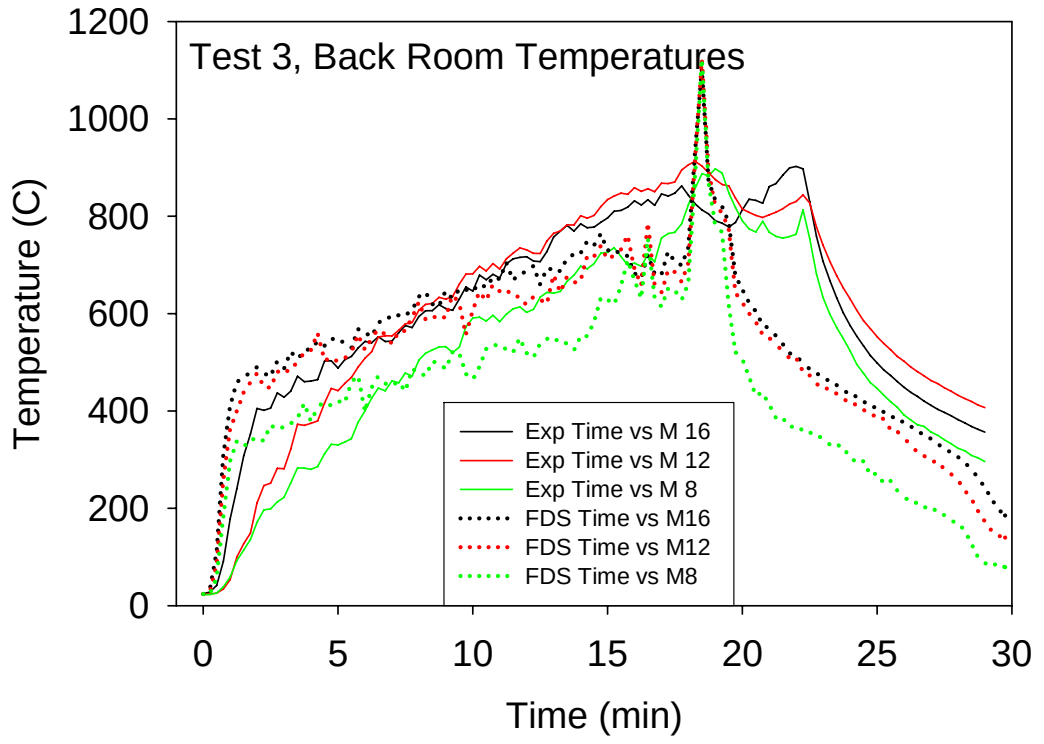

Fig. 5-4 Gas temperature comparisons for Test 3 (from Appendix A)

5.2.2 FDS (CFD Code) and CFST (Zone Model) Applied by M. Dey (USNRC, USA)

The following paragraph provides a comparison of semi-blind predictions by CFAST and FDS for the tests conducted for ICFMP Benchmark Exercise No. 4. CFAST Version 3.1.7 and FDS Version 3.1.5 were used for the computations.

The FDS code simulated Tests 1 and 3 successfully. The CFAST code simulated Test 1 to the end of the specified transient, however, instabilities were noted. There were convergence issues in the CFAST simulation of Test 3. The simulation halted at about 14 % to completion. CFAST is sensitive in cases with a high heat flux. The penetration of the thermal wave in the compartment floor and in less dense materials with low thermal conductivity poses numerical challenges for the CFAST code.

CFAST Code Description

CFAST is a widely used zone model, available from the National Institute of Standards and Technology (NIST), USA. It is a multi -room zone model, with the capability to model multiple fires and targets /JON 04/. Fuel pyrolysis rate is a pre-defined input, and the burning in the compartment is then modeled to generate heat release and allow species concentrations to be calculated. CFAST was used as a conventional two-zone model, whereby each compartment is divided into a hot gas upper layer and a cold lower layer. In the presence of fire, a plume sub-model (zone) transports heat and mass from the lower to upper layer making use of an empirical correlation. Flows through vents and doorways are determined from correlations derived from the Bernoulli equation. Radiation heat transfer between the fire plume, upper and lower layers and the compartment boundaries is included using an algorithm derived from other published work. Other features of CFAST relevant to the benchmark exercise include a one-dimensional solid phase heat conduction algorithm employed at compartment walls and targets and a network flow model for mechanical ventilation.

FDS Code Description

(See paragraph 5.1.1)

Input Assumptions for FDS and CFAST

For both codes the pre-defined heat release rate was used. The use of prescribed heat release rates neglects the feedback effect between the fire and the compartment conditions. Therefore, the use of prescribed HRRs will include some uncertainty due to the lack of complete simulation of the fire phenomena in the compartment. The given peak in the heat release rate for Test 3 and the assumptions made for Test 1 may lead to a larger source of uncertainty in the predicted results.

The lower oxygen limit needs to be input to the CFAST code for the simplistic submodel for predicting the extinction of the fire. There was no value for LOL included in the specifications, allowing judgment from users to define the most appropriate value for the experiments. The specification of this parameter has a large effect on the prediction of extinction and could be a large source of user effects, especially for underventilated conditions. In FDS internal values are used, generally eliminating the need for user intervention.

The barrel was not simulated in FDS or CFAST, due to its cylindrical geometry and multi-material configuration which cannot be modeled in the codes. Standard material properties have been used elsewhere.

The radiative fraction of the fuel was not specified. The value of the radiative fraction available in the literature for n-dodecane was assumed for the analysis. This parameter was identified as a key parameter effecting fire compartment conditions in ICFMP Benchmark Exercise No. 2.

The FUCHS fan system was simply modeled in CFAST and FDS with prescribed flow rates, without accounting for any feedback effects between the ventilation system and the compartment. Furthermore, the flow through the FUCHS system was assumed to be constant for the CFAST calculations as there is no direct means for providing input for varying ventilation flow rates in the code. The exhaust hood was not simulated in CFAST.

Code Results of FDS and CFAST for Test 1

The initial development of the HGL based on measured data seems erratic and may be due to discrepancies in the offset in the initiation of the transient. The measured data

shows the hot gas layer (HGL) interface reaches approx. 1.5 m at about 600 s. Both CFAST and FDS under-predict the steady state HGL interface height by 19 %.

Both CFAST and FDS predictions follow the same trend of temperature increase of HGL as the experimental data, but with CFAST over-predicting the increase by a larger amount. Once reaching the end of the rapid increase at approx. 360 s, the increase in temperature is greater in the experiment than that predicted by both CFAST and FDS. This discrepancy may be due to smaller heat loss in the experiments due to the presence of insulation that was ignored in the code calculations.

The O_2 level at GA1-O2, located at 3.8 m above the floor in the HGL (top of door is at 3.0 m), predicted by CFAST and FDS at the end of the transient phase is 8.9 % and 5.7 %, respectively. The measured O_2 level at the end of the transient is 13.5 %. Since the measured O_2 level does not decrease much after approx. 465 s, there is potentially an error in the measured O_2 level.

FDS predicts peaks in the plume temperature at approx. 50 s. These peaks are explained by the plume development predicted by FDS. Observations of the plume predicted by FDS indicate a steady vertical plume until approx. 50 s when the plume is pushed to the rear wall by flow into the compartment through the door. This causes peaks in the thermocouples, M2, M4, and M6 which are located directly above the fuel pan. The experimental measurements do not indicate this extensive movement of the fire plume. The measured temperatures M7 to M10 of measurement level 1 show a rapid increase in temperature followed by a more gradual increase until the end of the transient. The temperature measured at M10 is much higher than that measured at M7, M8, and M9. This is due to the tilting of the fire plume toward M10. FDS also shows a rapid increase in temperature followed by large oscillations and unexpected trends. These oscillations may be caused by oscillations in the flow through the door predicted by FDS. The temperature predicted at M8 by FDS is highest since the code predicts the fire plume to be pushed more toward the rear wall. For higher levels the effect of plume tilt is not evident.

The comparison of heat flux prediction with measured data poses several challenges. It is important that equivalent measures of flux are used in the comparison. The flux gauges in the experiments were cooled and maintained at a constant temperature (10 °C). The CFAST and FDS codes normally output the net heat flux on targets based on the target temperature. These fluxes were reformulated to give to the incident radiative

heat flux and the convective heat flux to a block with a constant temperature of 10 °C. Even with this reformulation, an exact comparison is not possible due to the inability to exactly measure the calculated values from the models. CFAST significantly over-predicts the heat flux with an uncertainty up to +215 %, whereas the uncertainties of the FDS predictions lie between 14 and 59 %. It should be noted that FDS predicts an increase in the heat flux toward the end of the transient phase, possibly due to the heat flux from the boundaries (walls etc) to the targets. This increase in heat flux toward the end of the transient phase is not observed in the measurements.

Corresponding to the overestimation of the heat flux in CFAST the calculated surface temperatures are also too high. The uncertainties in FDS are between 7 and 28 %.

The uncertainty of heat flux into the walls (WS3 and WS1) in the FDS calculation is about –45 %. The results for WS1 and WS3 are rather different, not observed in the experiment. The uncertainty of the surface temperature is about 26 %.

Code Results of FDS and CFAST for Test 3

The CFAST calculation crashed, so the results are not discussed here.

The measured HRR increases rapidly to 1500 kW in approx. 50 s, and then increases more gradually reaching 2700 kW at 850 s. The HRR increases rapidly from this point to 6000 kW at approx. 1050 s before being extinguished. Although the measured HRR has been input to the FDS code the FDS internal calculation of the HRR decreases after the initial rise at approx. 50 s. Although the HRR calculated by FDS starts to increase at about 200 s, it is less than the measured HRR. This may be due to the internal algorithm in FDS that inadvertently decreases the HRR for under-ventilated conditions.

FDS predicts the hot gas layer to develop and descend to about 0.6 m above the floor in approx. 90 s. The measured data shows the HGL interface starts to level to approx. 1.6 m (bottom of vent) at about 95 s. FDS predicts that a steady state level is reached more quickly after the initial drop compared to experiment. FDS under-predicts the steady state HGL interface height by 24 %.

The FDS prediction is similar to experimental observation until 840 s at which point FDS predicts a rapid reduction in O2 level to 0 %, while experimental observation indicates the O_2 level reaches 0 % more gradually at approx. 1095 s.

FDS predicts again that the flame is pushed significantly towards the rear wall by the flow of ambient air into the compartment through the door. Observations of the temperature fields show that FDS predicts that the flow through the door pulsates with a period of approx. 2 s. This pulsating behavior was noted during the experiments. The pulsating flow through the door provides sufficient oxygen to the fire and prevents it from being under-ventilated.

The plume temperature behavior is similar to Test 1 with an intermediate peak at about 50 s. These peaks are explained by plume development predicted by FDS. But the experimental measurements do not indicate this extensive movement of the fire plume. The measured data shows the plume to be fully developed at approx. 180 s after which the plume temperatures increase to approx. 1000 ^{O}C without any intermediate peaks.

The measured temperatures in the compartment at Level 1 for M7, M8, M9, and M10 show a rapid increase followed by a more gradual increase until the end of the transient phase. The temperature measured at M10 and M8 is higher than that measured at M7 and M9. This is due to the tilting of the fire plume toward the back wall. The plume temperature at M10 is higher than at M8 indicating that the tilt is more toward M10, but not as far as M8. FDS also shows a rapid increase in temperature followed by oscillations and a gradual increase in plume temperature, caused by flow oscillations at door opening.

The temperatures at higher levels (elevations) show a notable peak due to increased HRR at about 800 s. This was not simulated in the FDS calculations. The uncertainty was about 24 % to 33 %.

The uncertainty and the problem in comparing the heat flux and surface temperature for the material blocks are similar to those reported for Test 1. The uncertainty values are about 70 % for the heat flux and 35 % for the temperatures.

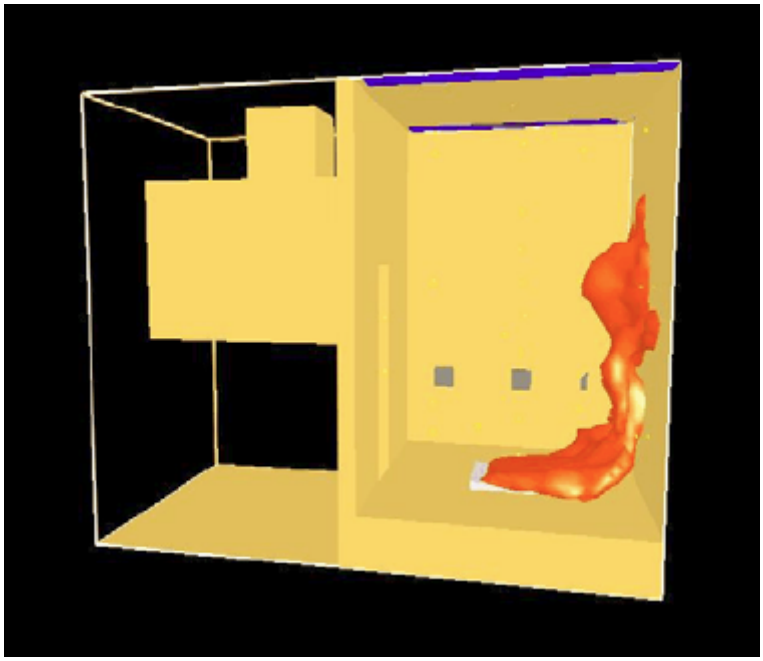

Fig. 5-5 View of flame sheet output from FDS - Test 1 (from Appendix C)

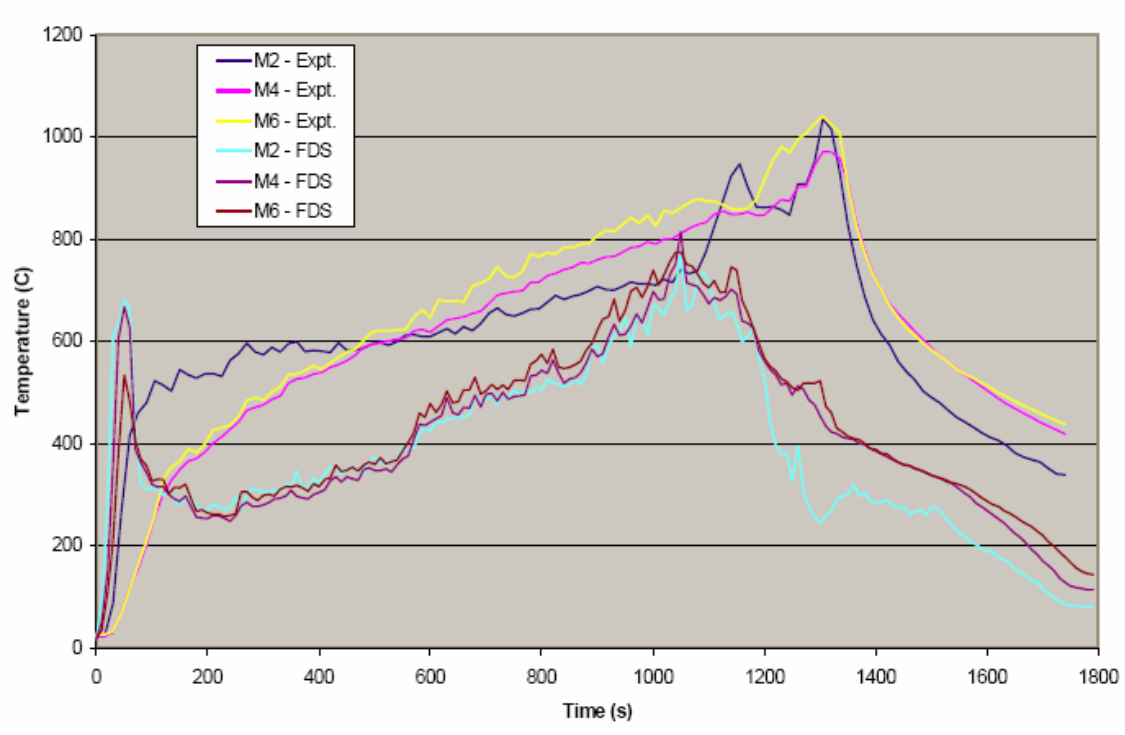

Fig. 5-6 Plume temperature (from Appendix C)

5.2.3 CFAST (Zone Model) and JASMINE (CFD CODE) Applied by S. Miles (BRE, UK)

Semi-blind calculations were made for Tests 1 and 3 with CFAST Version 3.1.6 and JASMINE Version 3.2.3. The main difference with the blind calculations was that the fuel mass loss measurement data were available, from which the fuel pyrolysis rates had been derived, allowing a more accurate fuel source term to be specified in the calculations. While most calculations had been conducted prior to the release of the other experimental measurements, some further calculations had then been conducted to explore various issues. The results of all these calculations are presented in detail in the Appendix B, and summarized below.

CFAST Code Description and Input Assumptions

CFAST is described above in paragraph 5.2.2. Version 3.1.6, without the FAST graphical user interface, was employed in all calculations. Additional information relevant to the application of CFAST to this Benchmark Exercise No. 4 is given below.

The dimensions of the OSKAR fire compartment and the doorway ventilation openings were modeled as in the problem specification. The thermal properties of the walls, floor and ceiling were included by creating new user defined materials with the required (concrete) properties. Conduction losses to the room walls, ceiling and floor were included, using the one-dimensional heat conduction sub-model.

The ventilation through the fan system was modeled using a mechanical exhaust vent. A limitation was that a fixed value for the volume flow rate was required, i.e. the time-dependent measured profile was not followed.

The fire was treated as a constrained fire (i.e. oxygen controlled) with an area 1 m^2, located at the center of the compartment at floor level. The fuel was modeled as kerosene, using a heat of combustion of 4.28 x 107 J kg^{-1}. The time-dependent pyrolysis rate was set to that measured experimentally for the initial calculations, and was then adjusted in subsequent parametric calculations. For Test 1 two calculations were conducted using a fixed fuel pyrolysis rate of 0.039 kg s^{-1}, based upon published engineering information. This provided a comparison with the blind JASMINE calculations where the same pyrolysis specification had been used.

In all calculations a two-layer gas assumption was assumed inside the room, but the 'ceiling jet' option was inactive. The radiative fraction was set to 0.3 in most calculations (0.6 was also investigated). While in most calculations the lower oxygen limit (LOL) was set to 0 %, it was adjusted to 10 % in some parametric calculations.

A required approximation in CFAST is that targets are treated as rectangular slabs. Furthermore, heat conduction is modeled in one-dimension, i.e. in the direction of the surface normal. The surface temperature of the three material probes was calculated, with the target surface normal directed into the compartment (x-direction). The response of the barrel target was not included in the CFAST calculations.

JASMINE Code Description and Input Assumptions

JASMINE is described above in 5.1.2. It was applied as described for the blind calculations with the main exception that the measured, transient fuel pyrolysis (or a fixed fraction thereof) was used to specify the fuel source term. In addition the effect of employing the discrete transfer radiation model was investigated. The influence of applying an oxygen concentration limiter on the combustion process was also investigated for Test 3. Furthermore, for Test 3 the consequence of reducing the imposed exhaust flow rate at the mechanical (FUCHS) duct by 50 % was explored.

CFAST Code Results

Appendix B presents details of the scenarios, for which converged CFAST simulations were achieved. Other parametric combinations were attempted for which a converged solution was not achieved, which is perhaps a consequence of the complex physics of the two experiments. The main observations and findings are summarized below:

For Test 1, the choice of a radiative fraction of 0.6, coupled to the measured fuel pyrolysis rate, resulted in an upper gas layer temperature reasonably close to that measured. The layer height predictions, with the layer dropping to approximately 1 m, were perhaps less representative of the actual experiment. For Test 3, the upper gas layer temperature predictions were less encouraging, with an over-prediction in all parametric calculations undertaken. This was observed, in particular, in the earlier stage of the experiment. It should be noted that radiative fractions higher than 0.3, and up to 0.6, were attempted but that converged solutions were not then obtained. Fig. 5-7 (from

Appendix B) illustrates gas temperature calculations for Test 1 using the measured and fixed (0.039 kg s^{-1}) fuel pyrolysis specifications.

For Test 1, the calculated oxygen concentration appears reasonable. For Test 3, the calculated oxygen concentration, while dropping to zero, does so much more quickly than suggested by the experimental measurement. This is most likely coupled to the fact that too much burning, and associated gas temperature rise, was predicted in the calculation compared to the actual experiment. For Test 3, where the oxygen concentration dropped to zero, whether the lower oxygen limit was set to 10 % or zero had very little influence on the calculated values.

Surface temperatures and incident fluxes for Test 1 were reasonable for the two calculations using a fixed fuel pyrolysis rate of 0.039 kg s^{-1}, but for the calculation using the measured pyrolysis rate they were notable higher than the measured values. Fig. 5-8 (from Appendix B) illustrates wall surface temperature calculations for Test 1 using the measured and fixed (0.039 kg s^{-1}) fuel pyrolysis specifications.

Test 3 calculations for wall surface temperature were reasonably close to the experimental measurements for all the parametric runs. Material probe surface temperatures and the heat flux densities were, however, over-predicted compared to measurement in all parametric runs. This may be due, in part at least, to three-dimensional geometry effects that cannot be captured using a zone model such as CFAST.

The limitation that the flow rate through the mechanical exhaust was fixed in value, and did not vary according to the measurement data, probably had only a small consequence.

Measured pyrolysis rate

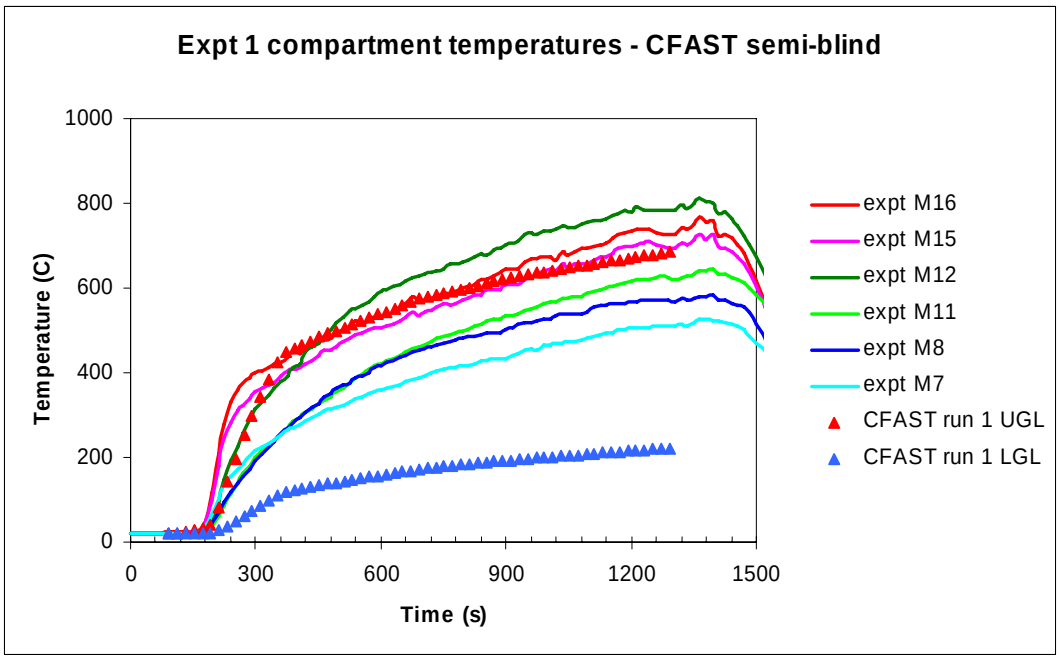

Pyrolysis rate = 0.039 kg s^{-1}

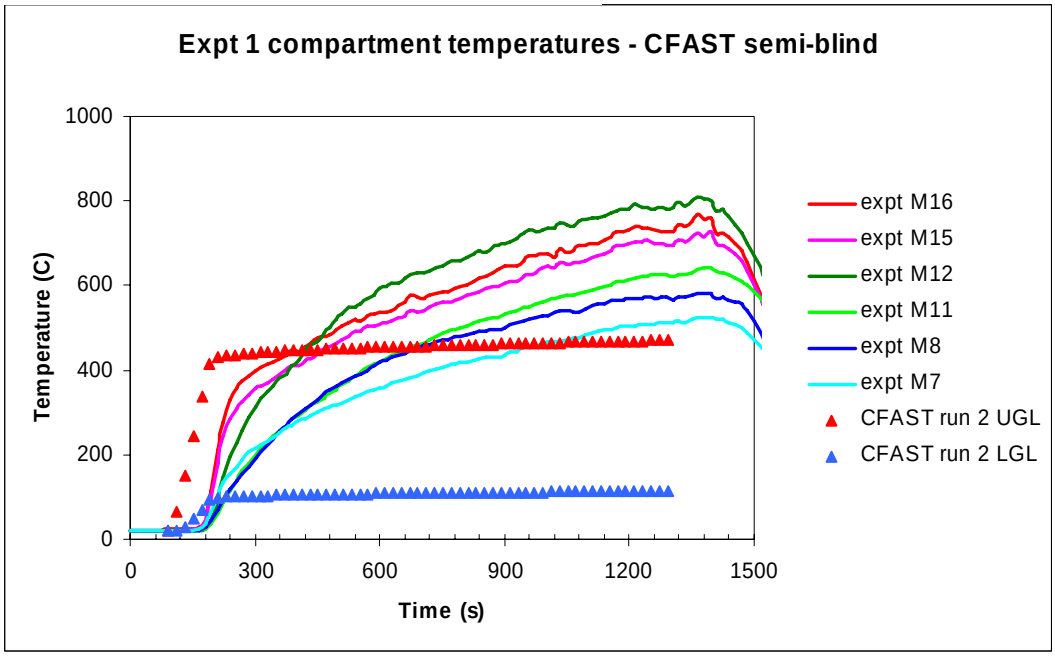

Fig. 5-7 Measured and predicted (open) gas temperatures for Test 1 (from Appendix B)

Measured pyrolysis rate

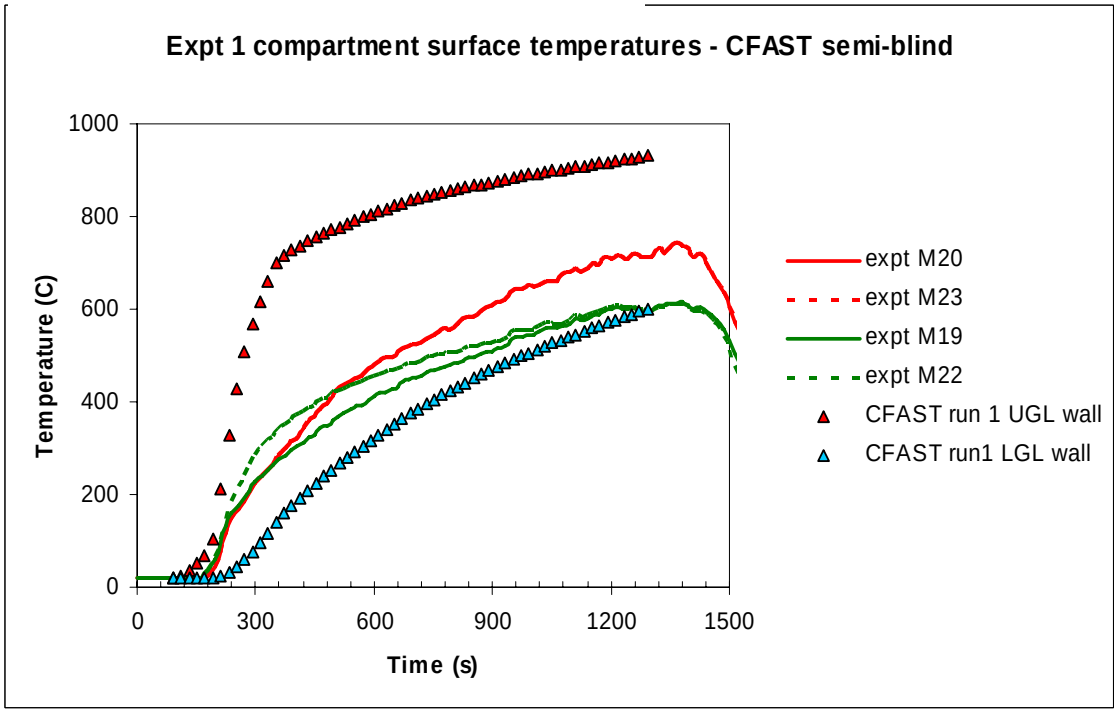

Pyrolysis rate = 0.039 kg s^{-1}

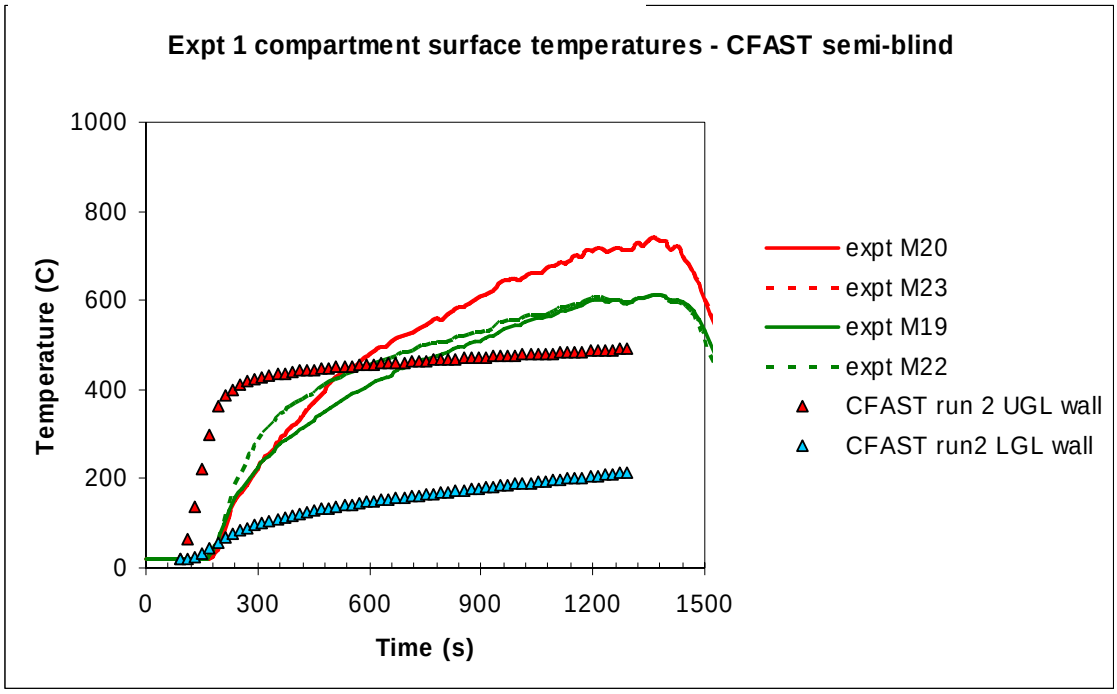

Fig. 5-8 Measured and predicted (open) wall surface temperatures for Test 1 (from Appendix B)

JASMINE Code Results

Appendix B presents details of the JASMINE calculations. These were conducted for the first 18 to 20 minutes of both experiments, after which time convergence problems were encountered. The main observations and findings from the JASMINE calculations are summarized below:

The calculations for Test 1, using the fuel pyrolysis rate derived from the experimental measurements (actually 75% of the measured pyrolysis rate - to account for radiation losses due to soot), were judged encouraging. The main features of the gas temperatures, doorway flows and radiation fluxes were captured quite well. The compartment temperature was arguably calculated to rise too quickly. Fig. 5-9 (from the Appendix B) compares gas temperature and doorway velocity predictions and calculations for Test 1.

While for Test 3 the calculations were generally considered quite reasonable, there was however greater discrepancy with the measured data compared to Test 1. In particular, the direction of the wall vent flow was predicted to be predominantly into the compartment compared to the actual experiment which exhibited a more pronounced two-way flow. Simulations using 75 % of the measured fuel pyrolysis rate generated, on average, results closer to the measurements compared to using the full pyrolysis rate or 50 % of the rate. Recall here that the justification for adjusting the pyrolysis rate is to account, in the overall energy balance, the heat lost from radiating soot particulates (not modeled in the JASMINE calculations), i.e. akin to the radiative fraction in a zone model such as CFAST.

It had been suggested that the level of the imposed exhaust in Test 3 might be the primary reason for the JASMINE calculations indicating less outflow from the wall vent compared to that suggested by the experimental measurements. However, while in a parametric simulation to investigate the effect of reducing the imposed exhaust rate by 50% the wall vent flow was then marginally more bi-directional, the overall effect was to reduce the level of agreement between predicted and measured temperatures and fluxes.

For both experiments the calculated flux densities at WS2 and WS3 were judged overall to be, qualitatively at least, quite reasonable. However, as illustrated in Fig. **5-10** (from Appendix B), the predicted flux density at WS4 (towards the front of the com-

partment) was significantly lower than that measured. This was initially attributed perhaps to the use of the six-flux radiation model, which misses some of the important angular radiant intensity information. However, further simulations using the more accurate discrete transfer also exhibited the same discrepancy in flux density at WS4.

There was no significant influence on the calculated variables when invoking the additional oxygen limitation mechanism on the combustion sub-model. It is perhaps not too surprising that little difference was observed due to the high compartment temperatures, as even with the additional oxygen limitation mechanism combustion still occurs if the local gas temperature is sufficiently high.

The energy 'budget' has been calculated in the JASMINE simulations, and is quite informative. Fig. **5-11** (from Appendix B) shows the energy budget for one of the Test 3 calculations, and illustrates that both heat losses to the solid boundaries and heat convected through the mechanical ventilation duct are significant.

A general note from the JASMINE work is that the presence of soot, and the subsequent radiation absorption and emission, may have an important bearing on the gas temperatures predicted. This in turn influences the radiation fluxes significantly (bearing in mind the T^4 dependency on radiant intensity), which then has a major influence on the conduction into the walls and targets and their temperature rise.

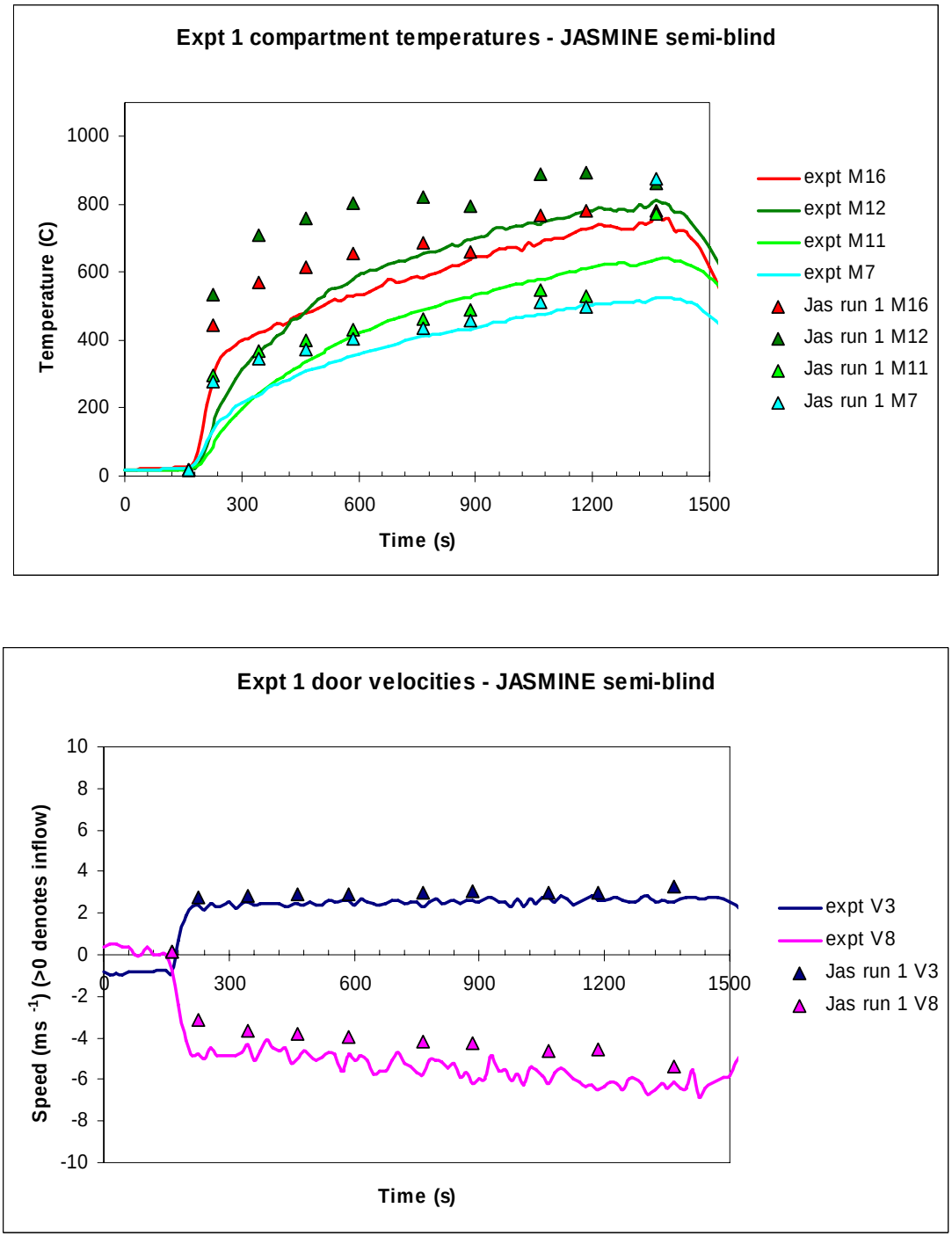

Fig. 5-9 Measured and predicted gas temperatures and door velocities for Test 1 (from Appendix B)

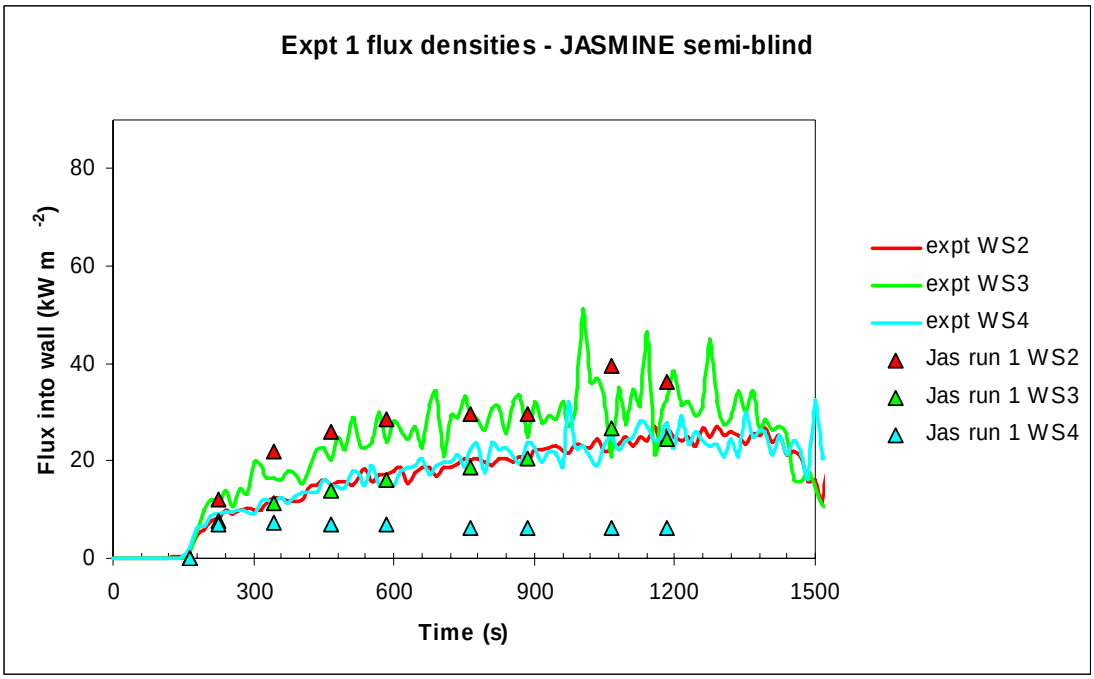

Fig. 5-10 Measured and predicted flux densities for Test 1 (from Appendix B)

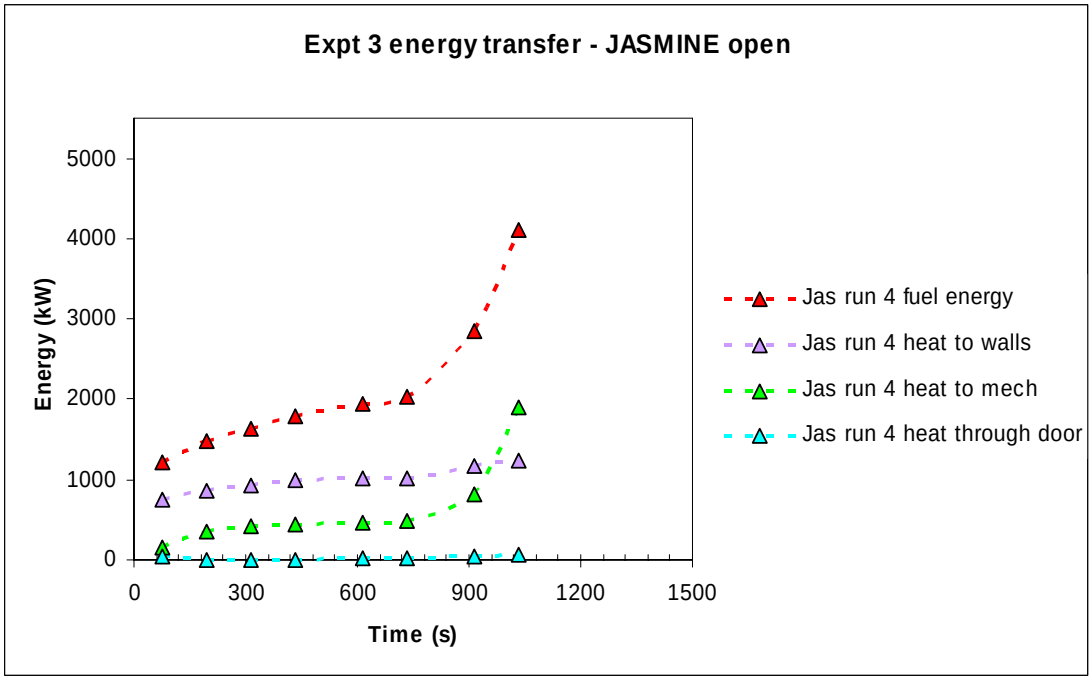

Fig. 5-11 'Energy budget' for a Test 3 simulation (from Appendix B)

5.3 Open Calculations

5.3.1 FATE (Zone Model) Applied by T. Elicson (Fauske & Associates LLC, USA)

The purpose of this benchmark exercise is to perform an integral validation of the FATE^{TM} 2.0 Computer Code fire models for use in nuclear power plants, fuel cycle facilities, and DOE (*D*epartment *o*f *E*nergy) material handling facilities. Calculations presented below have been performed with FATE Version 2.14 /PLY 04/.

FATE Code Description and Input Assumptions

The FATE^{TM} 2.0 Computer Code /PLY 04/ is used for this analysis. FATE, previously named HADCRT, is the successor code to the HADCRT computer program used in previous ICFMP activities. Specifically, FATE Version 2.14 is used in the following calculations. FATE Version 2.14 contains upgrades to address fire modeling issues. FATE stands for Facility Flow, Aerosol, Thermal, and Explosion Model, for PCs and workstations. FATE 2.0 is used for design, off-normal, and accident analyses of nuclear and chemical facilities. General capabilities of FATE 2.0 include: Fire model, multi-compartment thermodynamics including condensing species, arbitrary topology of flow paths, simulation of aerosol behavior including condensation, re-suspension, one-dimensional heat transfer through multi-layer slab on cylindrical heat sinks, combustion, thermal radiation networks, nuclear fuel and sludge models including chemical reactions. A more detailed description is given in Appendix D.

The fire compartment is simulated with a single region including 14 heat sinks. The wall heat sinks are modeled as “strips” that circumscribe the room perimeter and extend vertically between the indicated elevations. The advantage to this approach is input and computational simplicity, while the limitation is that a single surface temperature is reported for the North, East, South, and West walls at each elevation.

The doorway and the ventilation system are simulated by junctions and allow for buoyancy driven counter current flow. In addition, in flows through the doorway are assumed to be equally distributed between the smoky and lower gas layers, and, for Test 3, air in the lower 1.6 m of the room is assumed to be available for entrainment and consumption in the fire.

Two targets are included in the FATE model. The first target is the concrete material probe with lower corner coordinates of x = 0.0 m, y = 1.9 m, and z = 1.7 m. The probe is modeled with a single vertical rectangular heat sink, heat sink 16, with dimensions 0.3 m x 0.3 m x 0.1 m thick. This heat sink is divided into 20 nodes through the thickness to allow one-dimensional conduction through the probe. In addition, the heat sink is included in the radiation heat transfer network; therefore the heat sink surface is subjected to convective and radiative boundary conditions. The second target is the more complex barrel-type waste container. This target is divided azimuthally into four segments. The first three segments cover the cylinder half facing the fire, while the fourth segment is the entire back half side of the barrel facing away from the fire. Each segment height is equal to the height of the barrel. In addition, each of the four segments is represented as a composite heat sink consisting of three layers: an outer metal layer (5 radial nodes), a middle concrete layer (20 radial nodes), and an inner styrene granulate fill layer (20 radial nodes). The tinplate that makes up the inner barrel is defined as a contact resistance between the concrete and styrene. Radial conduction is allowed between the layers, while azimuthal conduction is modeled only in the outer most steel layer. The outer metal surfaces are also included in the radiation heat transfer network.

The given HHR were adjusted based on a 5-point moving average of the raw data and a delay based on the fuel ignition time. The fuel ignition time is taken as the time at which the heat sink temperatures begin to increase (160 s for Test 1 and 15 s for Test 3). FATE input also requires specification of the combustion products yield. The combustion yields used for input are based on real yields for high molecular weight/temperature hydrocarbons for well ventilated flaming fires.

Code Results

Test 1 is characterized by a kerosene fire with a steady state power in the range of 3 to 3.5 MW, peak fan vent flows of 2 m^3/sec, a doorway opening of 0.7 m by 3.0 m, and a multi-layer target in close proximity to the fire source. These conditions result in a flame that extends well into the smoky region and significant variation in temperatures across the x-y plane. As with other benchmark tests, the Benchmark Exercise No. 4 demonstrates that the two most influential aspects of the input are the fire power and the room ventilation behavior. To follow the measured ventilation flow rates, which are decreasing at the end of the experiment, the flow area as been adjusted from 0.176 m^2 to 0.0353 m^2.

The measured flows were estimated by reducing the reported velocities from doorway velocity probes V3 though V8. A volumetric flow rate was assigned to each measurement by taking the product of the reported velocity and 1/6 of the door area (0.35 m^2). The net volumetric flow was then taken as the sum of the individual volumetric flows and is assumed to represent the unidirectional flow rate. Even though the doorway area input to FATE is computed as 100 % of the geometric areas with no reductions taken for entrance and exit losses, the FATE unidirectional flow rate calculation under-predicts the estimated doorway flow rates.

For this particular geometry – a high powered fire in a relatively small and under-ventilated compartment – the measured gas concentration may be a better measure of room conditions rather than the smoky layer height. Reasonable agreement is indicated between the calculated and measured gas concentrations.

The temperature variation inside the fire compartment along the x-y plane is promoted by the room geometry in which the fire essentially blocks free inflow from the door (fire pan width is larger than the narrow doorway width). The FATE smoky layer calculations provide reasonable estimates of the average gas temperatures.

The peak wall temperatures in the back of the room are consistent with the peak gas temperatures, while the side wall temperatures are about 100 K lower. This may be influenced by air circulation which may be diminished toward the back of the room. The FATE wall strip heat sink model presents an average temperature of all four side walls at a particular elevation; therefore it is not surprising that peak wall temperatures are not predicted. The under-prediction of wall temperatures at upper elevations is a result of the overall lower predicted smoky layer gas temperature.

The container surface temperature is reasonably predicted, while the concrete probe temperatures are somewhat under-estimated. The under-estimation of the concrete probe temperature occurs because the probe remains in the lower gas layer in the FATE calculation, while test data indicates the probe is submerged in the smoky layer. Sensitivity calculations for which the probe is submerged in the smoky layer show good agreement with the test data. The significant heat up of the can surface, even though the waste can is located in the lower gas layer, is an indication of the radiative power received from the fire.

To perform a bounding analysis for nuclear power plant applications, the many uncertainties associated with a room fire must be addressed. Uncertainties identified in this benchmark include the fire power, ventilation flows, and air mixing. Perhaps the most straightforward approach to addressing uncertainties to obtain a bounding assessment appropriate for nuclear power plant applications is to increase the fire power. Therefore in a sensitivity calculation the HRR has been increased by 40 %, leading to a better temperature prediction.

The reduction of the door opening cross section leads to an under-ventilated fire. A key assumption used in modeling this case is the length along which oxygen is entrained and consumed in the fire. Finally, following guidance from other fire benchmark exercises, air flowing in through the doorway is assumed to be equally distributed between the smoky and lower gas layers.

The gas concentration is a better measure of conditions in the smoky layer. The measured smoky layer height is based on average of thermocouple readings at 4 separate elevations, with the lowest elevation at 1.5 m. Thus, the reported layer height does not provide indication of smoky layer heights below 1.5 m.

The gas and heat sink temperatures were found to be closely linked to the fire power. For this reason, adjustments were made to the reported fuel burn rate to conform to the times at which test data indicated the plume gas temperatures began to increase and decrease. Overall, reasonable agreement is obtained and no attempt was made to increase the fire power from its nominal value to provide a bounding estimate of the gas temperatures.

Calculation of the concrete probe and waste can temperatures as well as the concrete wall surface temperatures proved to be sensitive to whether or not each heat sink was submerged in the smoky layer.

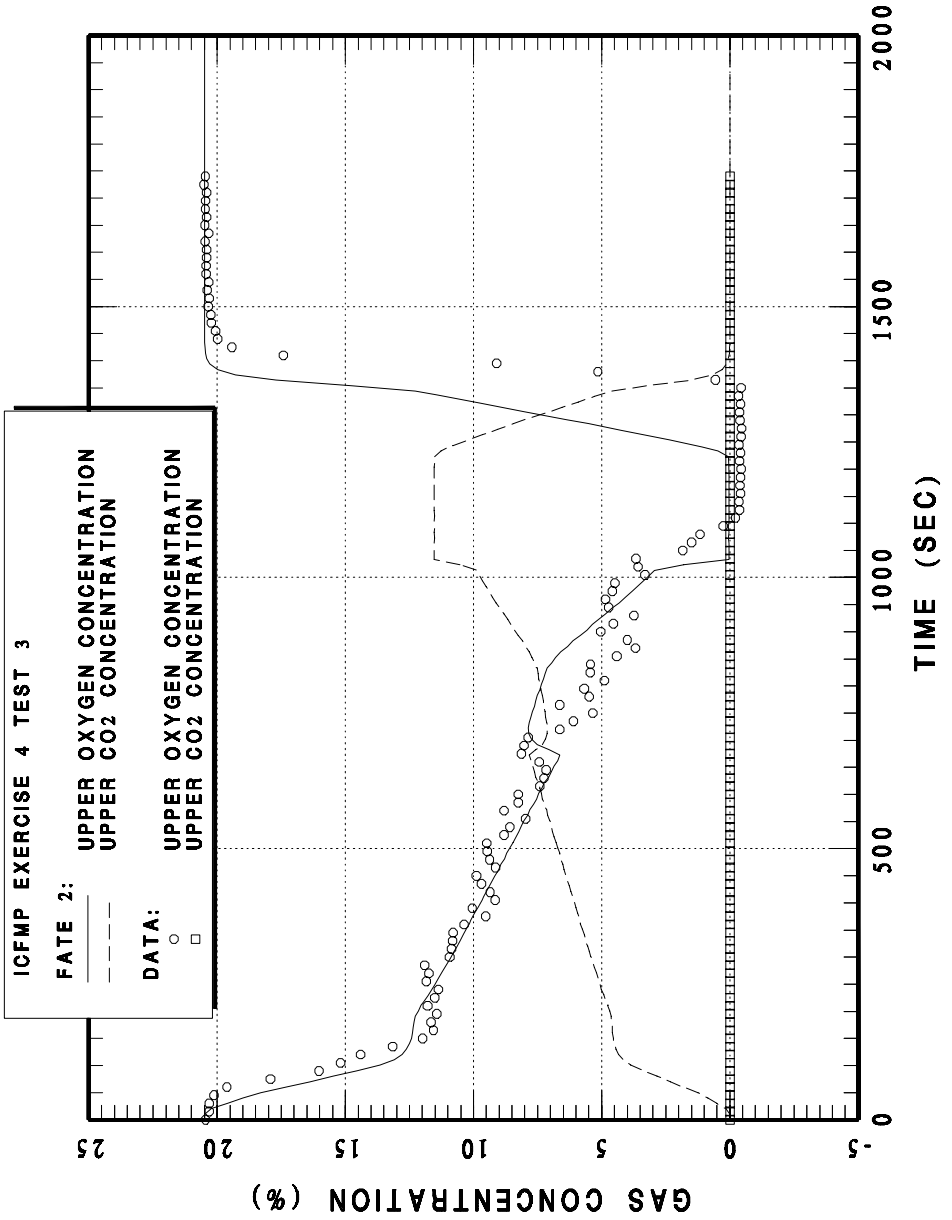

Fig. 5-12 Benchmark Exercise No. 4, Test 3 smoky layer gas concentrations (from Appendix C)

5.3.2 FLAMME-S (Zone Model) Applied by L. Rigollet (IRSN, France)

Tests 1 and 3 have been simulated with the two-zone model code FLAMME-S, Version.2.3.2 /BOU 02/, developed by IRSN. In this context, a remark must be made concerning the fact that the studied cases are outside the validation domain of FLAMME-S, specifically in respect to the two following conditions:

- The ratio of the pool surface area to the floor area of the facility is less than 5 %,
- The ratio of the heat release rate to the volume of the facility is less than 5 kWm^{-3}.

FLAMME-S Code Description and Input Assumptions

The FLAMME-S code is similar to the CFAST code described above. The fuel pyrolysis rate is a pre-defined input, and the burning in the compartment is then modeled to generate heat release and allow species concentrations to be calculated. FLAMME-S is a two-zone model, whereby each compartment is divided into a hot gas upper layer and a cold gas lower layer. In the presence of fire, the sub-model transports heat and mass from the lower to the upper layer making use of an empirical correlation. A notable difference in this context is that FLAMME-S uses the Heskestad correlation for the plume flow, whereas the McCaffrey correlation is utilized in CFAST. Flows through vents and doorways are determined in both codes from correlations derived from the Bernoulli equation. Radiation heat transfer between the fire plume, upper and lower layers, and the compartment boundaries is also included.

The side walls of the fire compartment are constructed from 25 cm of light concrete and 5 cm of insulation. The ceiling is made of a 25 cm concrete layer and a 5 cm insulation layer. For the floor, only 30 cm of concrete are taken into account: the aerated concrete implemented in the experiments in order to protect the mass loss measurement is not modeled. Two material probes, concrete and aerated concrete, are modeled.

In Test 1, the door is completely opened, with a free cross section of 0.7 m x 3 m. In the Test 3, the opening is partly closed, with a free cross section of 0.7 m x 1 m. The fan system, which is not used in the experiments, and the hood above the open front door are not modeled.

The energy released by radiation represents 32 % of the total heat released. A complete combustion reaction is assumed.

Two types of calculations have been performed: In a first step a constant pyrolysis rate has been assumed (Test 1: 65 g/m^{2}s; Test 3: 50 g/m^{2}s) and in a second step the measured rate was used. The LOL value was then reduced from 11.5 % to 0 %.

FLAMME-S Code Results

The layer height calculated by FLAMME-S is lower than that determined from the experimental data. The experimental interface height is determined from thermocouples located at three elevations: 1.5 m, 3.35 m and 5.2 m. Thus, in the experiment, the layer height never decreases under the elevation of the first thermocouple, i.e. 1.5 m. Tourniaire and al. /TOU 00/ have shown that the data reduction method is weakly dependant on the number of thermocouples except in the case of three thermocouples where the interface height does not reach the floor.

The gas temperatures calculated for the upper layer are in good agreement with the experimental results of Test 1. As the layer height calculated by the code is lower than the experimental interface, the calculated temperature of the lower layer is colder than the gas temperatures measured.

The oxygen concentrations calculated with the code in the upper layer are lower than those measured in the experiment; however, the comparison is difficult because the sensor GA2-O2 seems to be saturated.

In the experiment, total heat fluxes were measured at one elevation, i.e. 1.7 m. At the upper layer, the FLAMME-S code calculates slightly lower total heat fluxes.

The wall temperatures are not compared, because the FLAMME-S code calculates an average temperature for the first mesh of a wall and thus cannot be compared with a surface temperature measured experimentally.

However, the temperatures of two material probes (concrete and aerated concrete) are compared. Experimentally, the sensors seem to be reversed: M 28 and M 26 for the aerated concrete slab and M 32 and M 30 for the concrete slab. The calculated results are in good agreement with the measurements, if the four sensors mentioned above are indeed reversed.

In the first calculation for Test 3, using the lower oxygen limit (LOL) of 11.5 % rapidly leads to the fire extinguishing by itself, two minutes after the beginning. For the open calculations, even if the experimental pyrolysis rate is imposed in the data file, the code under-estimates the heat release rate: the pyrolysis rate is limited by the code, because the quantity of oxygen involved in the reactive zone is not sufficient for the combustion reaction. Therefore, it should be noted that the comparison of predictions with measurements for all other parameters cannot be expected to be necessarily close since the heat release rate is underestimated. During Test 3, a phenomenon seems to occur which is not modeled by the code. While the oxygen concentration measured in the experiment reached 0 %, the gas temperatures inside the compartment increased up to about 900 °C and a flame was observed at the opening. This experiment presents characteristics similar to those of ghosting flames described by various authors.

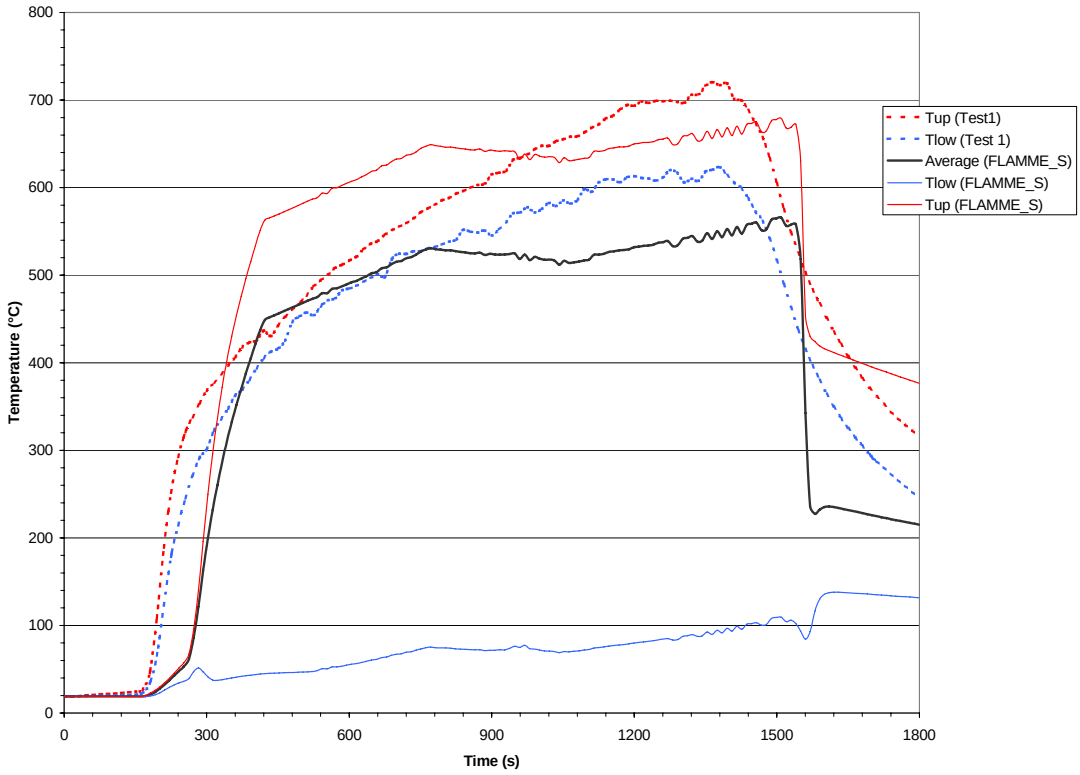

Fig. 5-13 Gas temperature in the compartment - open calculations (from Appendix D)

5.3.3 CFX (CFD Code) Applied by M. Heitsch (GRS, Germany)

Calculations with the CFD code CFX 5.7 have been carried out for Benchmark Exercise No.4 within the frame of the International Collaborative to Evaluate Fire Models for NPP Applications (ICFMP). Version 5 of the CFX family /CFX 04/ represents a completely new code structure compared with previous versions and offers new features.

CFX Code Description and Input Assumptions

CFX /CFX 04/ is a commercial Computational Fluid Dynamics (CFD) multi-purpose code. The latest generation is named version 5. The current release is 5.7. The main features which demonstrate the progress since the previous version 4 are the coupled solver and the ability to handle structured and unstructured meshes. CFX-5 is capable of modeling steady-state and transient flows, laminar and turbulent flows, subsonic, transonic and supersonic flows, heat transfer and thermal radiation, buoyancy, non-Newtonian flows, transport of non-reacting scalar components, multiphase flows, combustion, flows in multiple frames of reference, and particle tracking.

Thanks to the regular geometry of the test arrangement, the computational mesh was decided to be built exclusively with structured cells. The mesh has a total of 115700 cells in the fluid domain of the modeled test volume. Another 2548 cells are in the barrel target (inner and outer part) to describe heat conduction. It reveals that the horizontal resolution chosen may not be fine enough.

The gas mixture of air, fuel (kerosene) and combustion products is modeled by tracking the individual species, which are kerosene, oxygen, nitrogen, carbon-dioxide and steam. Soot is also created according to the Magnusson soot model implemented in CFX. In this model, a number of constants are used, which were not further investigated in this exercise. Nitrogen represents a background fluid, not participating in any reaction. The chemical reaction itself is represented by a single-step mixing controlled reaction within the Eddy Dissipation model. A complete combustion is assumed.

A predefined share of the reaction heat (40 %) is emitted from the surface of the fire pan as radiation flux and distributed by the P1 radiation model in CFX. This radiation model solves an extra transport equation and assumes direction independent radiation transport. It allows heating of the fluid due to radiation from a boundary (here the fuel pan). The radiation is not release from volume cells where the reaction takes place.

Flows through the venting (fan) system “FUCHS” and the hood are specified by flow velocities given in the specification of the tests.

A simplification was made concerning the heat flow into the surrounding walls. These walls are not included in the mesh and hence the heat flow calculated at constant wall temperature. This overestimates the removal of energy from the fluid.

CFX Code Results

The history of the fuel release corresponds exactly to the fuel consumption curve from the experiment. A total amount of 80.7 kg kerosene was added. The temperature distribution is affected by the inflow of cold air through the door and the hottest part of the gas plume is pushed towards the back of the room. The temperatures in the front location show a good correspondence to the measurements up to about 400 s but then change little up to the time when the fire intensity passes its peak. In the simulation this is expressed by a slight reduction of gas temperatures. Then the fire intensity remains constant for a long while and reduces to zero after about 1400 s. The measured temperatures however increase continuously up to the end of fuel combustion. A similar tendency can be observed for temperatures in the back part of the facility. Here, however, measurement and simulation show different trends. During the test the highest temperature was observed at the bottom of the room and decreased towards the ceiling. The simulation predicts the opposite. This was true for all columns of thermocouples.

The measured data for oxygen at GA1 are captured quite well. Only at the beginning and the end of the fire scenario are some differences seen. This may be related to the kerosene release curve, which was specified as an input. The measured CO_2 mole fraction is lower than the values predicted by CFX. This may be due to the fact that the modeled chemical reaction does not include any production of CO and assumes only CO_2 and H_2O.

In the door opening a number of flow sensors recorded the flow speeds in a vertical line. In the upper locations the predictions compare quite well with the measurement, in the lower probe locations however the flow is underestimated.

The barrel inside the fire compartment is built as a cylindrical double vessel container. The inner section was filled by a type of granulate and the outer cylinder by concrete.

In the computer model these two materials have been included but not the vessel walls. The mesh was probably not sufficiently fine to model the temperature rise accurately, and this was over-estimated.

This measured HRR history for Test 3 was input to the code according to the test description. The sudden stopping of kerosene release after about 1100 s can also be identified in the temperature plots and causes some disagreement after that time. The gas with the highest temperatures is pushed towards the back wall. They show a similar good correspondence with the measured data up to the moment the fire is stopped. There might also be some thermal inertia of the thermocouples including continuing radiative heat flux from walls, which causes a slower decrease than predicted by the simulation.

The agreement for oxygen concentration at GA1 is as good as for Test 1.

For the lower velocity probe at the door opening the comparison is very good. At the upper location, however, negative values (inflow) were measured but were not predicted. At the time of about 800 s there is only flow into the test compartment through the door.

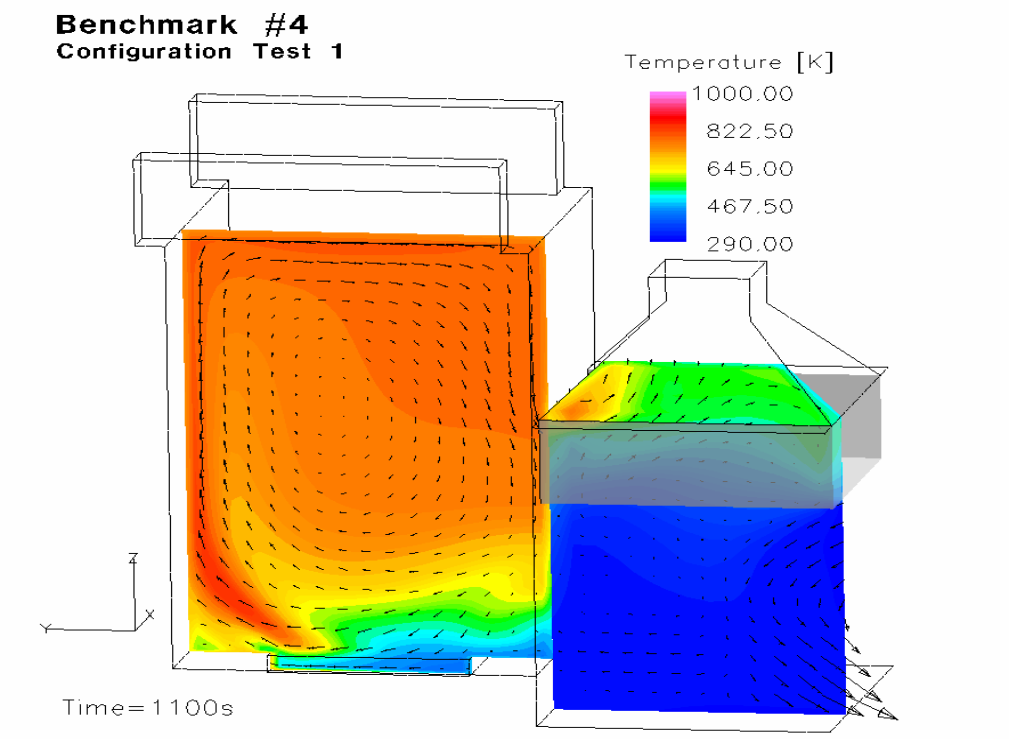

Fig. 5-14 Vertical temperature distribution at a plane x = 0.95 m (from Appendix E)

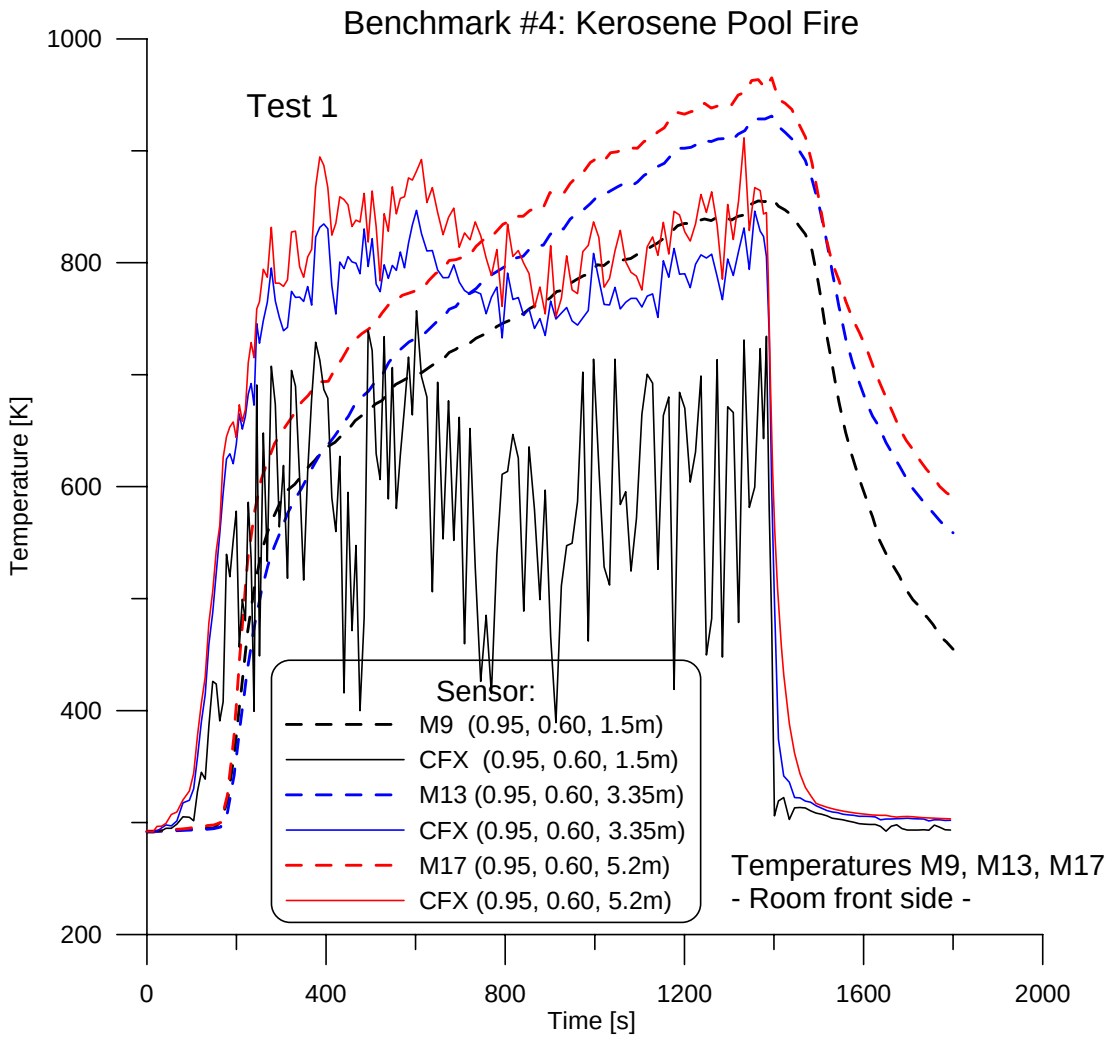

Fig. 5-15 Comparison of selected gas temperatures close to the front of the test facility for Test 1 (from Appendix E)

5.3.4 FDS (CFD Code) Applied by W. Brücher (GRS, Germany)

As an extension to earlier calculations with FDS2 and FDS3 within a project outside the ICFMP, open calculations have now been performed with FDS3 and FDS4 to investigate the influence of different FDS versions and the differences due to the chosen grid.

FDS Code Description and Input Assumptions

The FDS code has already been described in chapter 5.2.1. One major difference between FDS3 and FDS4, with some influence on the results is a different default LOL condition, where the ‘no burn’ area in under-ventilated conditions is extended to higher temperatures.

FDS Code Results

Actual heat release rates differ from the heat release rate obtained from the prescribed pool mass loss data. Fig. 5-16 shows all heat release rates calculated with different model configurations. Depending on the model configuration not all released fuel is burnt immediately or in some cases it is only partly burnt. The mass release peak in particular is not accompanied by an equivalent strong increase of the heat release due to the under-ventilated conditions in Test 3.

Both calculations with FDS3 use exactly the same set of parameters except for the grid cell size. Temperatures are generally slightly underestimated by the model for most of the time (Fig. 5-17 to Fig. 5-19). The temperature peak appears too early compared to the measurements, which is partly due to the mass loss rate of the benchmark specification. A different (smoothed) interpolation of the questionable weight scale data in former calculations resulted in a better agreement of the temperature development. However, peak temperatures are also underestimated in that case. No obvious increase in the simulation quality of the temperatures is found, although this effect would be expected as a consequence of a better resolution of the flame area. A possible explanation for the slightly worse overall performance with the fine grid may be the missing extension of the fine grid to the whole door area which is crucial for the development of the fire inside. The calculated fine grid gas flow into the compartment is higher than the measured one, resulting in lower gas temperatures inside the compartment. This effect is also found in the calculation for oxygen concentration inside the fire compartment, which is over-estimated.

Due to the modification of the default temperature dependent LOL limit in FDS4, lower heat releases are found in FDS4 compared to FDS3, also including lower gas temperatures and surface heat fluxes. The default LOL definition seems to be a major problem in under-ventilated conditions for both model versions.

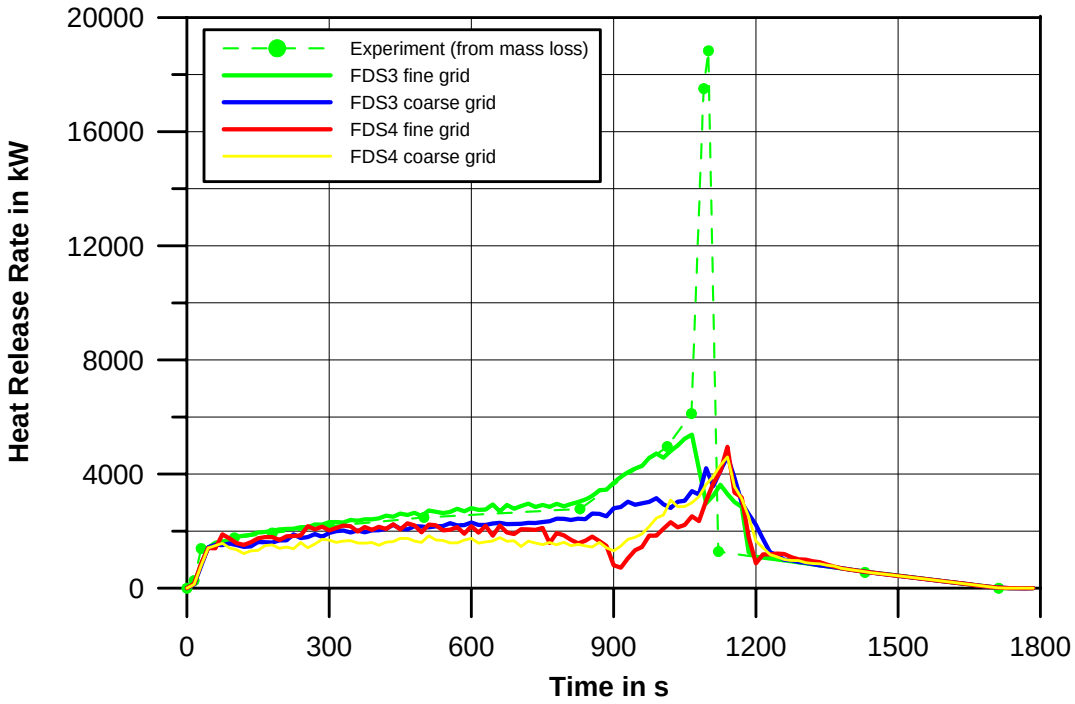

Fig. 5-16 Heat release rates of all FDS3 and FDS 4 calculations for Test 3 (from Appendix G)

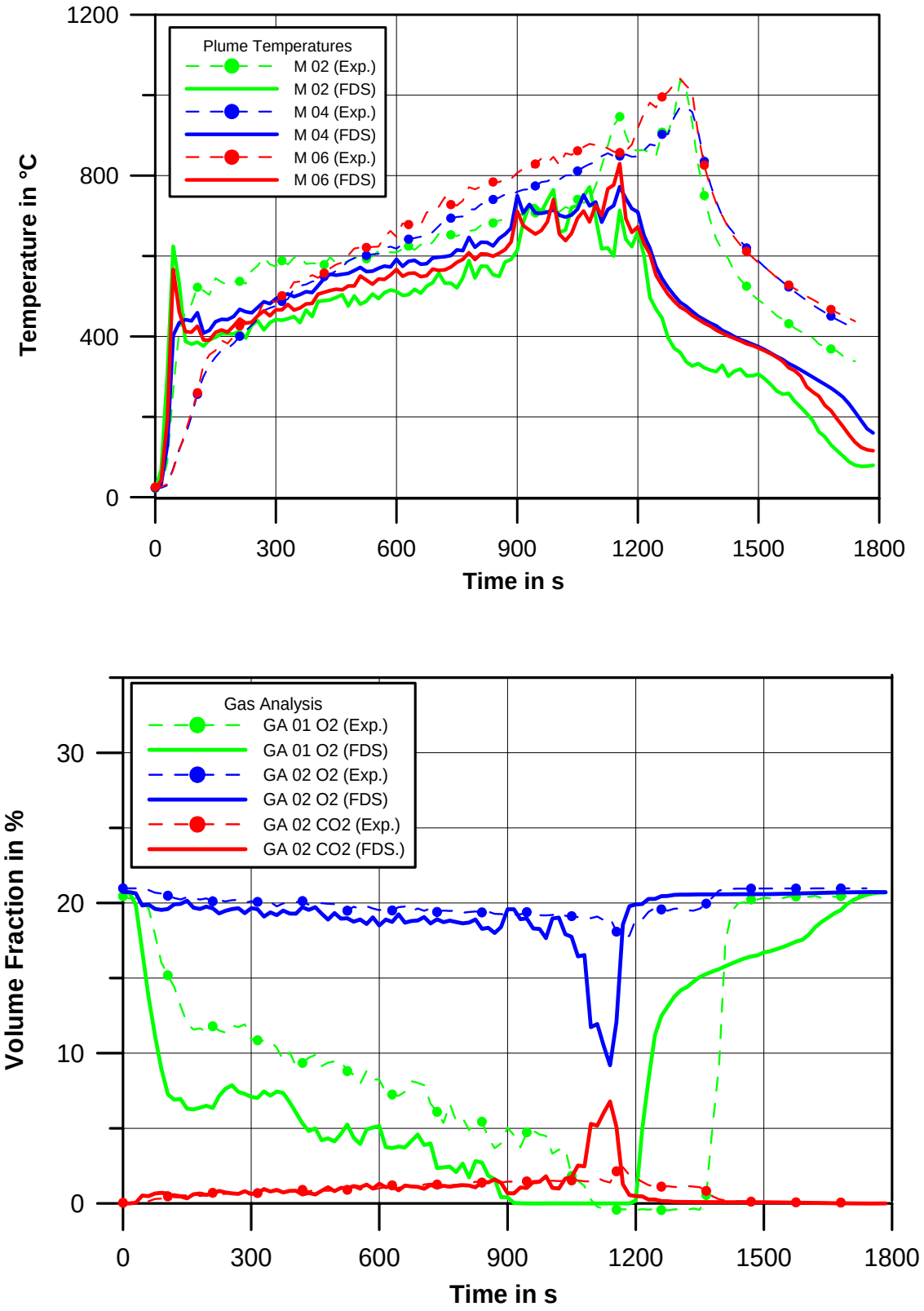

Fig. 5-17 Comparison of FDS results (FDS3 coarse grid; from Appendix G)

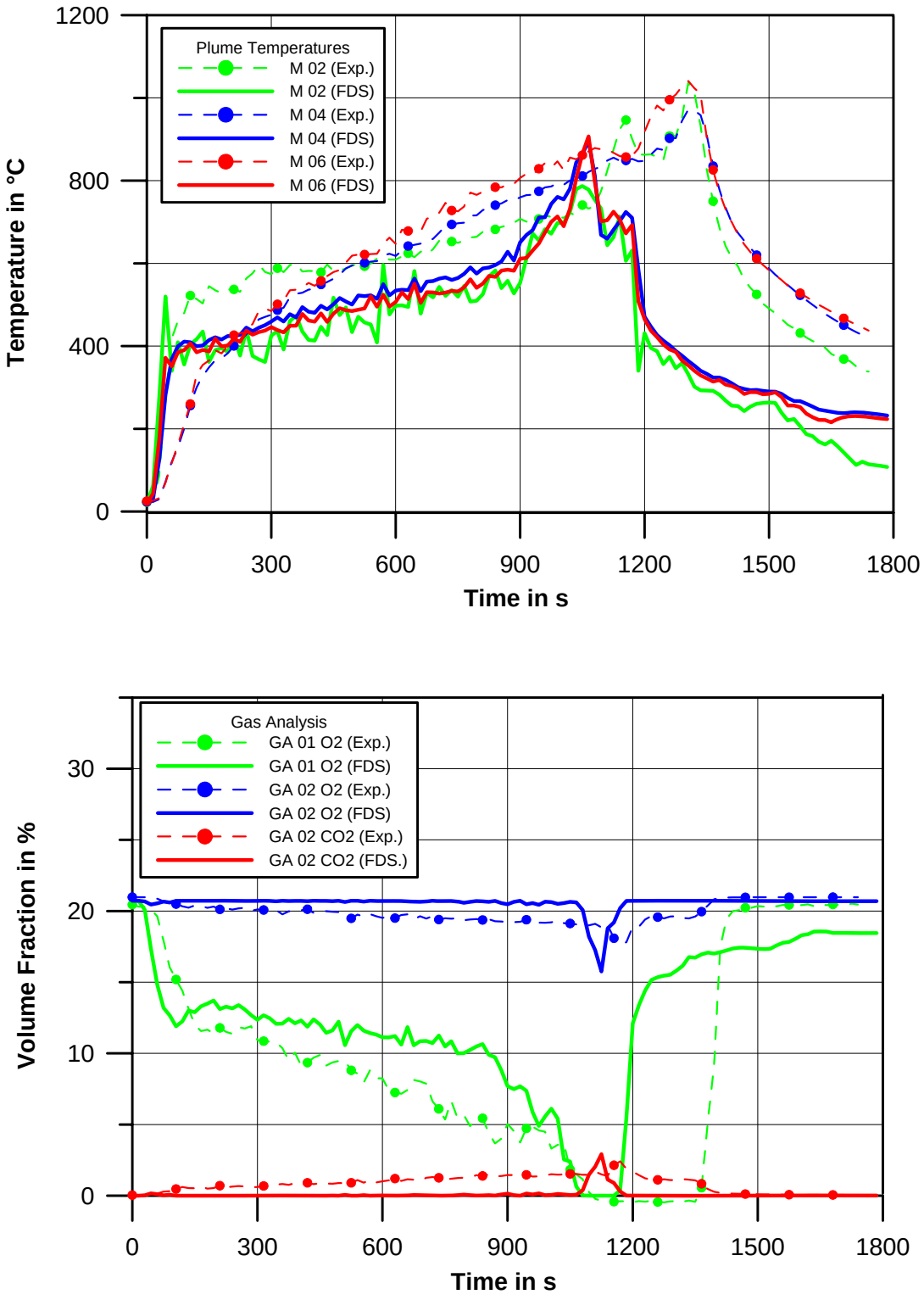

Fig. 5-18 Comparison of FDS results (FDS3 fine grid; from Appendix G)

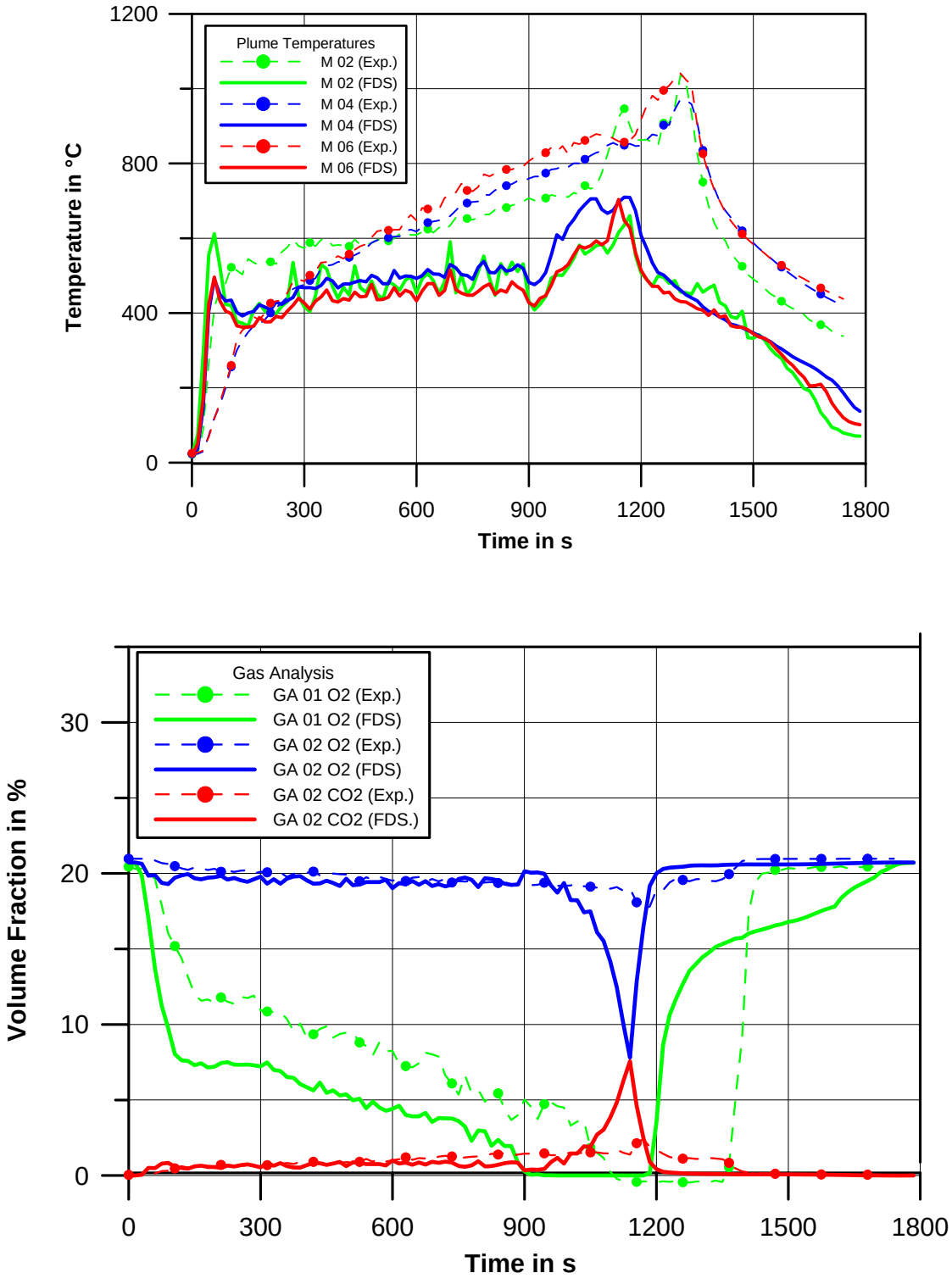

Fig. 5-19 Comparison of FDS results (FDS4 fine grid) (from Appendix G)

5.3.5 COCOSYS (Lumped Parameter Code) Applied by B. Schramm (GRS, Germany)

Both experiments of Benchmark Exercise No. 4 have been simulated with COCOSYS with knowledge of the experimental results. Because of the flame being extinguished due to oxygen depletion in Test 3, the pyrolysis rate has been modified in some parametric calculations.

COCOSYS Code Description and Input Assumptions

The lumped parameter (LP) code COCOSYS /ALL 05/ has been developed and validated for the comprehensive simulation of severe accident progression in light water reactor containments. This code system is to allow the simulation of all relevant phenomena, containment systems and conditions during the course of design basis accidents and severe accidents. In COCOSYS, mechanistic models are used as far as possible for analyzing the physical and chemical processes inside reactor containments. Essential interactions between the individual processes, e.g. feedback from fission product decay heat on thermal hydraulics, are treated in a thorough way. With such a detailed approach, COCOSYS is not restricted only to relevant severe accident phenomena, but will also be able to demonstrate interactions between these phenomena as well as the overall behavior of the containment.

For the simulation of oil and cable fires, pyrolysis and burning models have been implemented in the thermal hydraulic module of COCOSYS. This process is divided into two steps: first the release of pyrolysed species from the oil or cable surface and second the burning processes inside the atmosphere and on the surface of the burning material itself. Two different types of concepts have been implemented in COCOSYS: a very detailed one simulating the combustible materials (oil and cables) with a 1D heat flow model and a simplified concept to handle user specified pyrolysis rates including in some way the feedback from the thermal hydraulic boundary conditions.

In the oil fire model, the material to be burned is represented by a usual structure subdivided into several layers for the calculation of temperature profiles in the material (Fig. 5-20).The surface temperature is calculated by a spline interpolation using all layer temperatures. The heat flux on the surface (e.g. reaction heat, convective heat transfer, radiation) is distributed into the uppermost layer and the second layer according to the volume fraction of the uppermost layer. The released CH_X fractions are

burned above the oil pool considering the oxygen concentration. In case of too little oxygen available, the CH_X components can be transported to other zones and be burned according to user specified mixing factors. In the burning process of CH_X, CO and steam components are formed. The CO mass will be further burned according to the oxygen content and the Boudoir equilibrium.

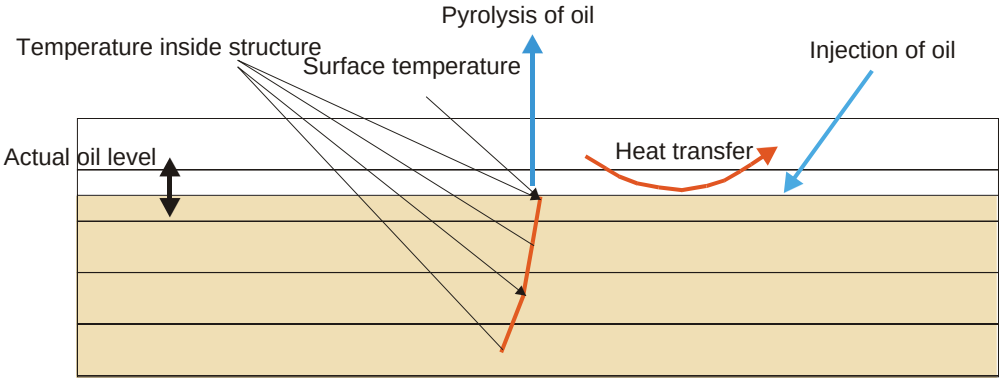

Fig. 5-20 Concept of the pyrolysis model for oil burning

A grid of 102 control volumes with 235 connections in between was used to model the fire compartment. The compartment was divided into 9 vertical levels at the height of 0.0 m, 0.36 m, 0.6 m, 1.1 m, 1.6 m, 2.6 m, 3.6 m and 4.6 m. The difference in the setup between the levels is that the size of the center zone in the fire compartment is increasing with the height. To enable a counter flow through the door opening the fire compartment has to be subdivided so that there are at least be two levels of control volumes at this door elevation. To enable a more detailed flow simulation through the door four levels of control volumes have been used.

COCOSYS Code Results

Especially for Test 3 COCOSYS had some problems in simulating the correct temperature stratification. The plume temperatures as well as most of the other temperatures in the lower part of the fire compartment (level 1) are underestimated by 100 to 200 K but at higher elevations inside the fire compartment the temperatures are over-predicted by 50 - 100 K. After 950 s the temperature in the lowest COCOSYS zone is decreasing rapidly, even though the pyrolysis rate is at its peak. The reason is that all the O_2 in this zone is consumed in the combustion process and not enough air is transported to this control volume. This indicates that the provided pyrolysis rate does not fit to the simulated thermal conditions of COCOSYS. Comparing the temperatures in the material

probes of aerated concrete and concrete it can be observed that the temperature near the surface (x = 0.02 m) is under-predicted in the simulation. This can be easily explained with the significant under-prediction of gas temperature in the simulation in this region. The gas composition has been measured at the point GA1 in the fire compartment. In the simulation, the O_2 concentration is lower than in the experiment for the period 0-800 s. From 800 – 1000 s both values show a good agreement. After 1000 s, the O_2 concentration is nearly zero in the experiment, but in the simulation it is increasing again. These discrepancies can be explained by looking at the O_2 concentration over the fuel surface. The flame is extinguished in the lower part of fire compartment above the pan.

Due to the problem of the extinguishing flame, a parametric calculation with a modified pyrolysis rate has been performed. The aim of this calculation was to investigate if better results could be obtained if the pyrolysis rate was reduced in order to prevent the extinguishing of the flame. For the first 900 s the measured fuel weight seems to be realistic, thus the pyrolysis rate was not changed for this period. The measured temperatures show that the combustion process is nearly over after 1300 s. Hence, the pyrolysis rate has to be very small for this period. With the modified pyrolysis rate the temperature stratification is not satisfactorily predicted. At a lower elevation, the temperature is still under-predicted in the simulation and the temperature increase measured during the first 100 - 200 s is over-estimated.

The COCOSYS results of Test 1 are now summarized. The plume temperature increases earlier than in the experiment at the measurement points (M1-M6). In the experiment it took about 180 s until a fast temperature increase was measured, in the simulation this temperature increase is predicted at 100 s, and is less strong. After 200 s the temperature is over-predicted at all measurement points in the plume by 100 - 200 °C (M1-M6). Outside the plume, the characteristic of the results are similar to Test 3. At lower elevations the temperatures are under-estimated and at higher elevations the temperatures are over-estimated with deviations up to 200 K. In the simulation, the mixture of the gas is not simulated correctly. In the calculation, very little hot gas mixes with the cold gas at the lower elevations. It moves due to buoyancy upwards and gathers at the top of the room. It leaves the room via the FUCHS fan system or through the upper part of the door. The gas composition was measured at the point GA1 in the fire compartment. In the experiment, the O_2 concentration was significantly higher than in the simulation. Accordingly, the CO and the CO_2 concentrations predicted in the simu-

lation are too high. An explanation would be that the chemical reaction mechanism is not valid, or, which is more likely, there is a problem with the simulation of the mixing between hot and cold gas layer.

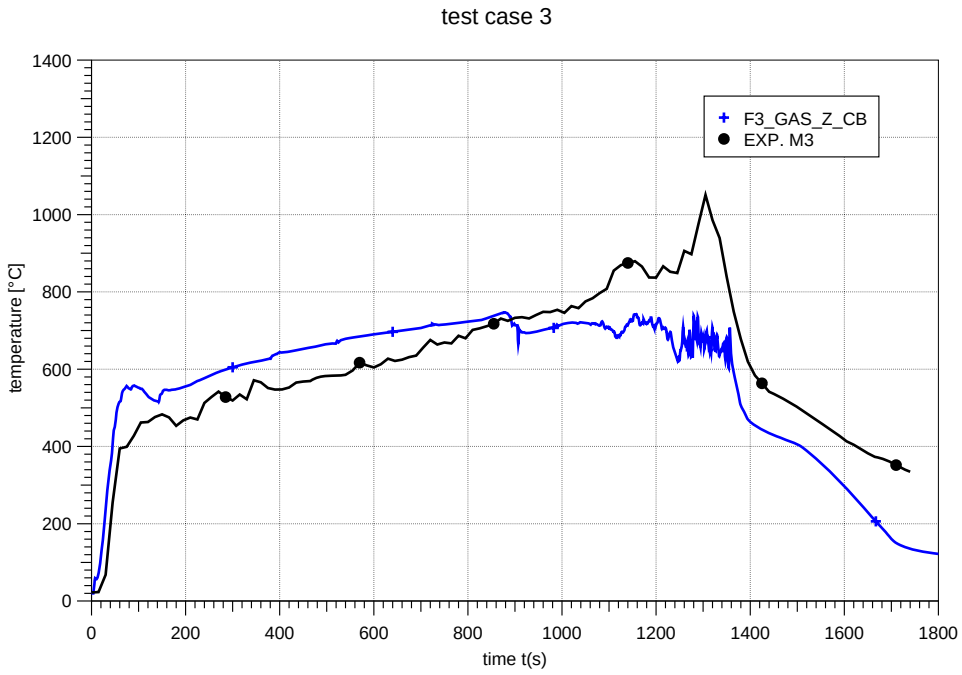

Fig. 5-21 Test 3: Plume temperature at M3 (from Appendix H)

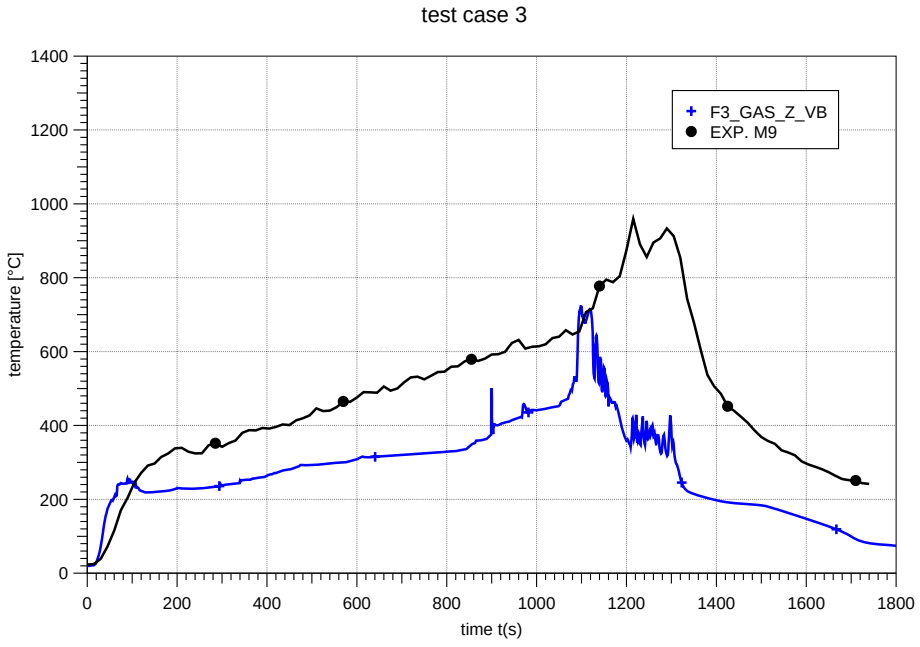

Fig. 5-22 Comparison of measured temperature M9 (z = 1.5 m) and COCOSYS results (from Appendix H)

5.3.6 VULCAN (CFD Code) Applied by V.F. Nicolette (SNL, USA)

The CFD code VULCAN has been used for open calculations of Test 3. However, the results have not been optimized to match the available experimental data.

VULCAN Code Description and Input Assumptions

VULCAN is derived from the Kameleon Fire code /HOL 90/. It models the transport and burning of vaporized fuel, as well as the transport of combustion by-products and their thermal impact on targets. Conservation equations are solved for mass, species, momentum, energy (enthalpy), turbulence quantities, and radiation intensity. Convective and radiative heat transfers to targets are included in the code, as well as the subsequent thermal response of the targets. VULCAN contains the following sub-models (algorithms):

– A fuel vaporization sub-model for the estimation of the rate, at which the fuel is transferred from the liquid phase (for liquid fuels) to the vapor phase.

- A k-ε turbulence model;
- Eddy Dissipation Concept (EDC) combustion model. Reactions are modeled as either 1-step or 2-step reactions, with irreversible, infinitely fast chemistry (relative to the mixing process);
- A soot generation and transport model;
- Discrete Transfer Method (DTM) of Shah and Lockwood is employed to solve the thermal radiation;
- VULCAN uses an extension of the SIMPLEC method of Patankar and Spalding, 1972, to solve the conservation equations using a control volume formulation. A structured three-dimensional Cartesian grid is used. First- and second-order accurate upwind schemes can be used for the convective terms.

A non-uniform grid of 38 x 55 x 46 (y direction is from the front door to the back of room) control volumes was used for the majority of simulations, and was developed based on previous modeling experience. Additionally, a refined mesh simulation was performed using 74 x 104 x 84 control volumes (essentially dividing the physical length of each control volume side by a factor of 2). This yielded a control volume length scale of order 0.07 – 0.15 m in the x and y directions. The control volumes in the z direction

were somewhat larger in the upper regions of the room, where gradients were expected to be small. The computational domain was taken as the fire compartment plus some reservoir space outside of the fire compartment.

For some simulations, the measured fuel evaporation rate was specified for the code. For other simulations, the fuel evaporation rate was calculated by the code based on the thermal response of the fuel. The chemical reaction was modeled as a two-step reaction with production of intermediate species. In the first step of the chemical reaction, the fuel is assumed to combust to form carbon monoxide and hydrogen. The second step of the reaction converts the intermediate species to water vapor and carbon dioxide.

VULCAN Code Results

A simulation was performed in which the experimentally measured mass loss rate was directly calculated based on the thermal response of the fuel pool (Fig. 5-23).

Oxygen depletion was observed to occur significantly sooner in the simulations than in the experiment. The agreement between simulation and experiment is best discussed when separated into 2 time periods: pre-oxygen depletion, and post-oxygen depletion of the room. Prior to oxygen depletion, very good agreement was obtained for the pool mass loss rate and the majority of heat fluxes to targets. The agreement was not as good for thermocouple temperatures, target thermal response, and doorway velocities. For times that are post-oxygen depletion, the agreement is generally not as good as for the pre-depletion period. This is understandable since the post-oxygen depletion environment is highly dependent upon the locations and amounts of leakage into the compartment. A fine mesh simulation produced essentially the same results as with the coarse mesh, suggesting the coarse mesh results were adequate. The inclusion of buoyancy generated turbulence in the simulations did not change the results substantially, but did improve the prediction of temperature low in the plume and the lower doorway velocity, while resulting in even faster oxygen consumption (relative to the standard k-ε model).

The sources of discrepancies between the predictions and data could not be definitively resolved due to uncertainties in the experiment and documentation. These discrepancies are believed to be primarily due to inputs to the code being significantly different than existed in the experiment. In that context, this experiment is not recom-

mended for code validation purposes, but does provide useful information regarding the potential uncertainties in code predictions when key inputs (e.g., leakage paths) are not accurately specified.

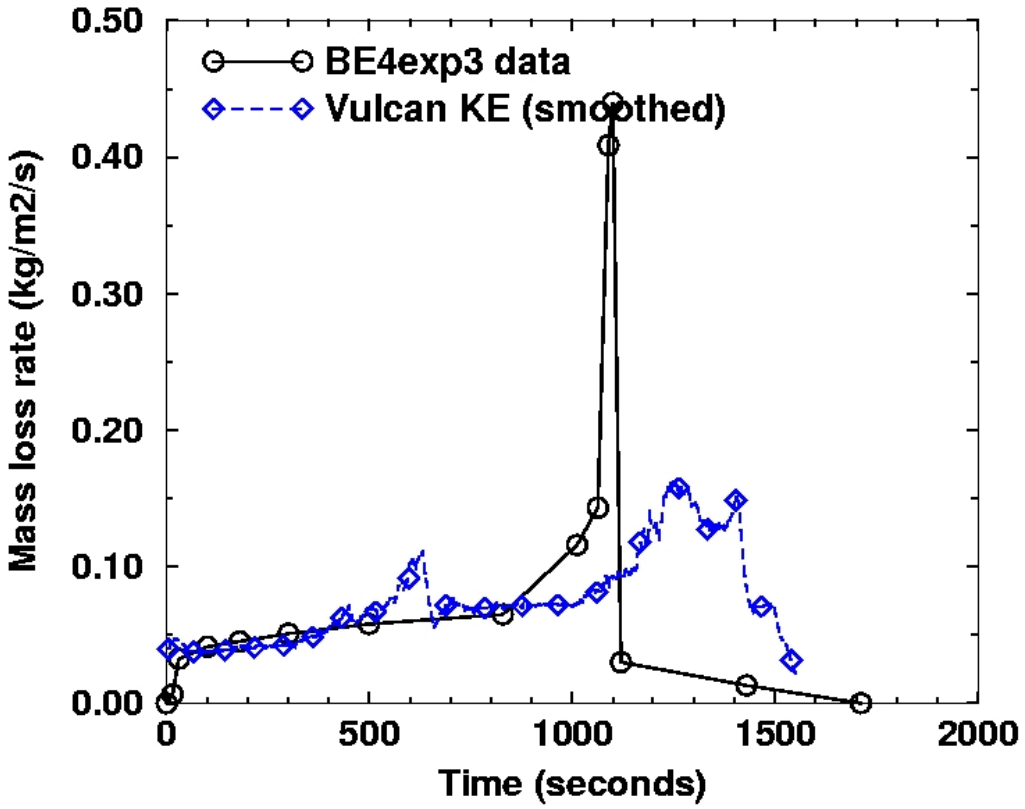

Fig. 5-23 Mass loss rate (smoothed) versus experiment (from Appendix I)

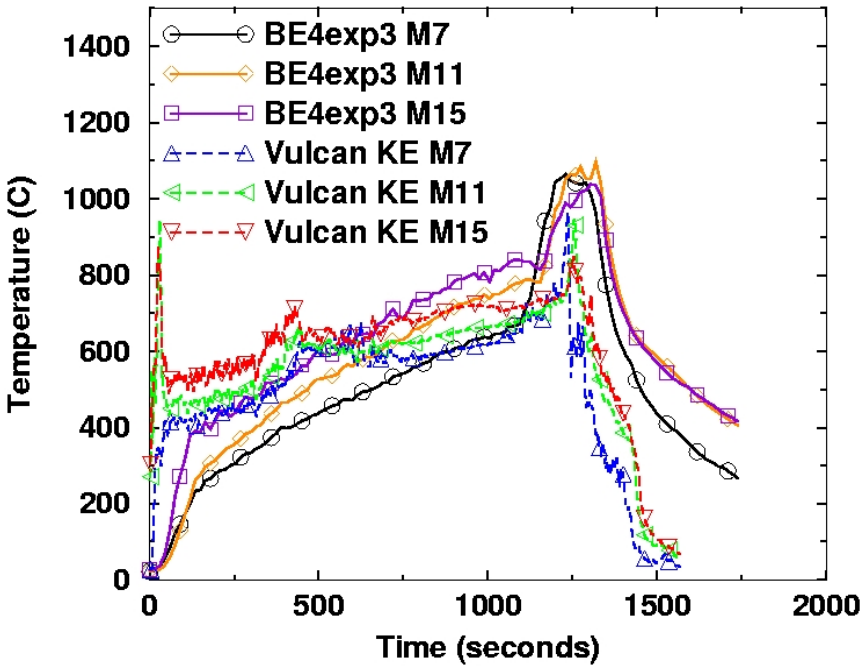

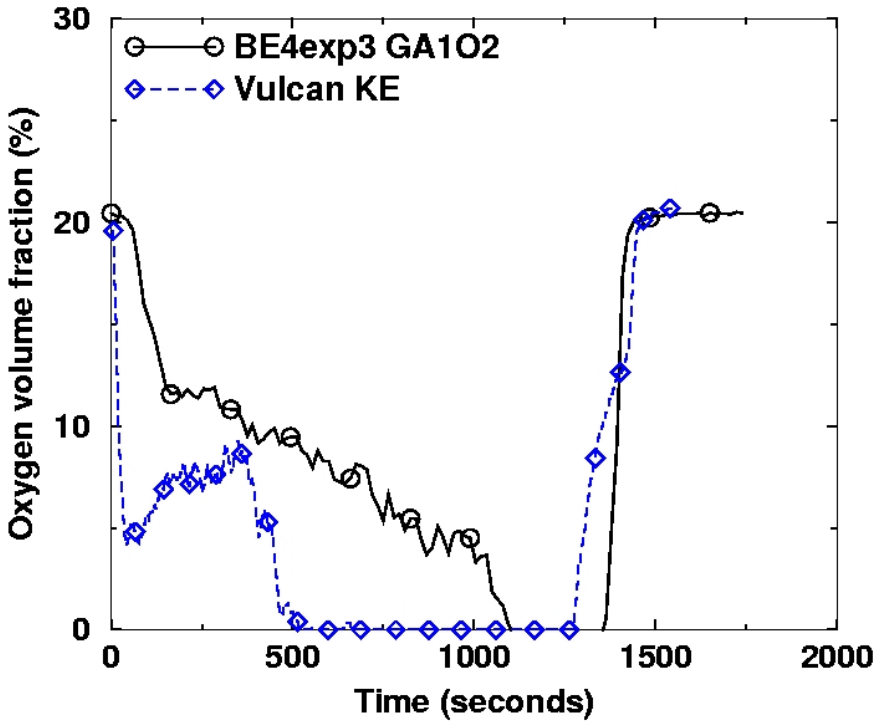

Fig. 5-24 Front room temperatures and oxygen concentration (from Appendix I)

5.3.7 MAGIC (zone code) Applied by B. Gautier (EDF, France)

The zone model MAGIC has been used for open calculations of Tests 1 and 3. Some additional parameter studies concerning the heat release and the effect of light concrete floor have been performed.

MAGIC code description and input assumptions

The calculations presented here were performed with MAGIC V4.1.1b /GAY 06/. The code is used in its standard version using input variables corresponding to a normal risk study approach. MAGIC uses a two-zone model including most of the classic features, like gaseous phase combustion, governed by the properties of emitted products and the air supply attributable to the plume flow, smoke production and transport of unburned products, heat exchange, natural flows and forced ventilation, simulation of targets and sprinkler systems.

The shape of fire compartment has been simplified, and has conserved the total volume. The distances between targets or openings and fuel surface are conserved. The hood in front of the door is not modeled. The ventilation has been simplified to one global exhaust vent at the ceiling. The lower oxygen limit is fixed to 0 % which is the EDF recommended value. The radiation fraction is set to 0.35.

MAGIC code results

MAGIC results appear more realistic in Test 1 (open door) than in Test 3 (semi-closed door). In Test 1 the gas temperature are realistic while target temperature and flux are significantly over-estimated. In Test 3 gas layer temperature is little under-estimated, while the target predicitions are in good agreement.

In Test 3, the configuration induces more complex phenomena: the reduction of the opening cross section produces under-ventilated conditions. It seems that the flame was inclined to the door in the experiment. These phenomena are not represented in MAGIC.

Some experimental data appears to be questionable, especially the HRR in Test 3 and the interface height (due to the low number of thermocouples used in the interface height calculation).

More information on the vent system would have allowed it to be modelled and permitted a more realistic "fire risk study" type of approach to the test. Especially in Test 3, the ventilation due to the vent is comparable to the one due to the door (in calculation and probably also in the actual test). It seems that the door flow is under estimated in the calculation, maybe due to the hood effect.

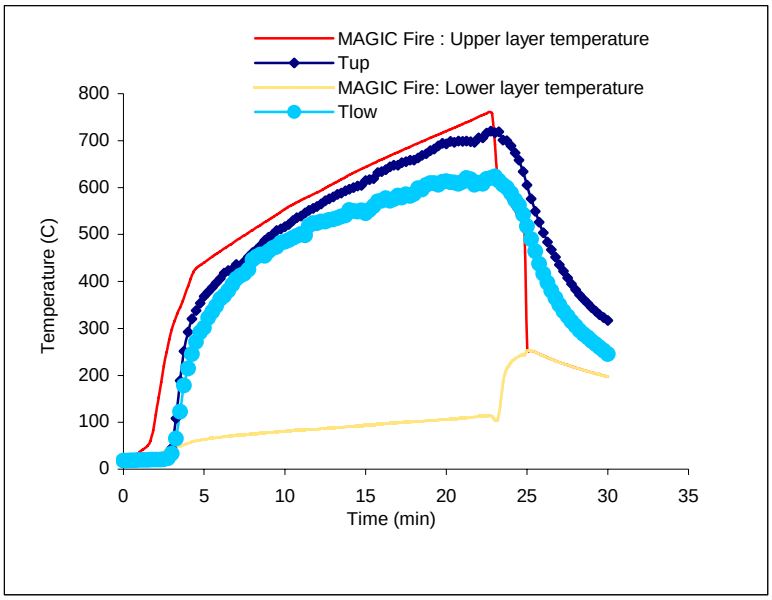

Fig. 5-25 Upper and lower temperature in Test 1 (from Appendix J)

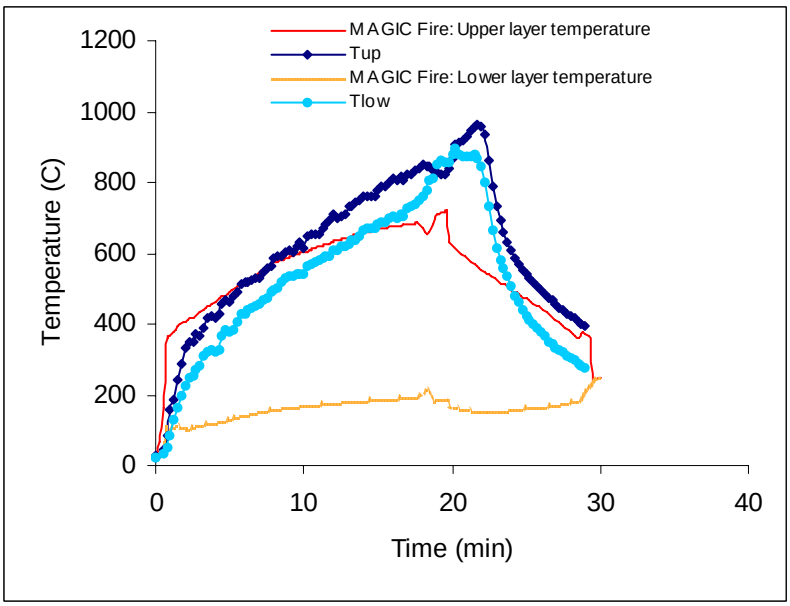

Fig. 5-26 Upper and lower temperature in Test 3 (from Appendix J)

6 Code to Code Comparison

In this chapter the results of the different codes and types of codes are compared to each other. It is clear that the results of simulation tools depend on the quality and capabilities of the models themselves as well as on the experience of the users. Furthermore, it is obvious that this comparison is specific to the Benchmark Exercise considered, with partly oxygen depleted conditions and a relative strong fire.

The objective of this chapter is to look at the overall results of fire simulation tools for:

- characterization of deviations from the experimental results to give some indications on uncertainties, particularly for PSA studies;
- identification of minimum and maximum values of code results;
- characterization of user effects as well as differences between blind and open calculations;
- characterization of potential uncertainties of the experiment itself and the experimental results.

Due to the limited number of participants and calculations it is quite difficult to identify the real causes of deviations of the calculated values from the experimental measurements. Nevertheless, this Benchmark Exercise does give some view on the possible uncertainties of fire simulations.

6.1 Test 1

6.1.1 Plume Temperatures (M1 to M6)

Fig. 6-1 and Fig. 6-2 compare the results for blind and open calculations of the plume temperatures at positions M2 and M6. In comparison to the blind simulations, the results of the semi-blind FDS calculations are much better, having used the pre-defined pyrolysis rate. Larger deviations between semi-blind FDS simulations occur for temperatures closer to the fire surface (like M2). It seems that the user has to be careful to get good results at positions close to the fuel surface. The blind simulations of JASMINE also show an underestimation of the temperatures. This underestimation was not so significant in the semi-blind simulations of JASMINE. The open COCOSYS

simulation overestimates the temperature by approx. 200 K. MAGIC temperature in the flame appears excessively high in the flame zone (M2 and M4 appear in the flame zone in the calculation, M6 is between flame and plume). In contrast, the temperature increase was not predicted in the open CFX calculation. This could be the result of constant wall temperatures assumed in the CFX calculation.

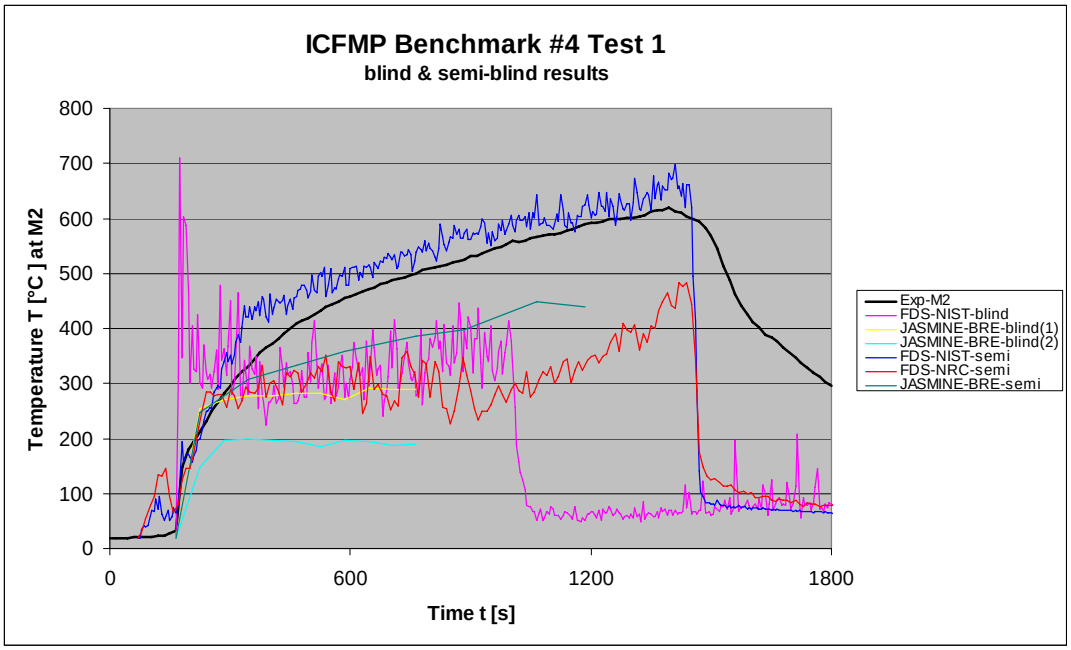

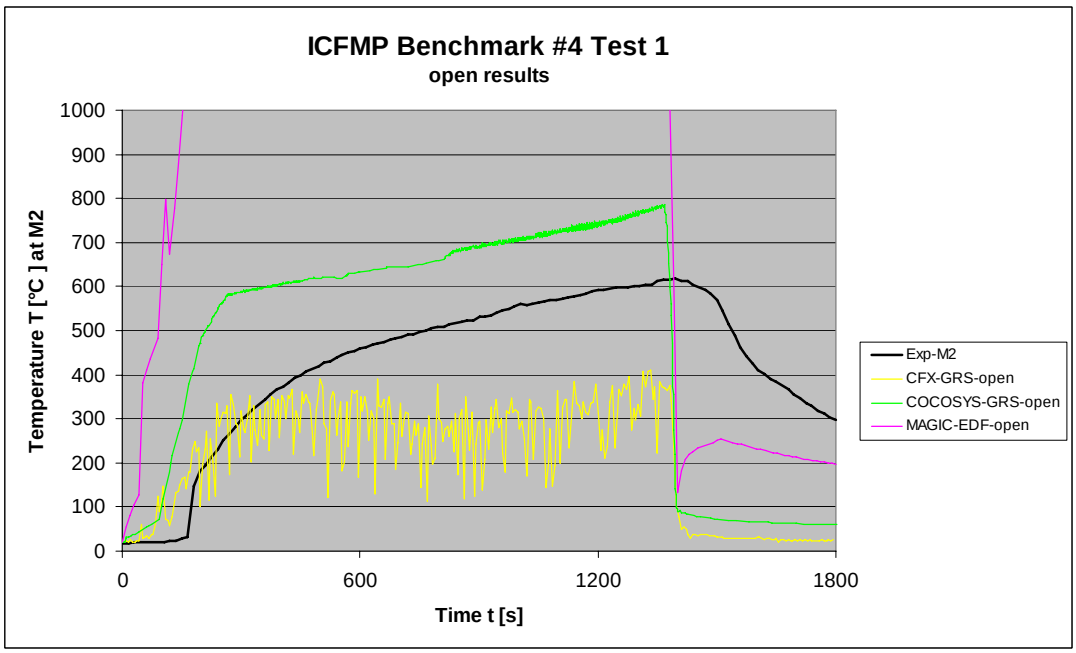

Fig. 6-1 Comparison of plume temperatures M2 (blind & open)

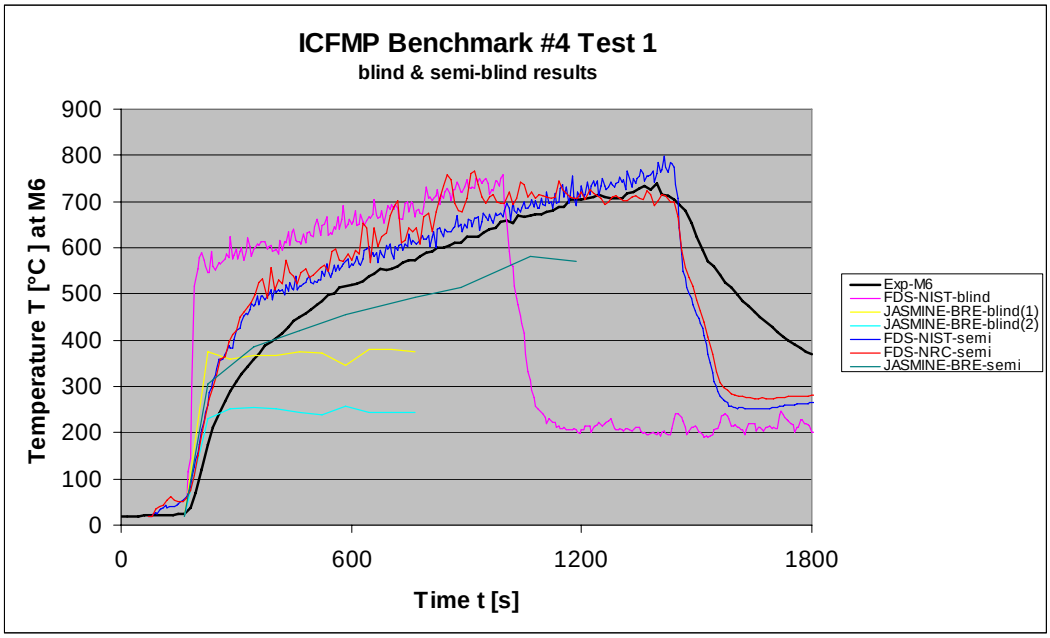

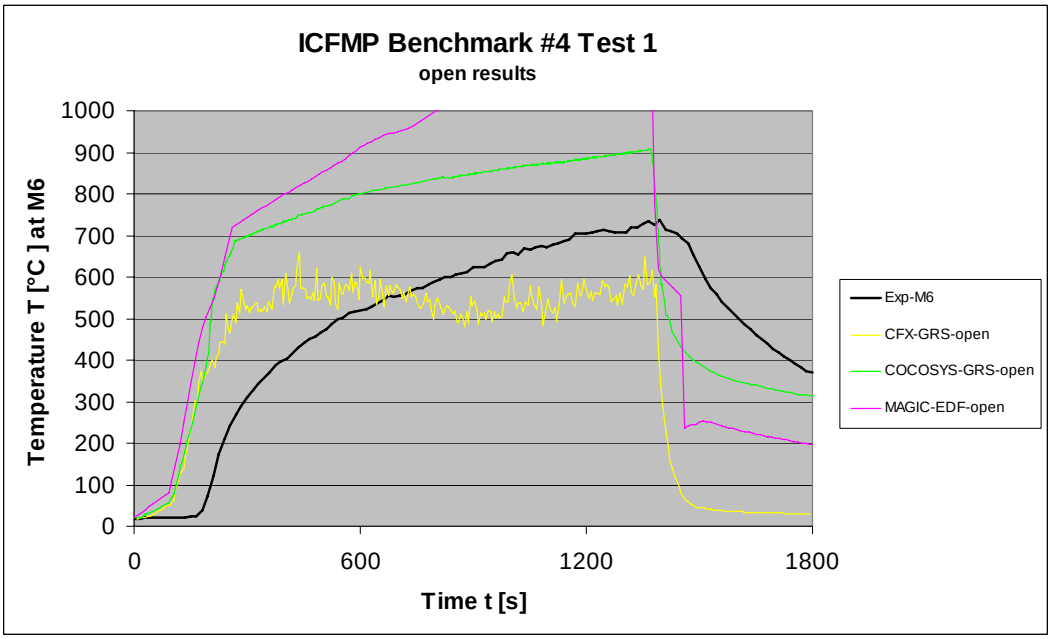

Fig. 6-2 Comparison of plume temperatures M6 (blind & open)

6.1.2 Temperatures inside the Fire Compartment

Fig. 6-3 to Fig. 6-8 present the comparison of the temperatures at the temperature thermocouple tree locations at the front and rear of the fire compartment. The differences between front and back are not very large, indicating that a shift of the fire plume

did not occur. The results of the semi-blind calculation with FDS performed by NIST are very good. The results of FDS performed by NRC underestimate the temperatures at the front. This corresponds to the much lower temperature in the lower part of the fire plume. Most of the semi-blind simulations with JASINE and FDS are reasonably better compared to the blind calculations. This shows again that the knowledge of the pyrolysis rate is highly important for obtaining good results. COCOSYS could not really reproduce the temperature stratification inside the fire compartment. The results at lower elevations are much too low, where in the upper part the temperatures are overestimated by about 100 K.

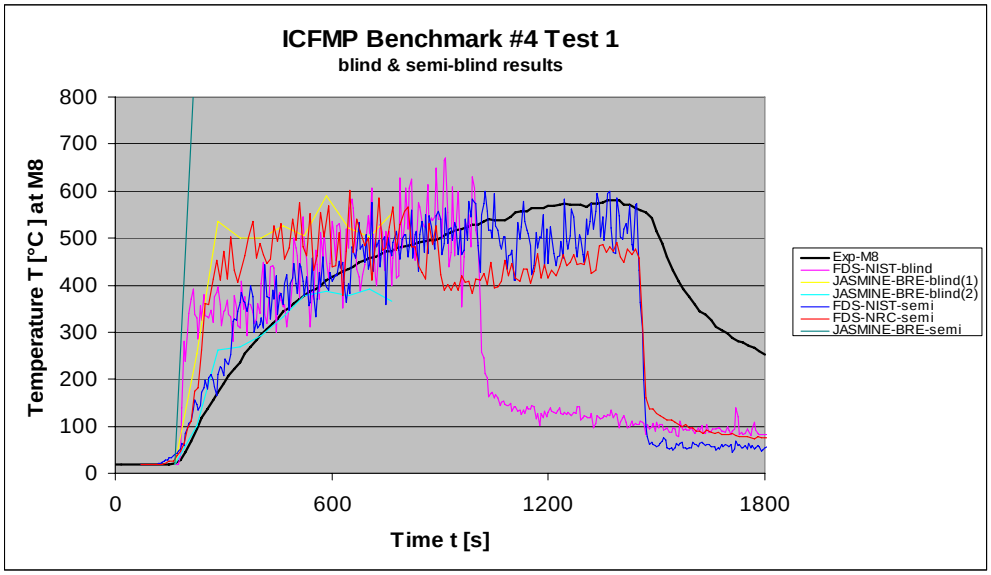

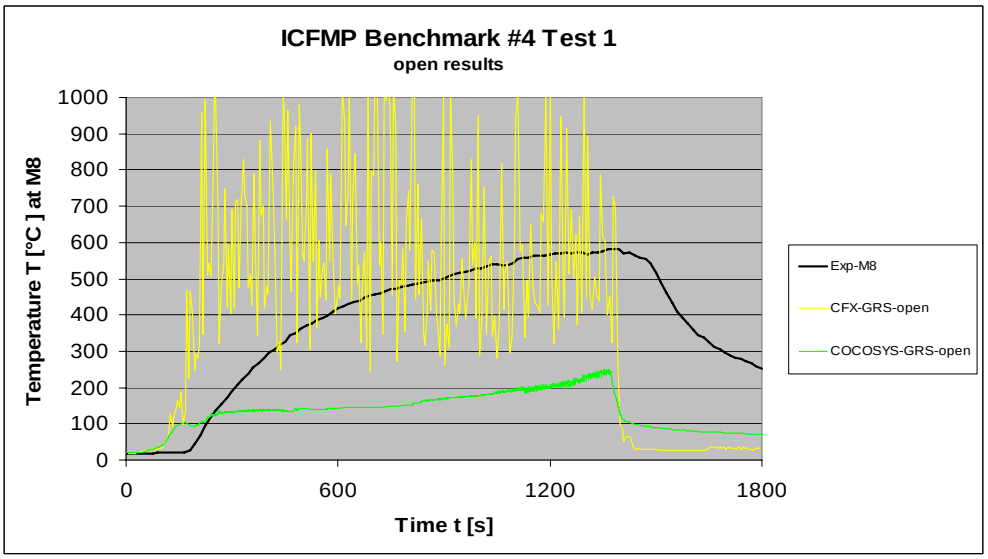

Fig. 6-3 Temperatures on the back side of the compartment (M8, blind & open)

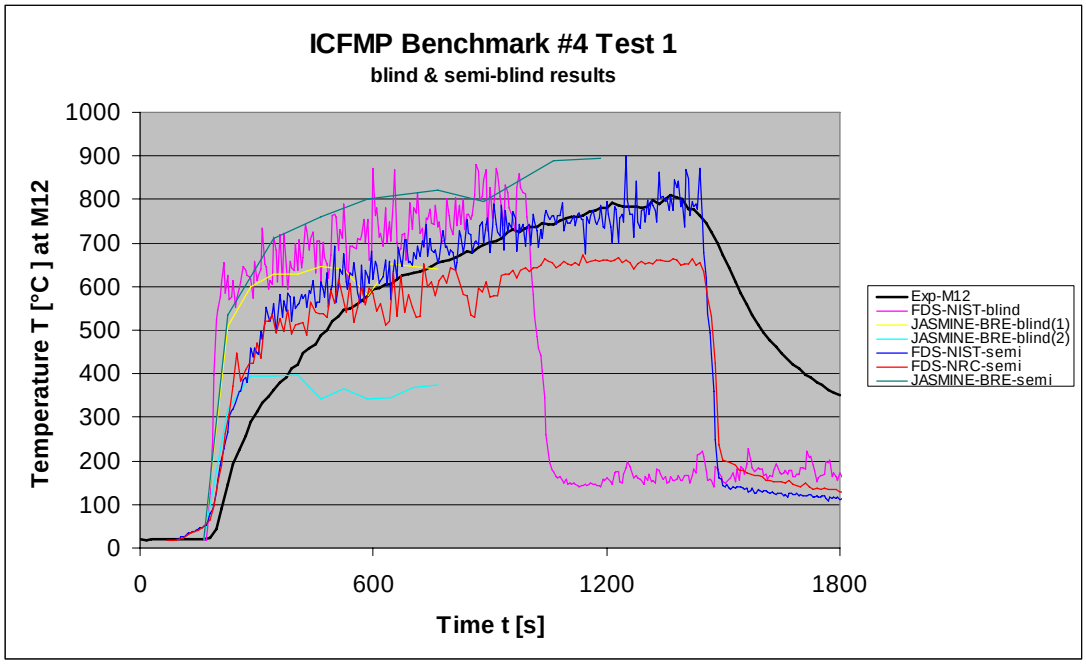

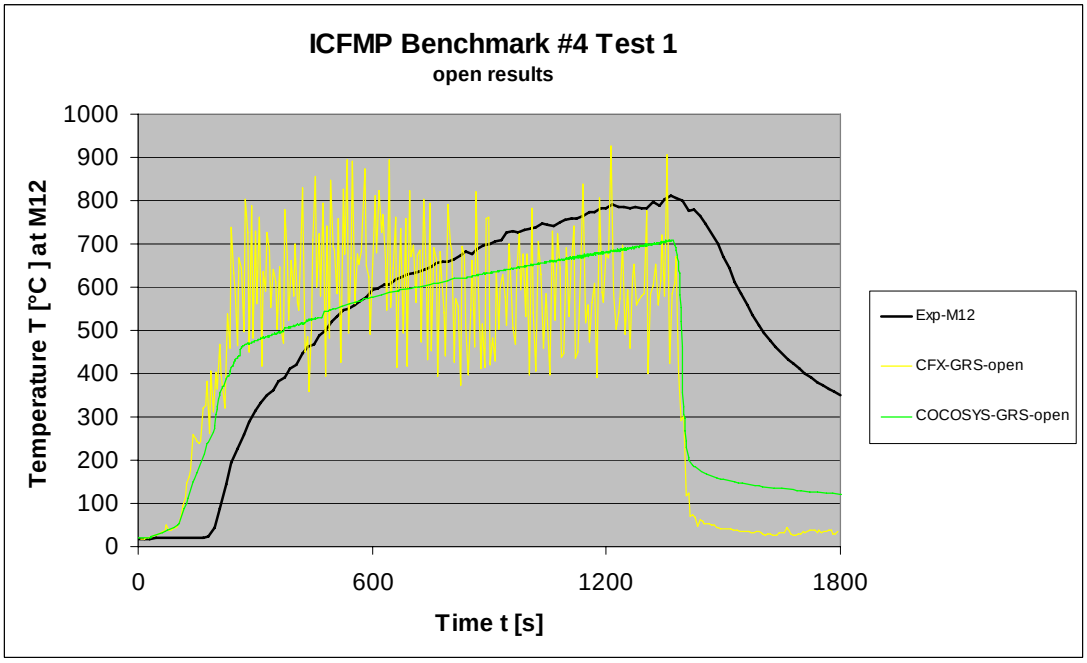

Fig. 6-4 Temperatures on the back side of the compartment (M12, blind & open)

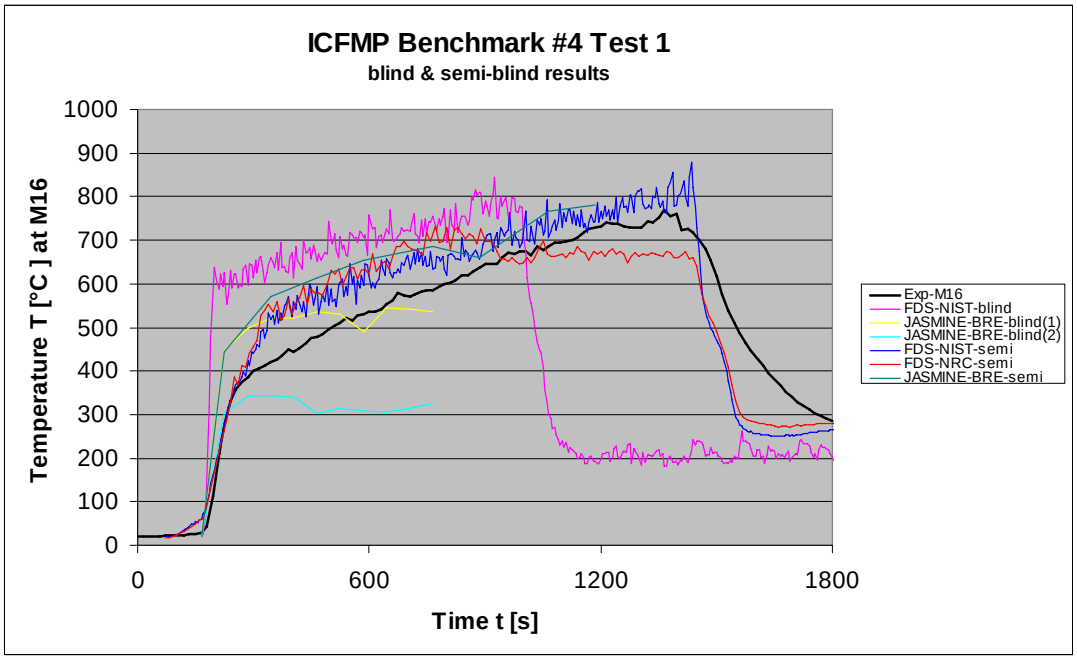

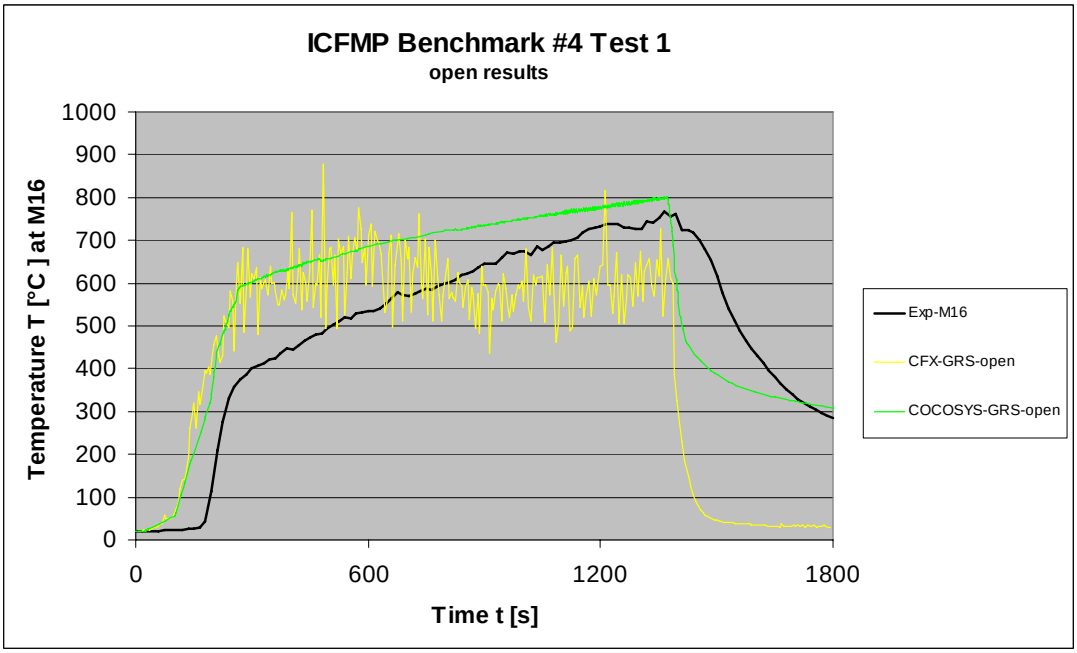

Fig. 6-5 Temperatures on the back side of the compartment (M16, blind & open)

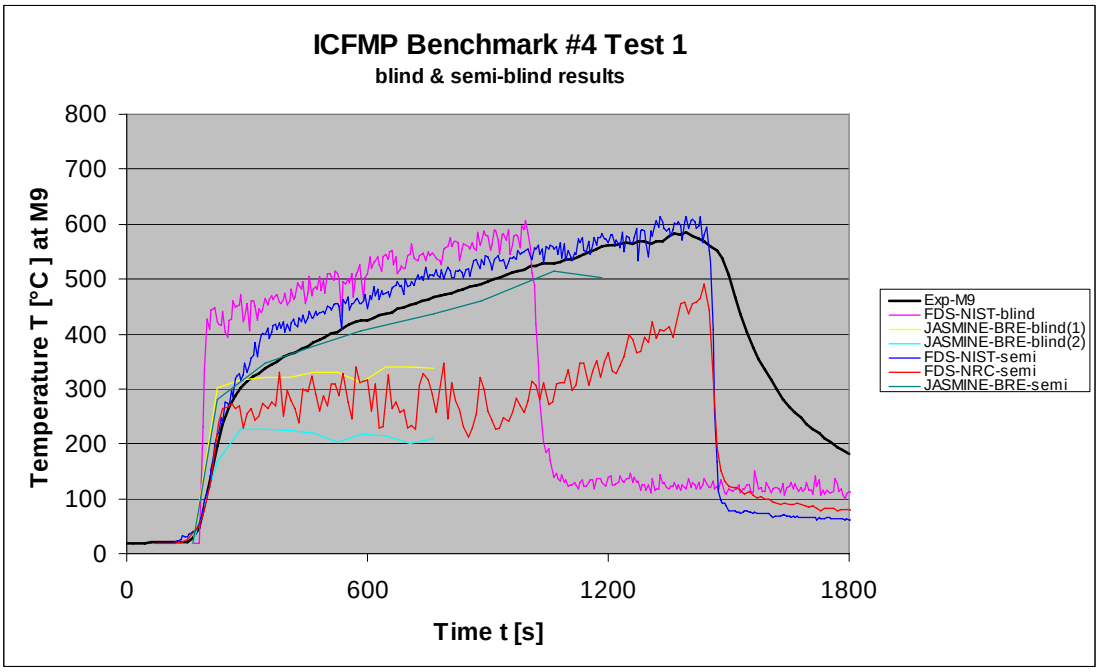

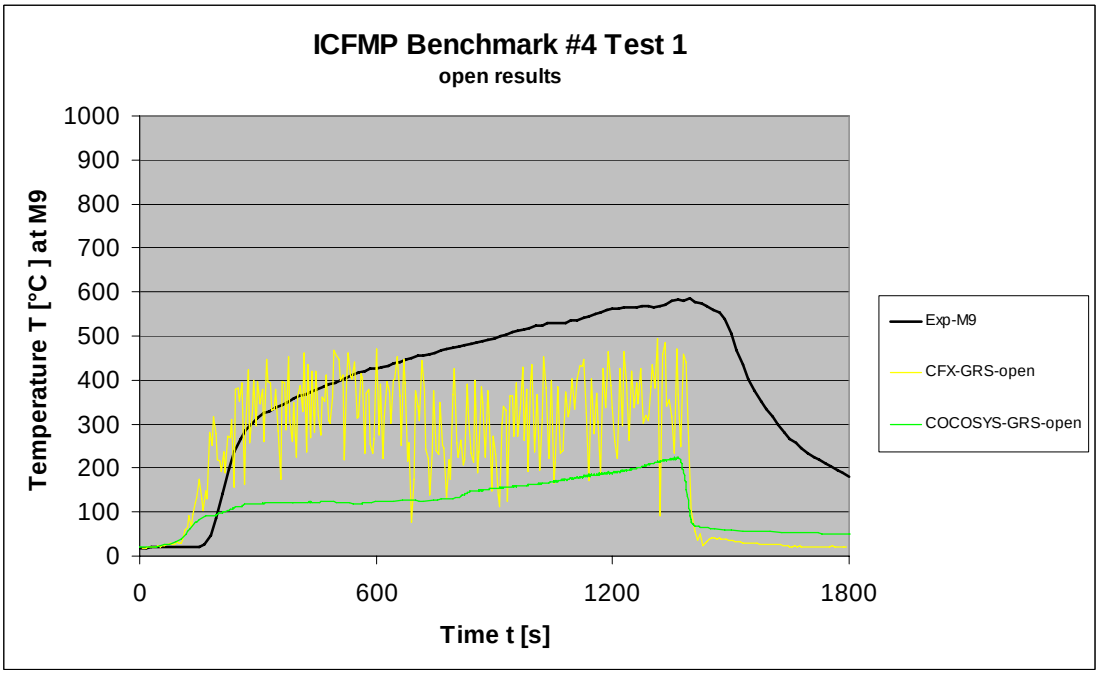

Fig. 6-6 Temperatures on the front side of the compartment (M9, blind & open)

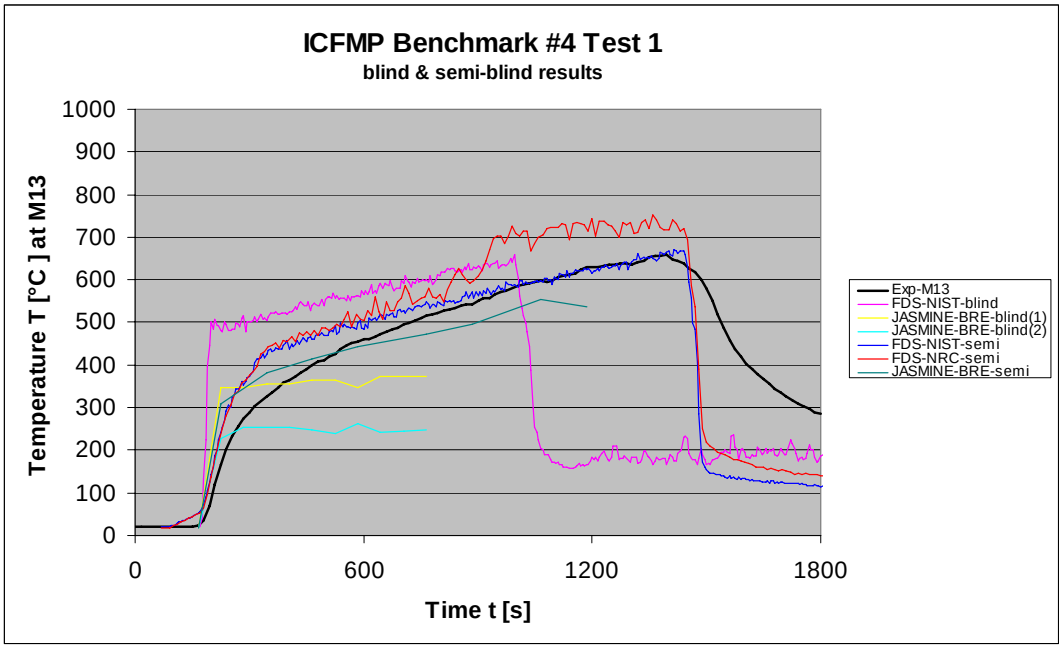

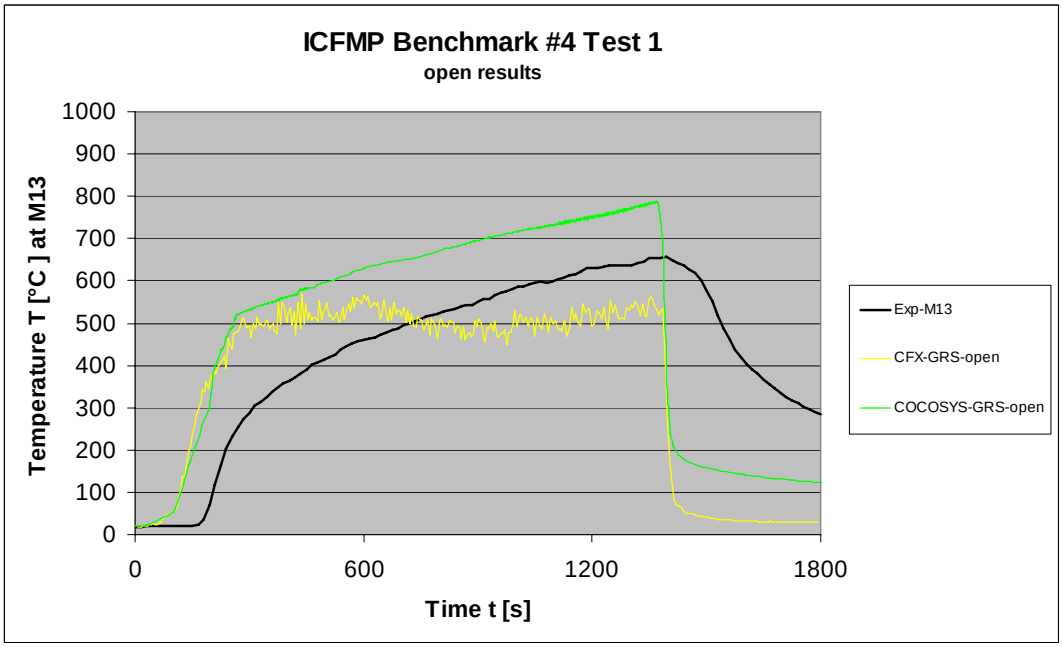

Fig. 6-7 Temperatures on the front side of the compartment (M13, blind & open)

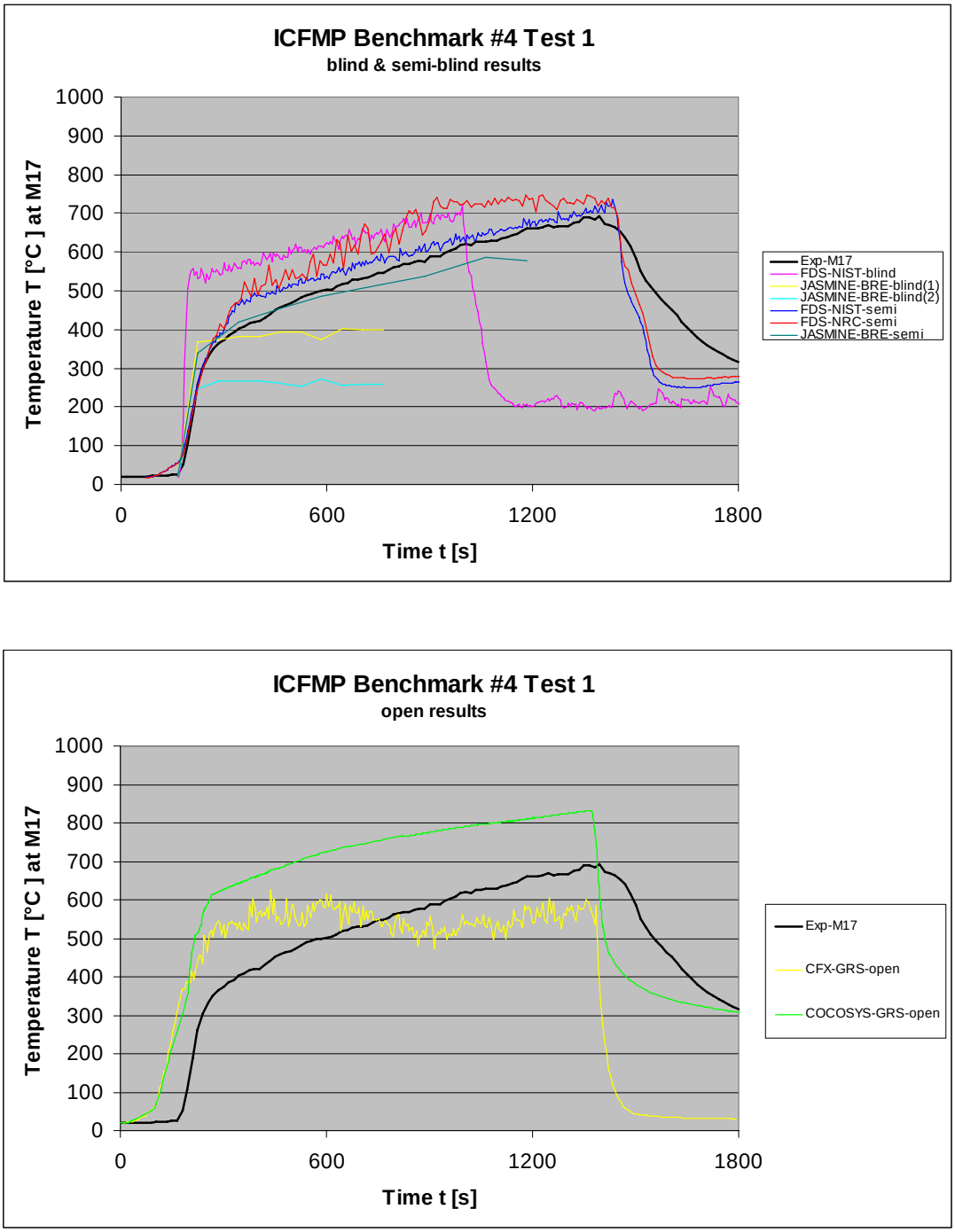

Fig. 6-8 Temperatures on the front side of the compartment (M17, blind & open)

6.1.3 Layer Height and Upper Layer Temperature

Fig. 6-9 and Fig. 6-10 present the hot gas layer height and upper layer temperature. It has to be mentioned in this context, that due to the low number of elevations of measurement positions the calculation of a layer height is not really possible. Therefore, only the general characteristics should be compared. The results of the different codes and code types for the upper layer temperature are reasonably good. The different semi-blind calculations with CFAST show a wide range of about 300 K for the upper layer temperature.

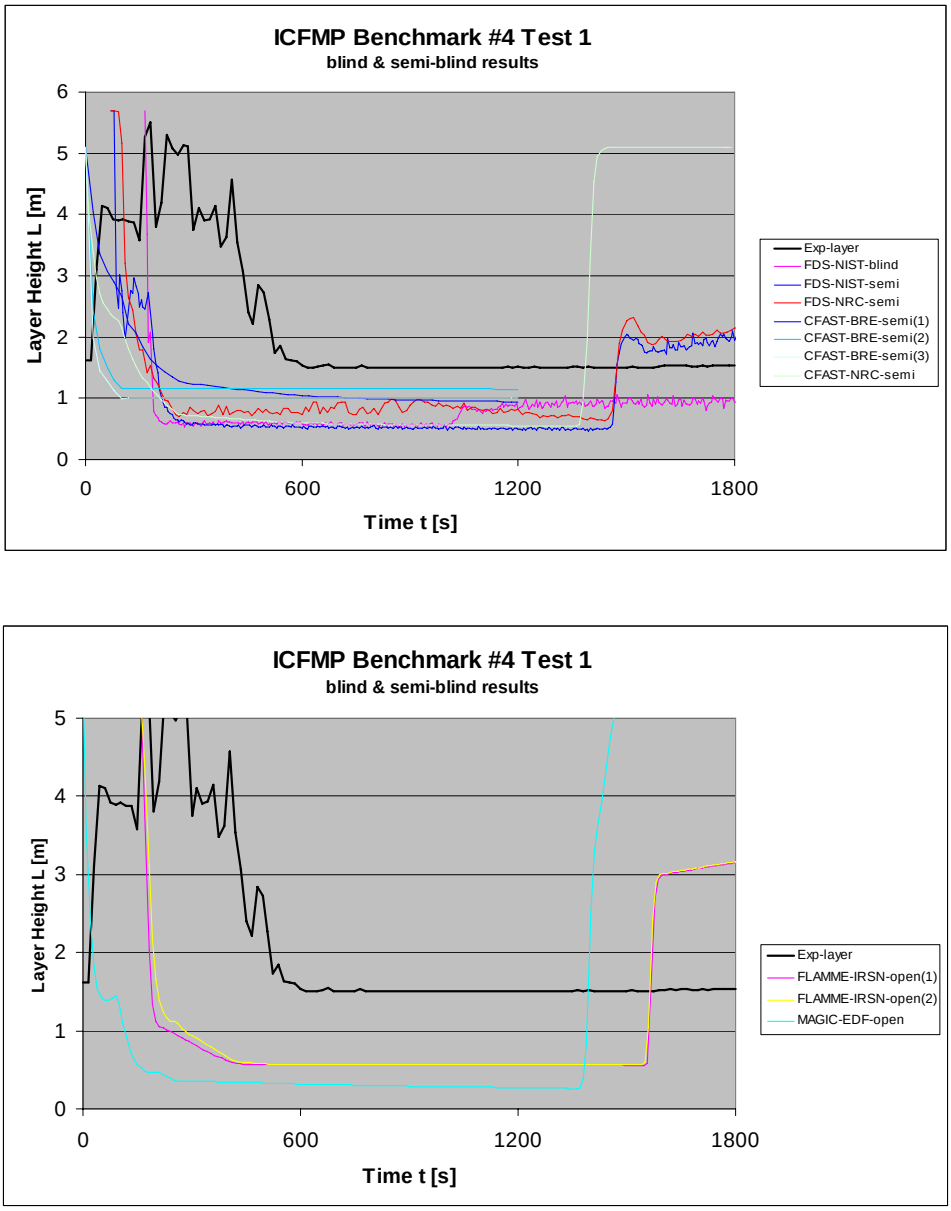

Fig. 6-9 Layer height (blind & open)

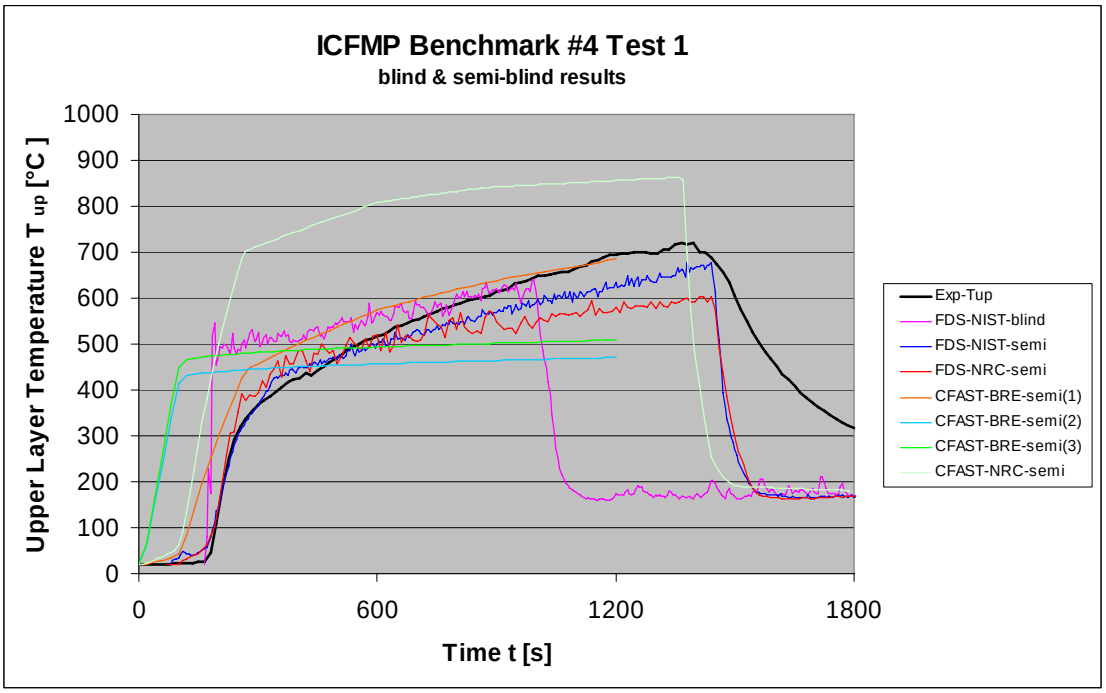

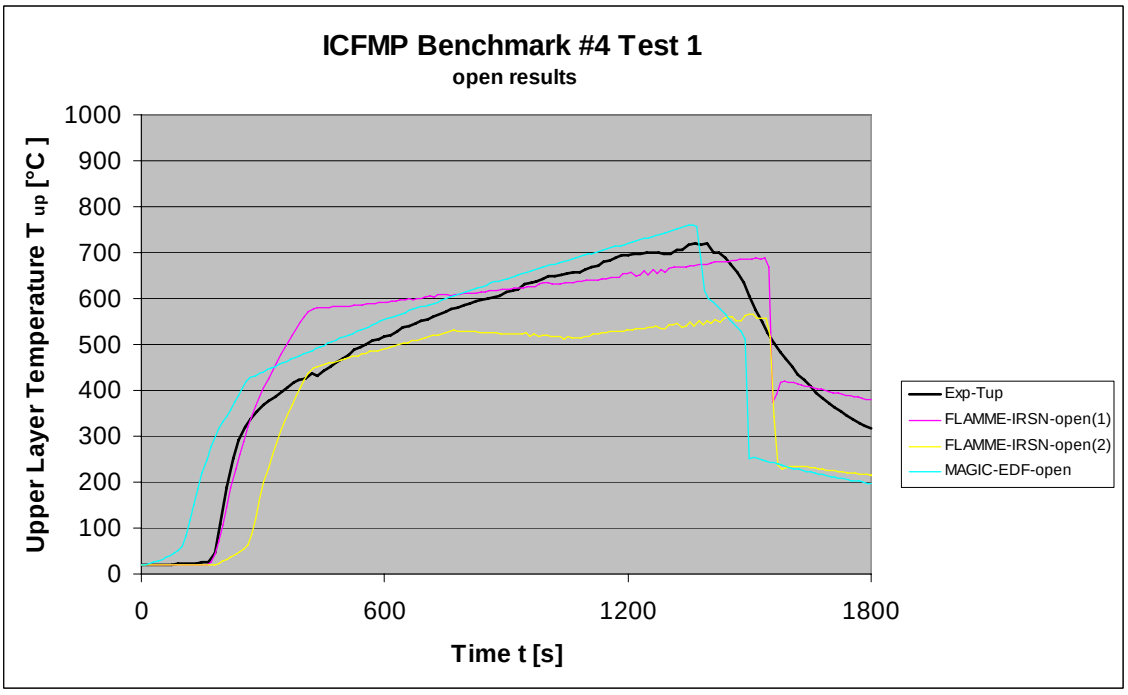

Fig. 6-10 Upper layer temperature (blind & open)

6.1.4 Gas Concentration inside the Fire Compartment

The main difference between Test 1 and Test 3 is the ventilation condition leading to oxygen rich conditions for Test 1. Fig. 6-11 to Fig. 6-14 show the comparison for the gas concentrations of O_2 and CO_2 inside and outside the fire compartment. All codes except CFX underestimate the oxygen concentration inside the fire compartment. Since the experimental values at the measurement position GA1 are quite constant in contradiction to the values at the position GA2, the measurement at GA1 seems to be somewhat questionable. The results of the semi-blind FDS calculation performed by NIST outside the fire compartment are very good. In addition, the measured CO_2 concentration at GA1 does not seem to be reasonable. The value is lower compared to the value at the position GA2.

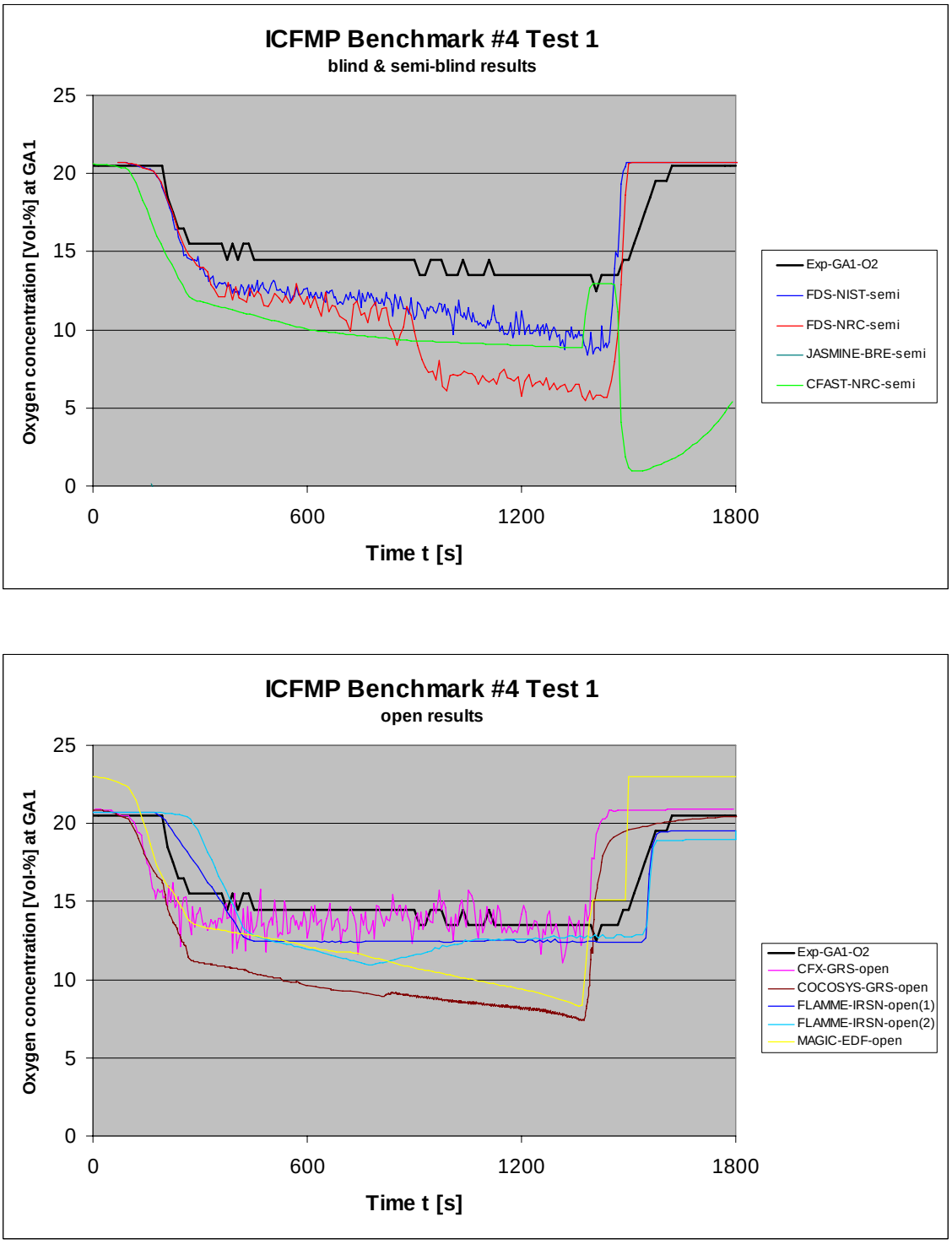

Fig. 6-11 Oxygen concentrations inside the fire compartment (blind & open)

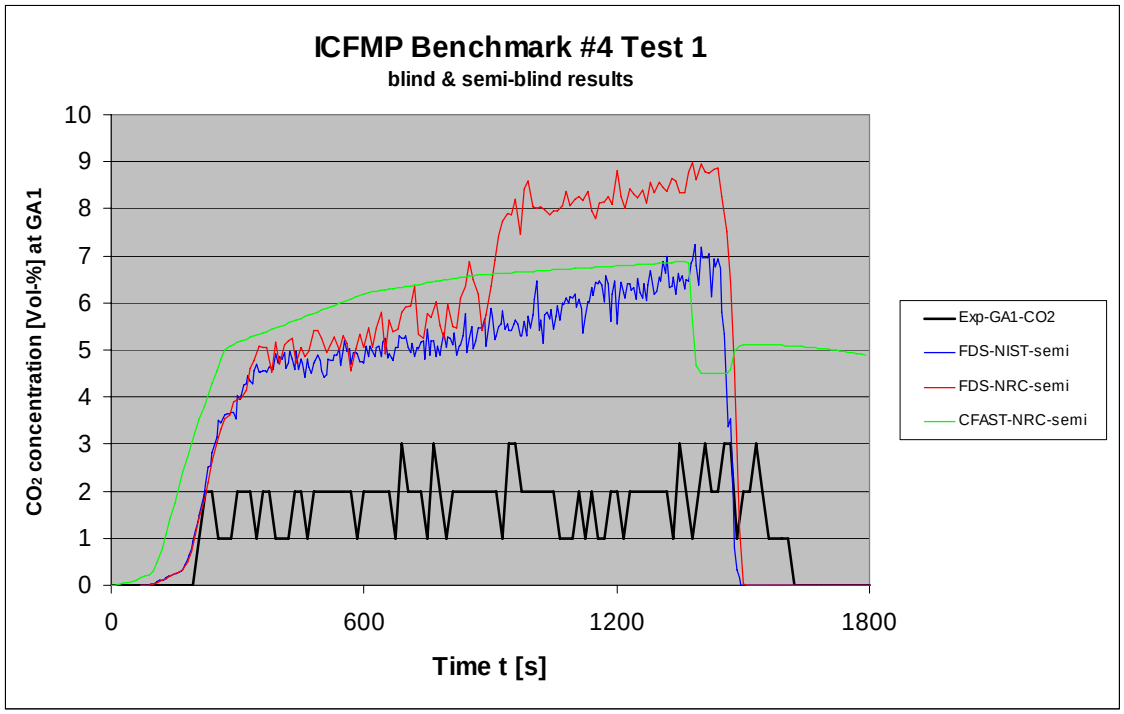

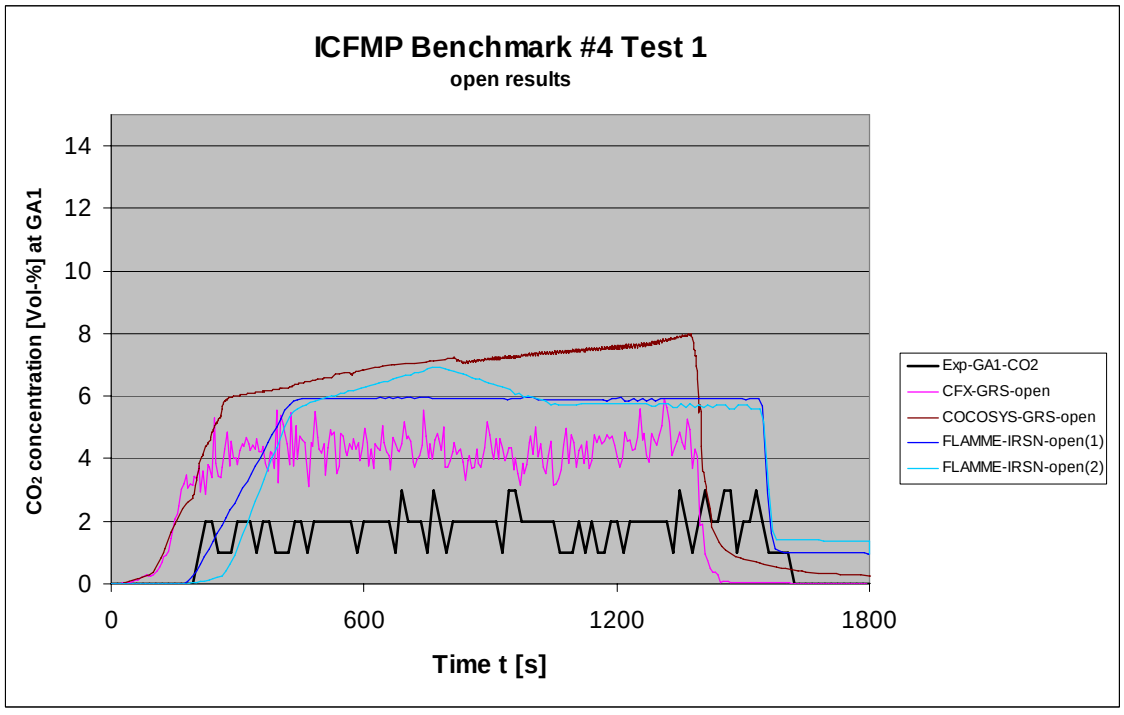

Fig. 6-12 CO_2 concentrations inside the fire compartment

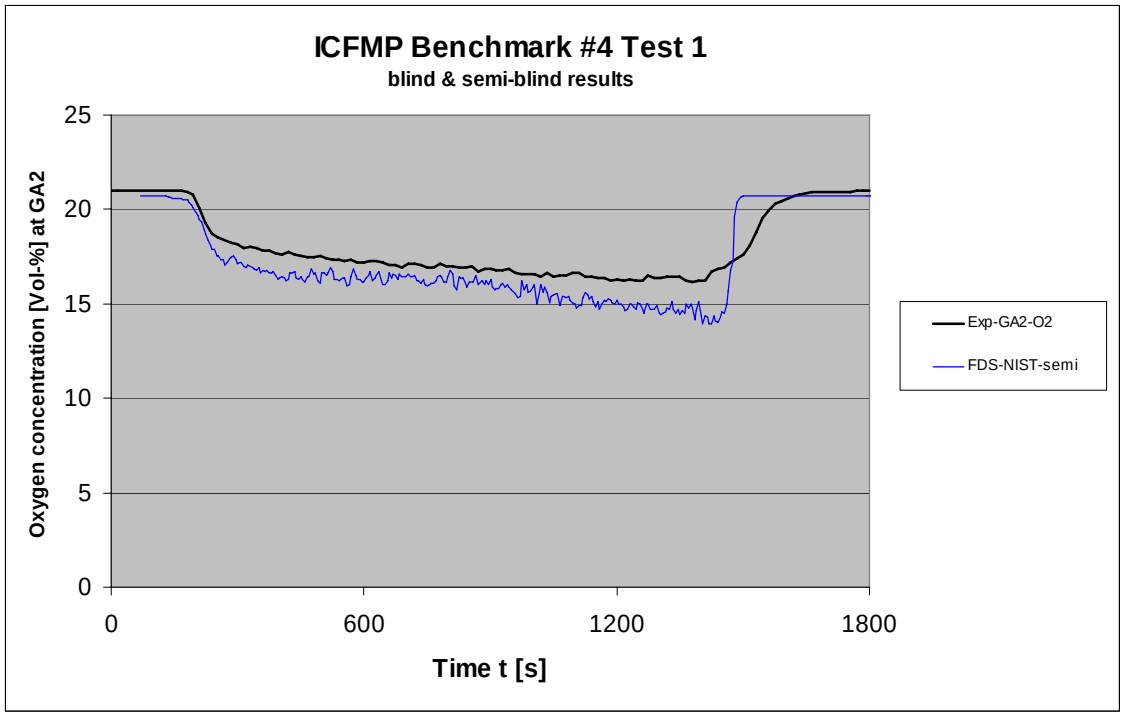

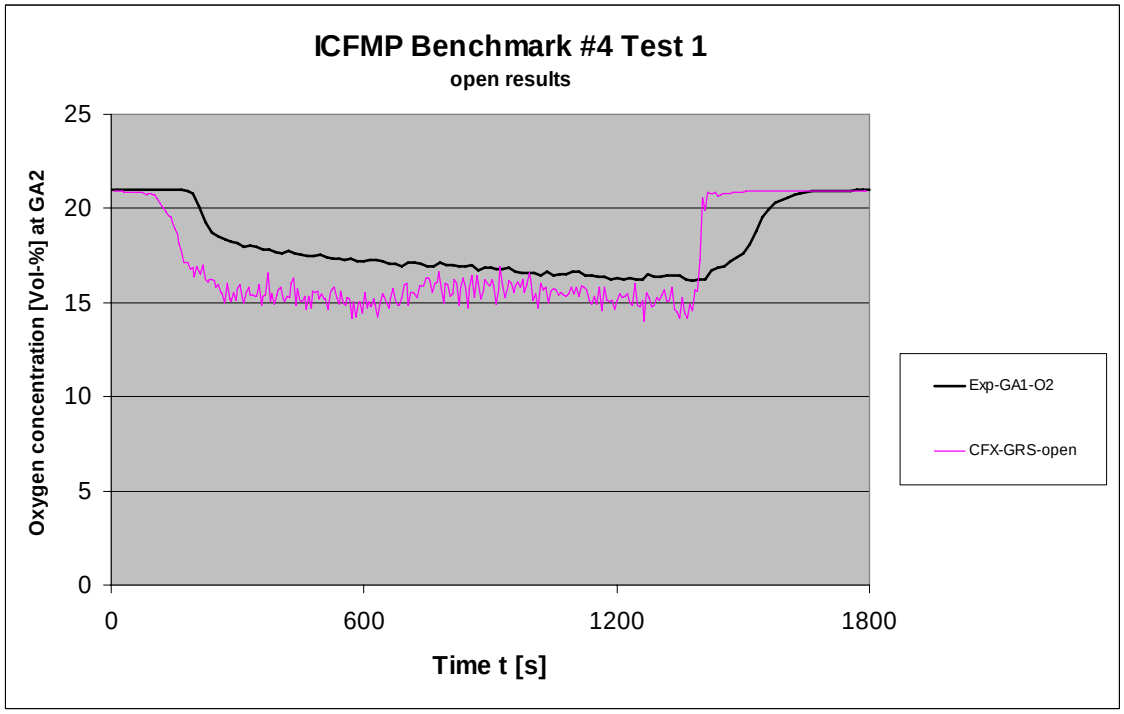

Fig. 6-13 Oxygen concentration outside the fire compartment (blind & open)

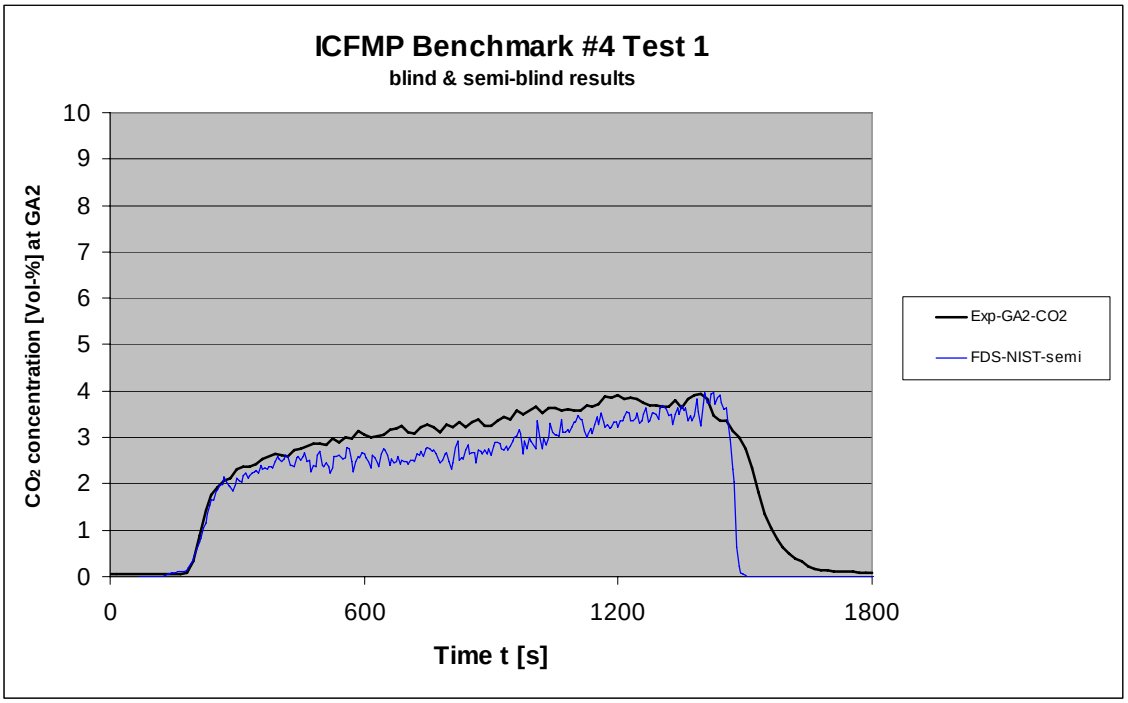

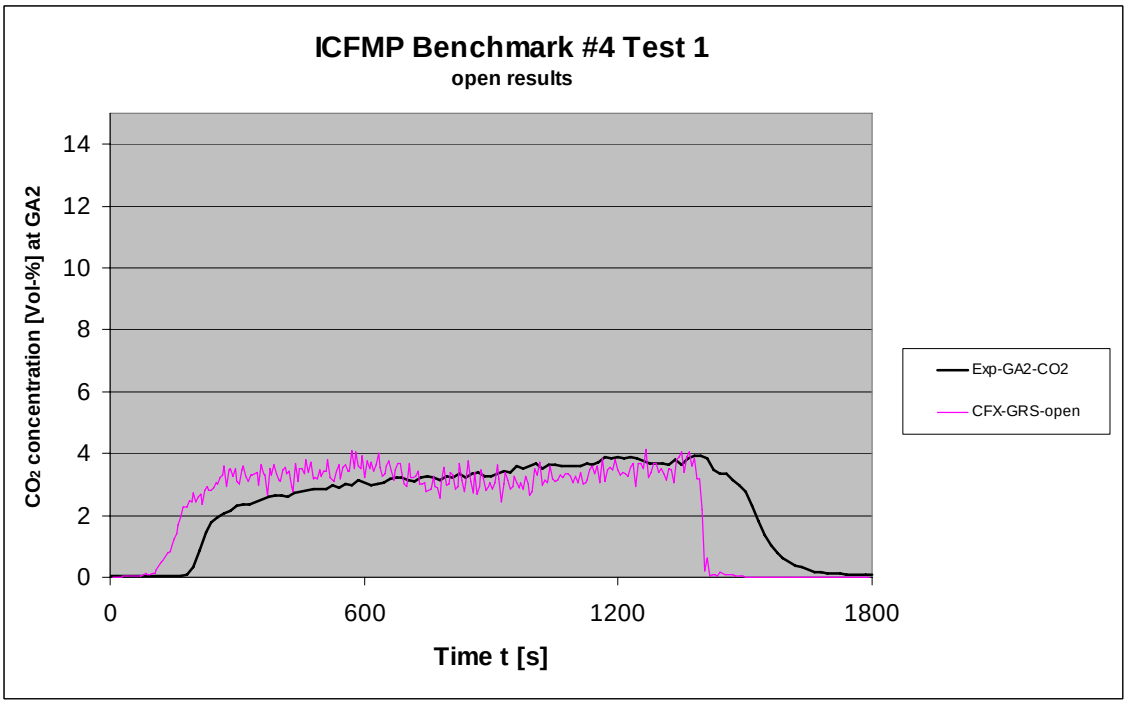

Fig. 6-14 CO_2 concentration outside the fire compartment

6.1.5 Probe Temperatures

The results of the probe temperature measurements have been delivered for the semi-blind and blind calculations only. The simulation results of CFAST performed by NIST show an unstable behaviour for aerated concrete. The calculated surface temperatures for concrete and steel are much too high. Most of the other CFAST calculations overestimate the surface temperatures. The results of the blind JASMINE simulations are too low. FDS overestimates the temperatures at least approx. 100 K in the semi-blind simulations. For the open calculations probe temperature results have been delivered for MAGIC only. The calculated target temperatures are generally higher than measurements.

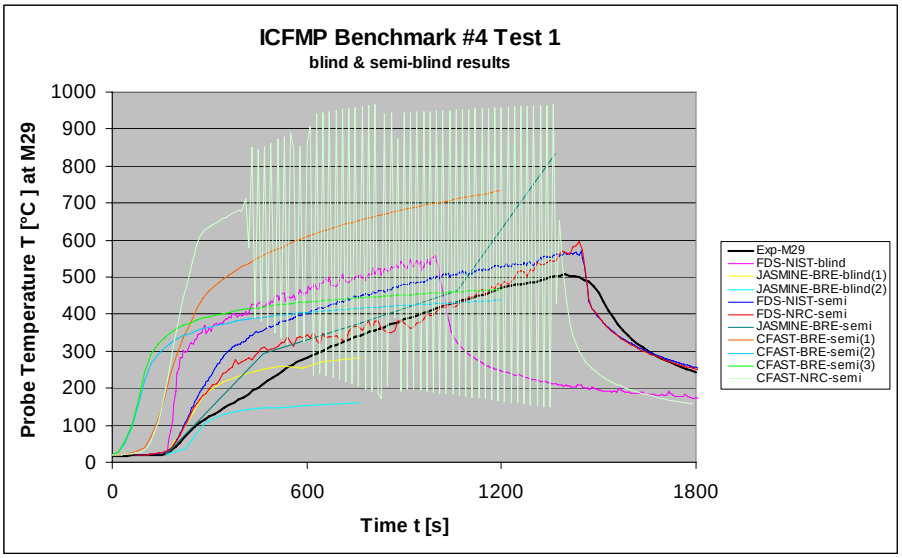

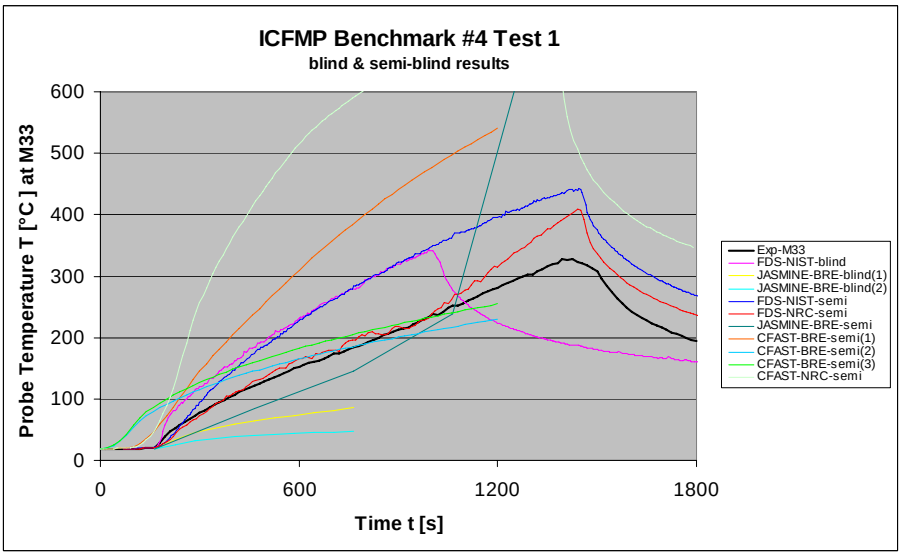

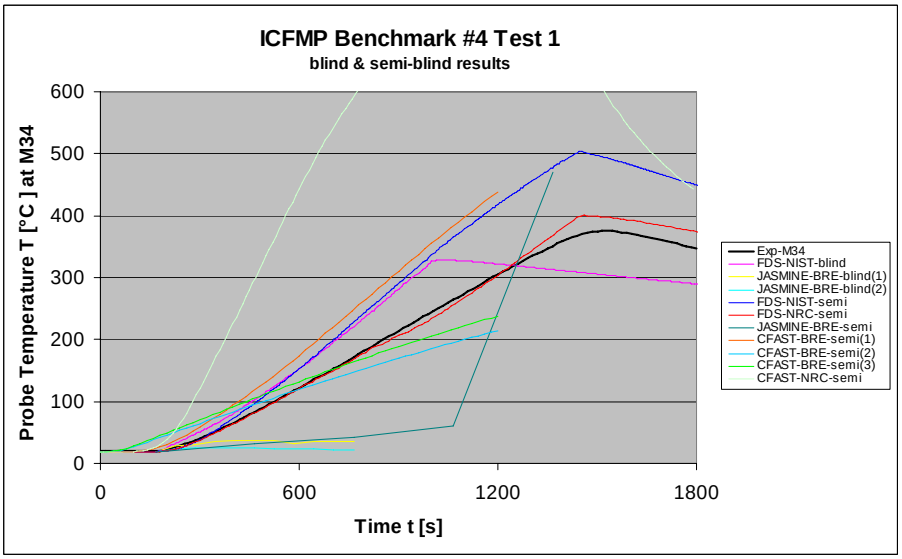

Fig. 6-15 Probe temperatures (blind results)

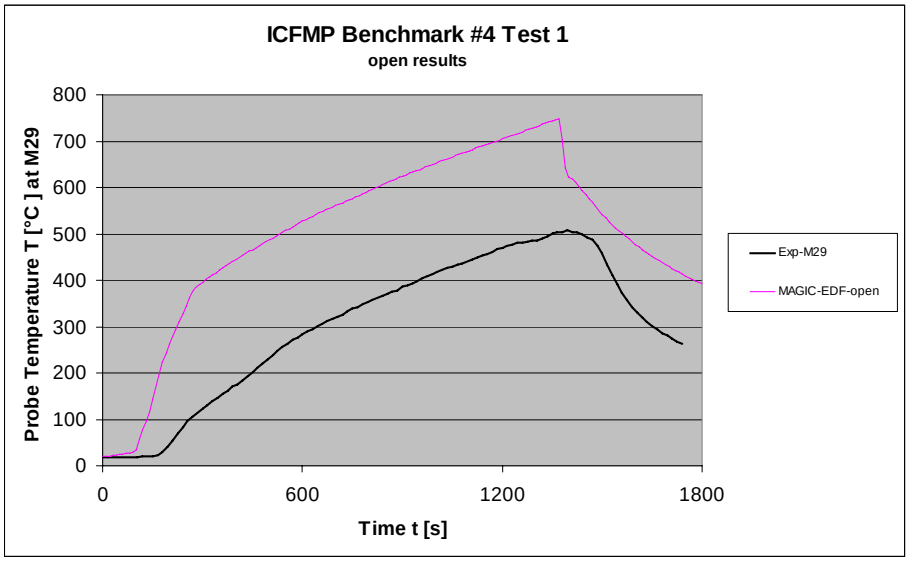

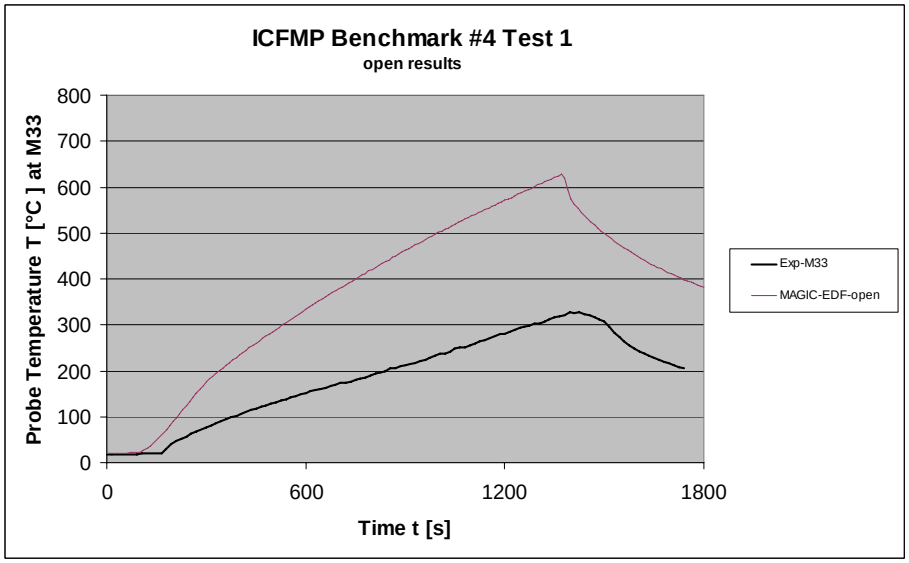

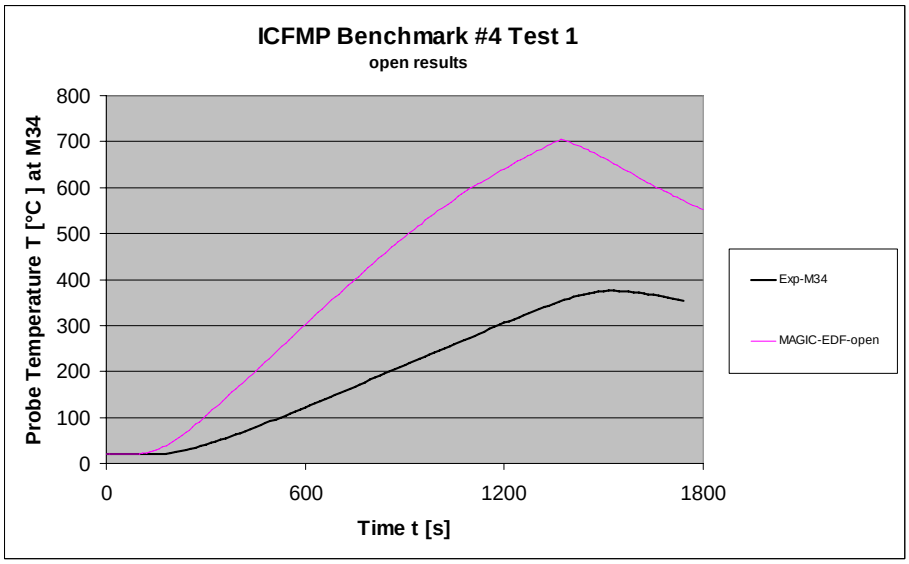

Fig. 6-16 Probe temperatures (open results)

6.2 Test 3

6.2.1 Plume Temperatures (M1 to M6)

Fig. 6-17 and Fig. 6-18 shows the comparison of the plume temperatures M2 and M6 for blind and open calculations. The measured plume temperature in the lower part of fire compartment, such as M1, show a strong temperature increase in the initial phase to values up to 700 °C. At the end of the fire, the temperatures increase again, reaching values of approx. 900 °C. Most of the codes predict temperatures that are much lower that measured toward the end of the experiment. The differences are about 100 to 200 K. In the upper part of the plume, the measured temperature rise is much slower than the calculated ones. Starting with values of approx. 350 °C, values up to 900 °C are reached with a final peak at about 1000 °C. In the blind simulations, the plume temperature increase is underestimated. The results are partly better in the open calculations (e.g. CFX). However, deviations of up to 200 K are possible. It has to be stated that the situation at the end of the fire is more questionable. The simulation strongly depends on the assumptions which have been made for the pyrolysis rate. The peak is simulated approx. 250 s too early. The pyrolysis rate provided to participants could be examined for improvement.

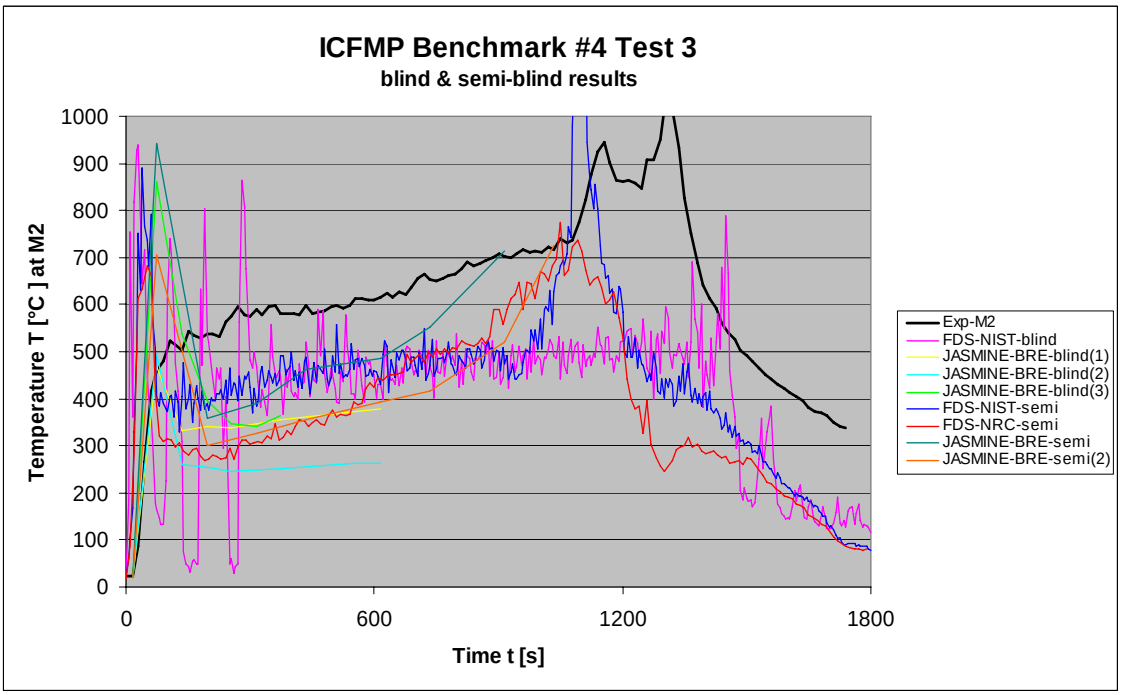

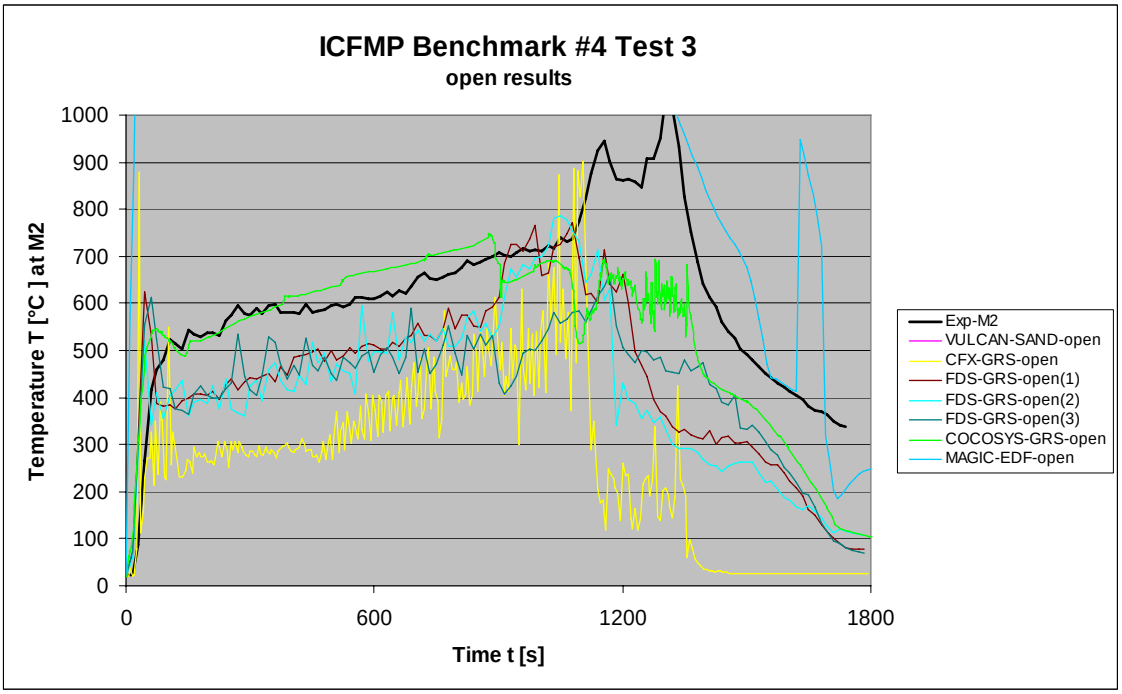

Fig. 6-17 Comparison of plume temperatures M2 (blind & open)

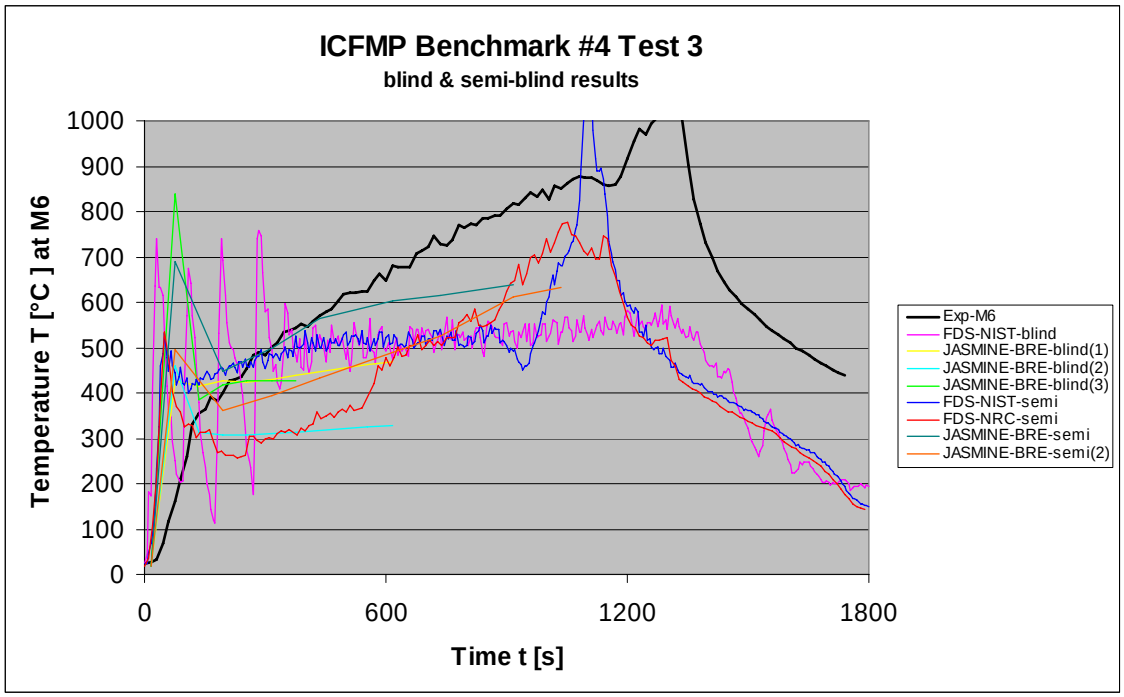

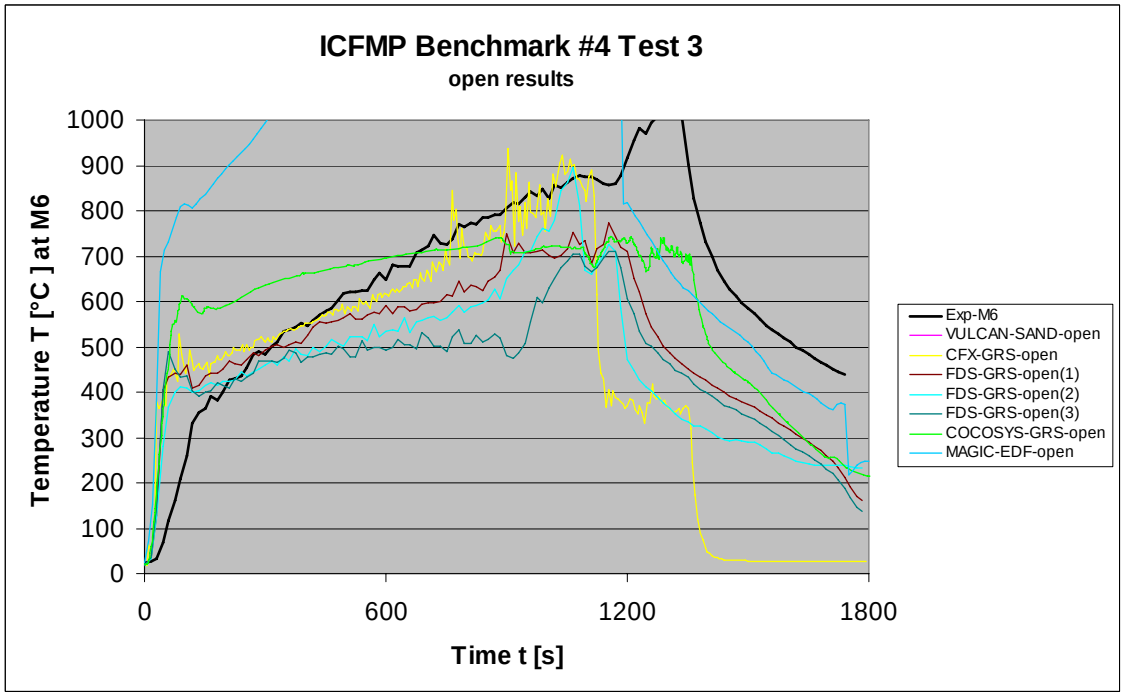

Fig. 6-18 Comparison of plume temperatures M6 (blind & open)

6.2.2 Temperatures inside the Fire Compartment

Fig. 6-19 to Fig. 6-24 present the comparison of blind and open calculations for two temperature trees. These are the measurement positions M8, M12 and M16 at the rear of the fire compartment close to the wall and the positions M9, M13 and M17 at the front. The deviations between the code results are partly quite high with approx. up to 500 K. JASMINE calculates very high temperatures at the rear (position M8), while the results are much better at the front. A possible reason is that a strong shift of the fire plume was calculated in the simulation. Similar to the plume temperatures, the temperature gradient is underestimated by most of the codes. The open CFX calculation shows a somewhat better simulation of the temperature gradient. But, similar to the plume temperature, the measured temperature peak was not calculated. At about 550 s the VULCAN simulation shows a temperature decrease, which was not observed in the experiment. COCOSYS does not solve the momentum balance. Therefore, a plume shift can not be calculated and the results for back and front side are very similar. A temperature peak was also not simulated.

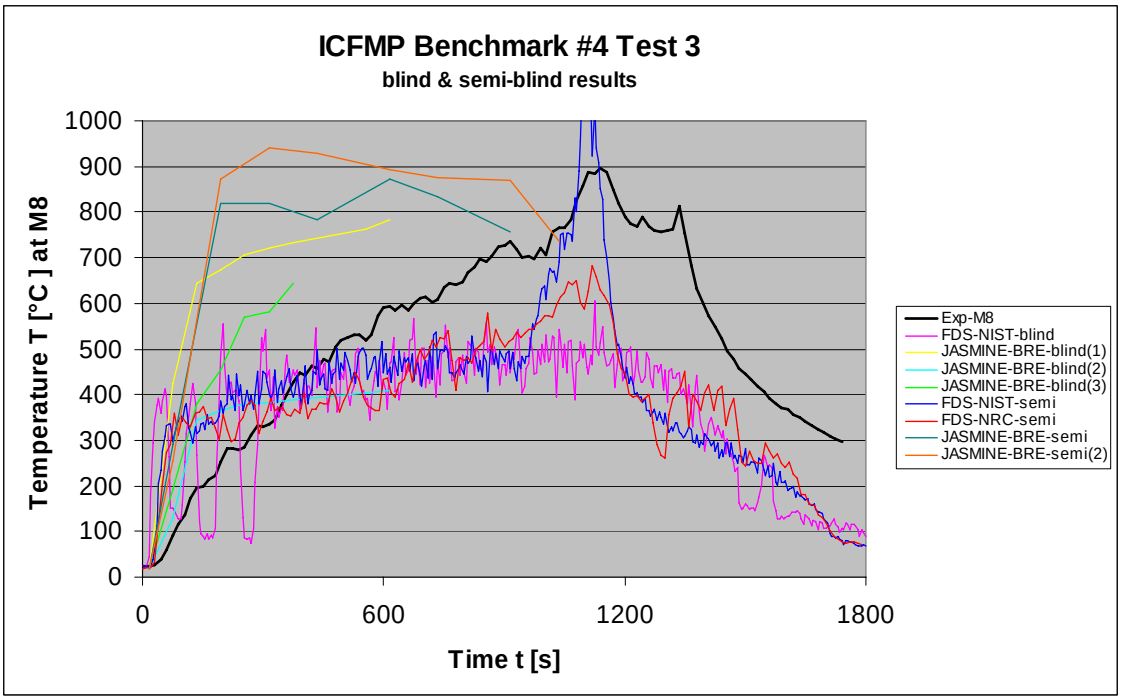

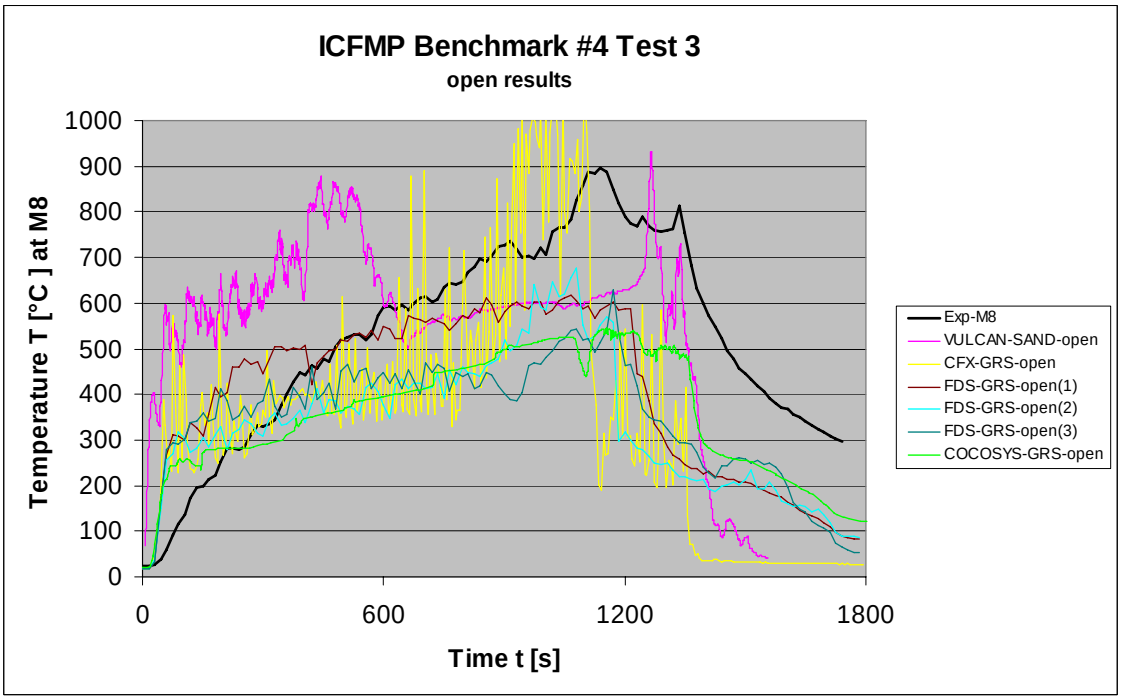

Fig. 6-19 Temperatures on the back of compartment (M8, blind & open)

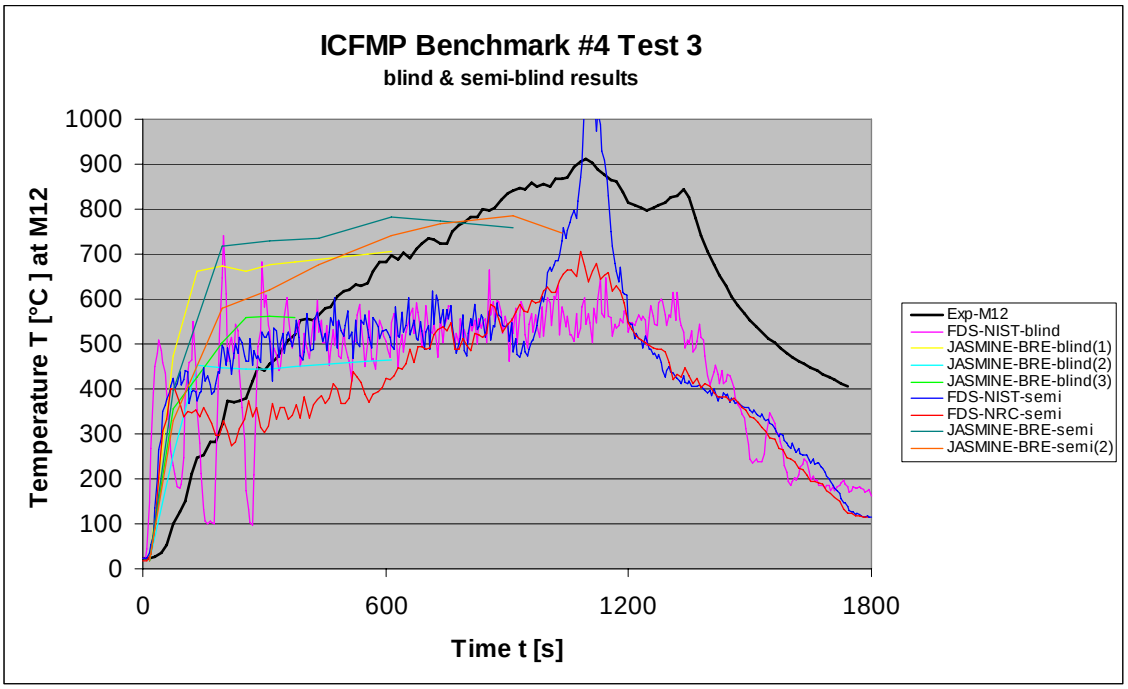

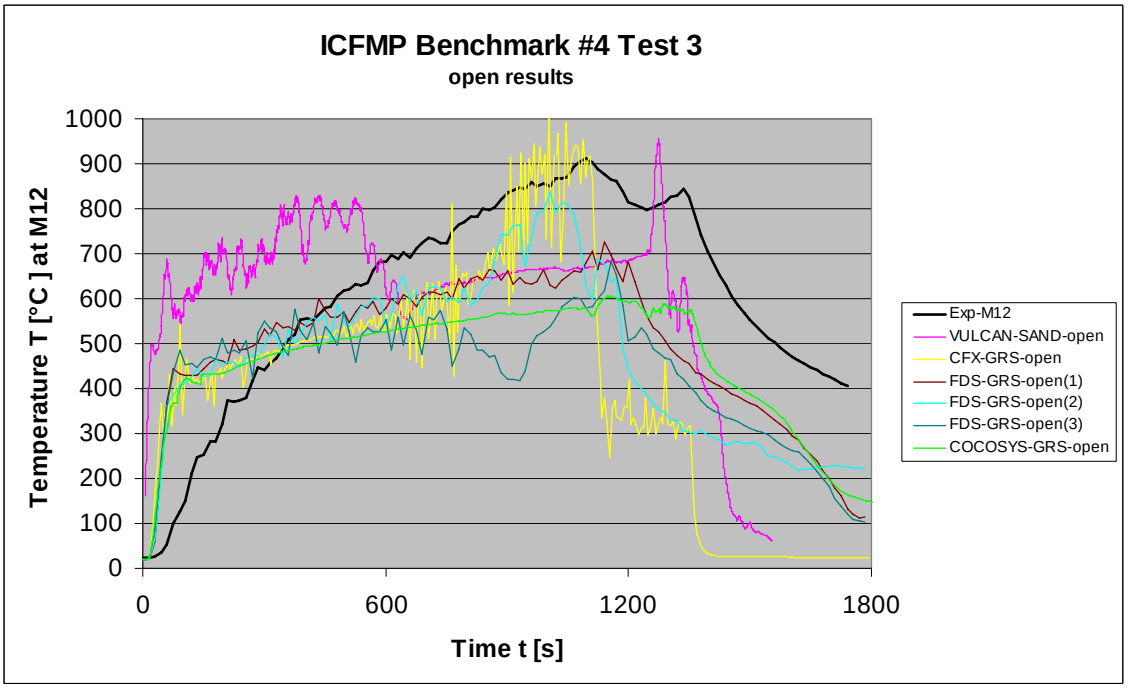

Fig. 6-20 Temperatures on the back of compartment (M12, blind & open)

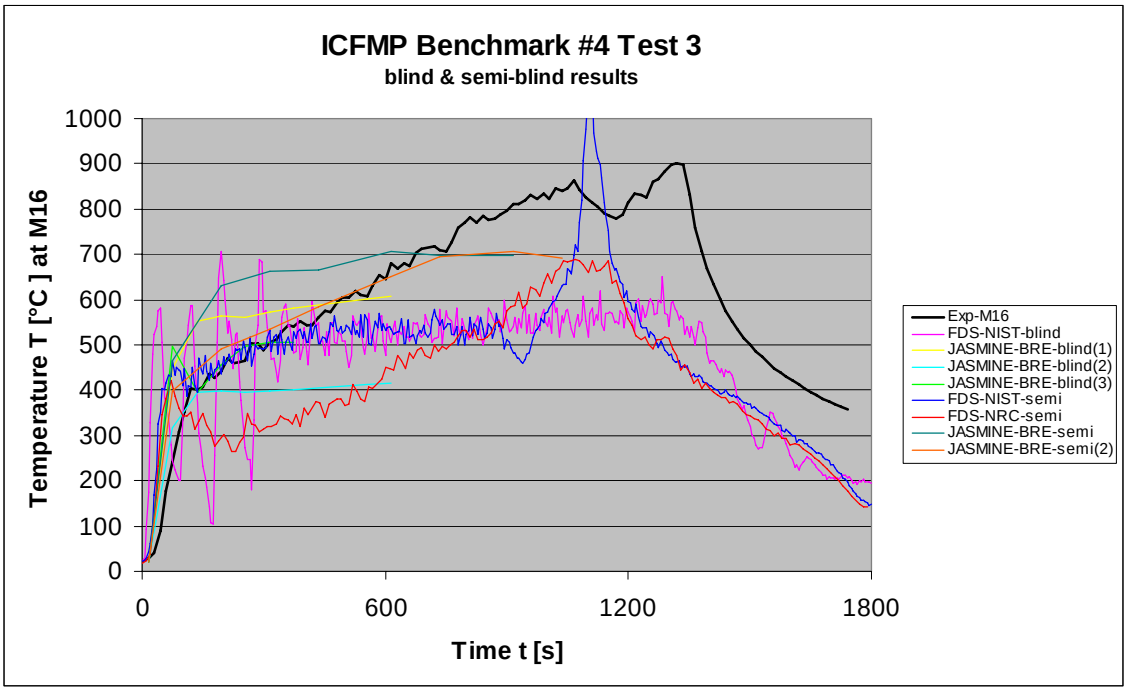

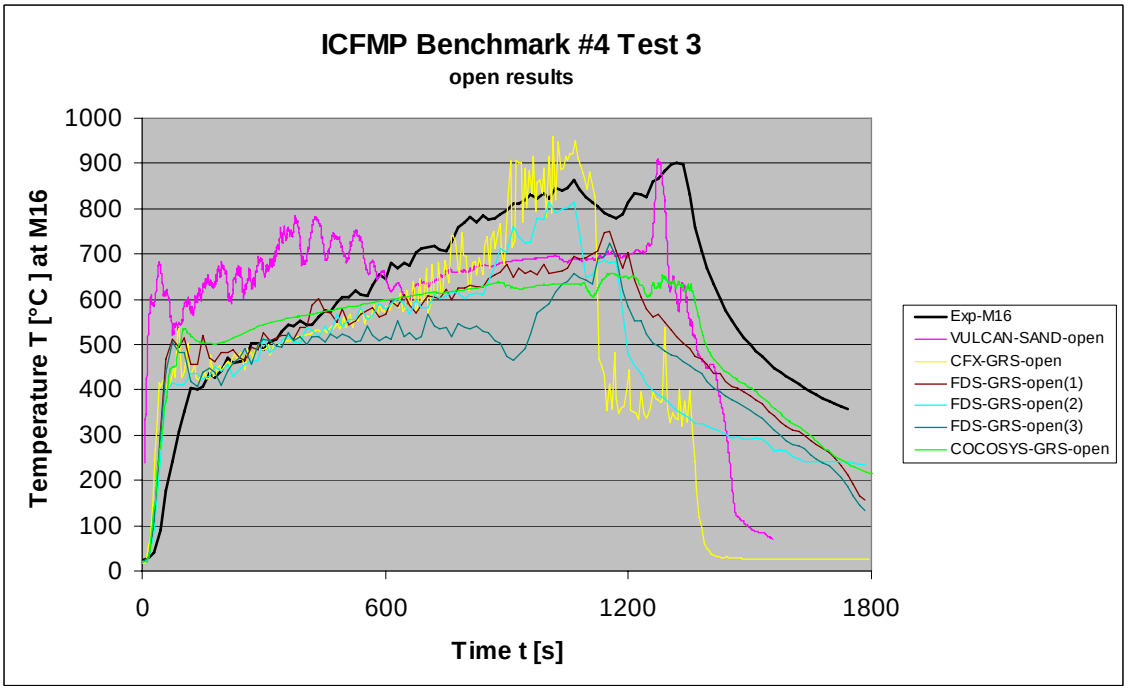

Fig. 6-21 Temperatures on the back of compartment (M16, blind & open)

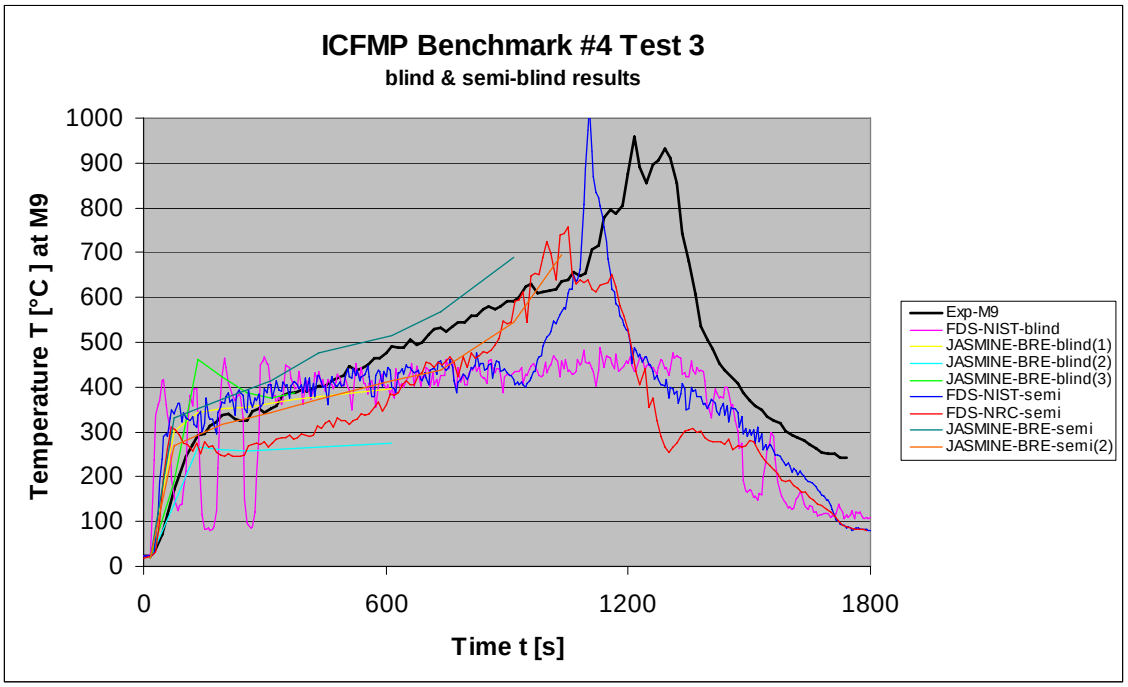

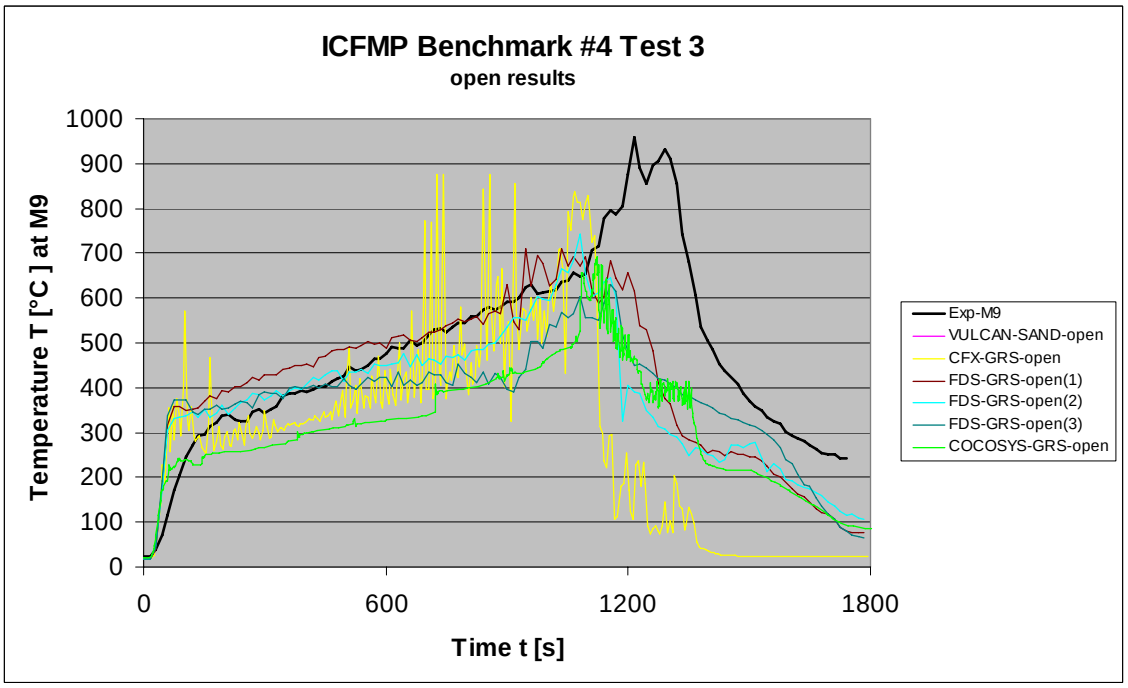

Fig. 6-22 Temperatures on the front side of compartment (M9, blind & open)

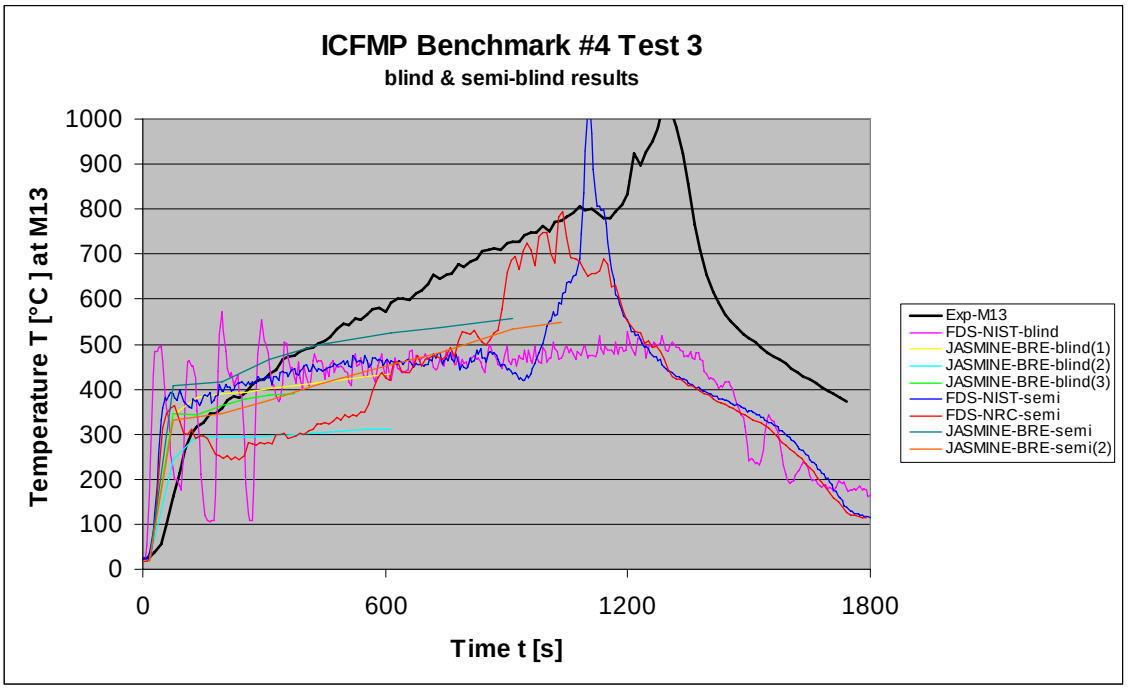

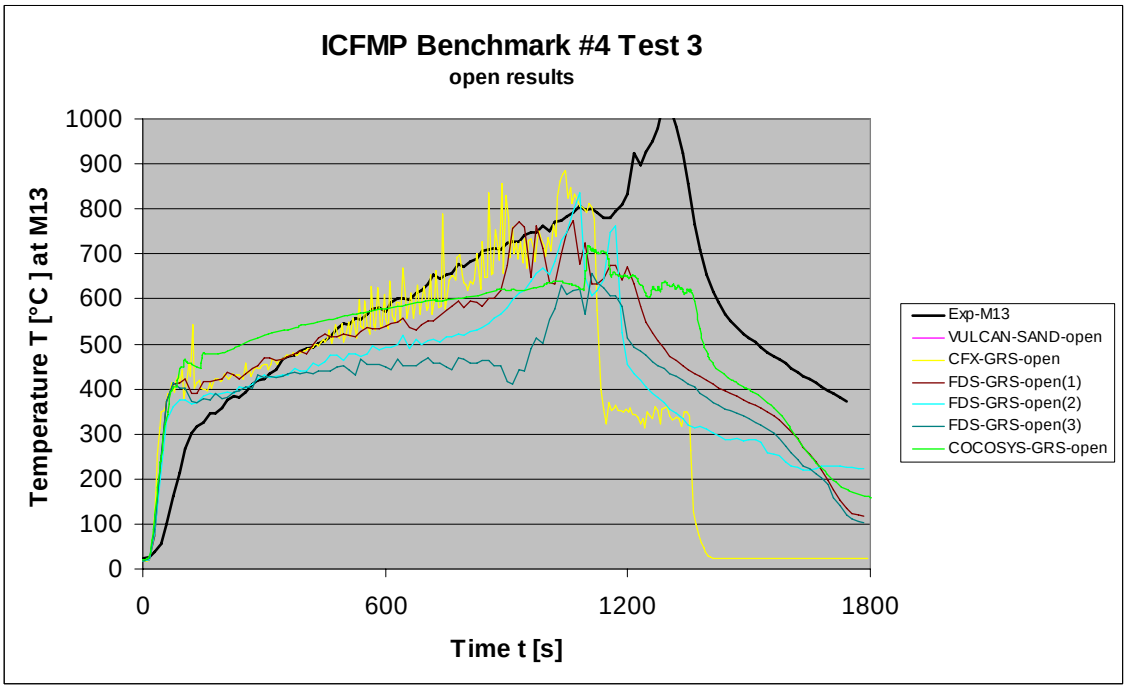

Fig. 6-23 Temperatures on the front of compartment (M13, blind & open)

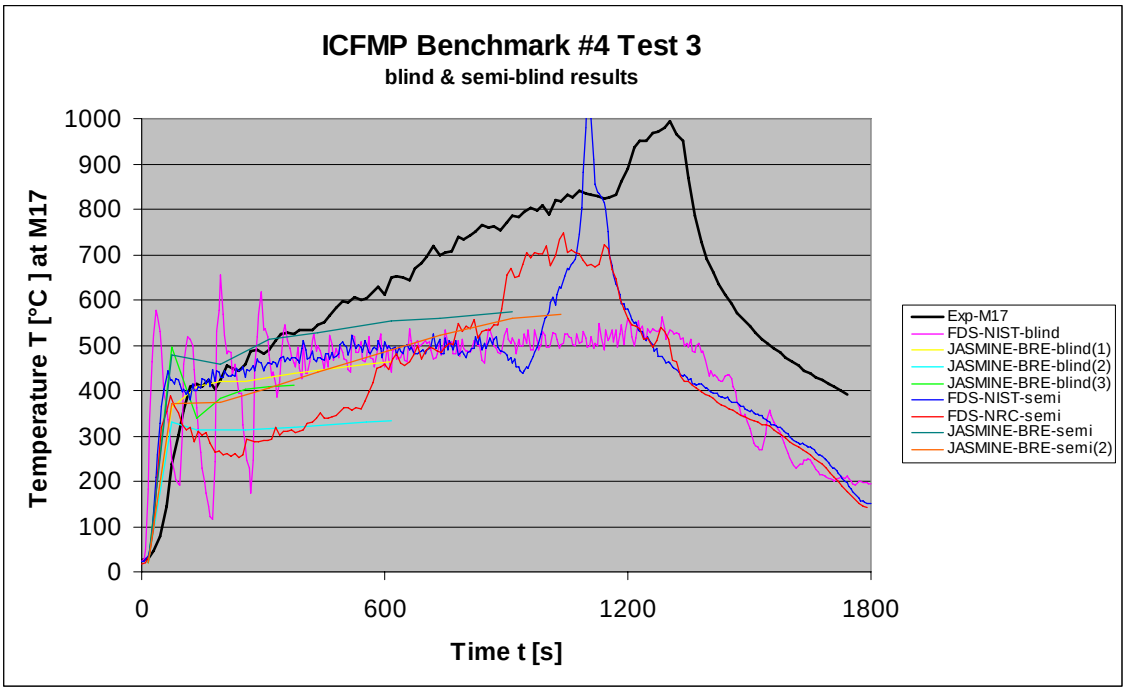

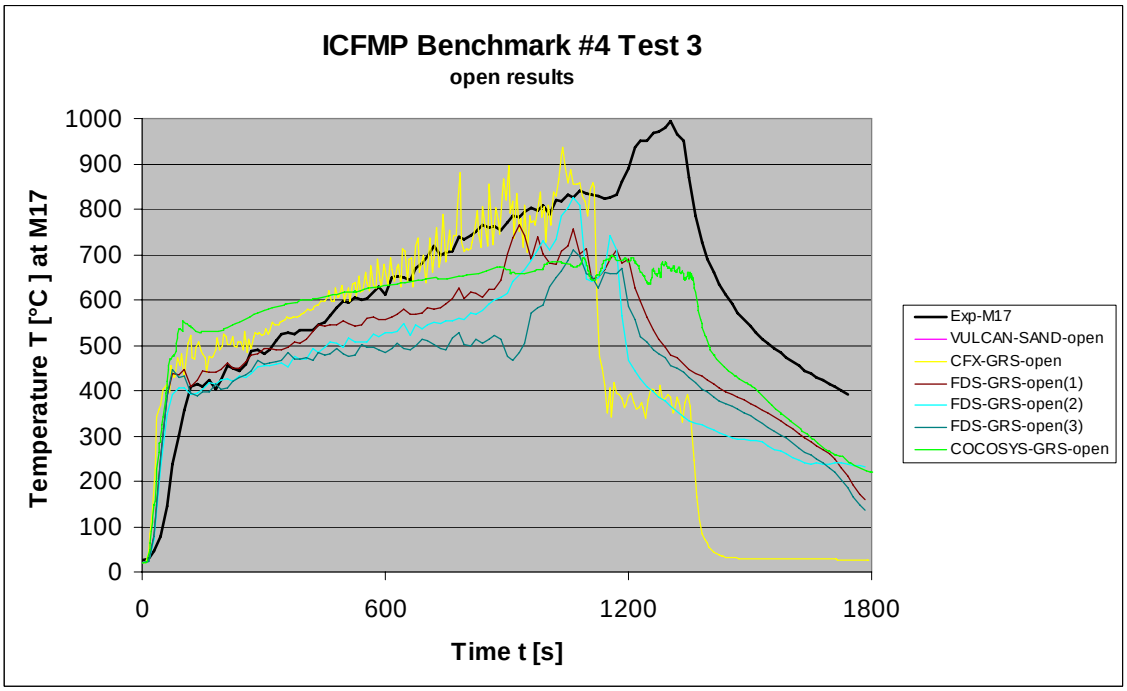

Fig. 6-24 Temperatures on the front of compartment (M17, blind & open)

6.2.3 Layer Height and Upper Layer Temperature

Only three levels of measurements are available inside the fire compartment. Therefore the calculation of the upper layer temperature and the hot gas layer height is questionable. Fig. 6-25 and Fig. 6-26 present the comparison between the results of zone models and experimental results. The calculated layer heights are lower compared to the experiment, In particular close to the floor level. Because the lowest elevation of the measurement is located at 1.5 m, the experimental result cannot be lower.

The semi-blind CFAST calculations performed by different users show a strong deviation of 300 K for the upper layer temperature. Results from open calculations are provided by the code FLAMME-S and MAGIC. The results of MAGIC are quite close to the experimental results. Concerning FLAMME-S it has to be pointed out that this Benchmark Exercise is out of the validated range of this code. The simulated temperatures are too low in comparison to the experimental data.

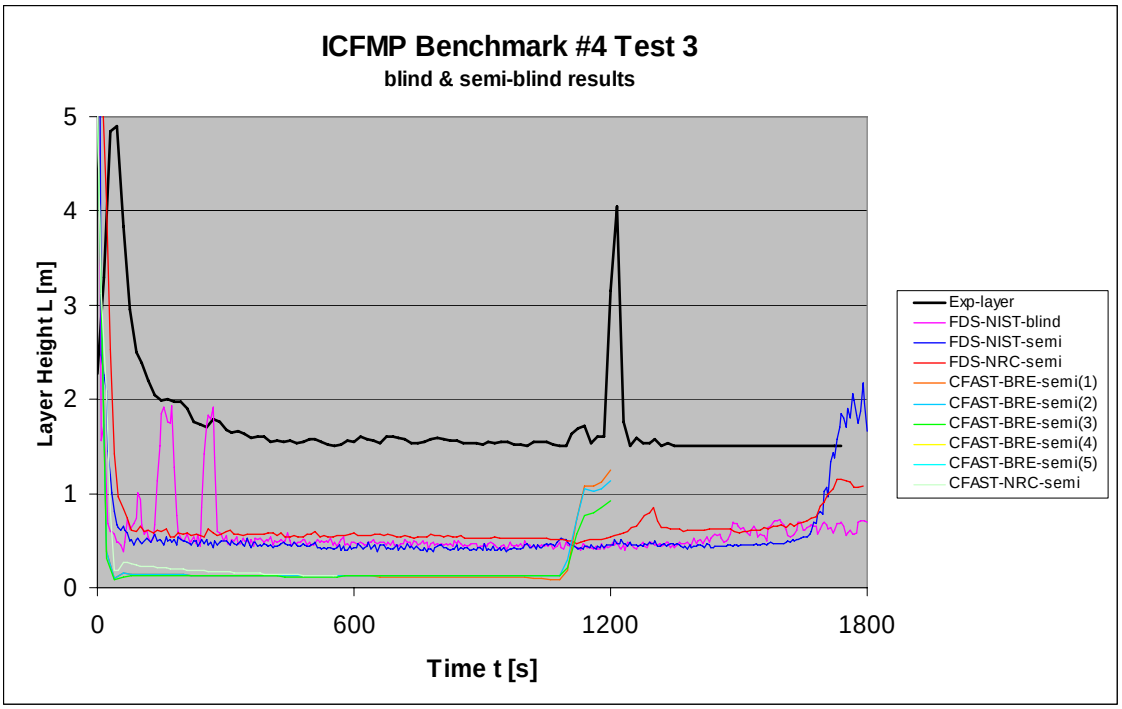

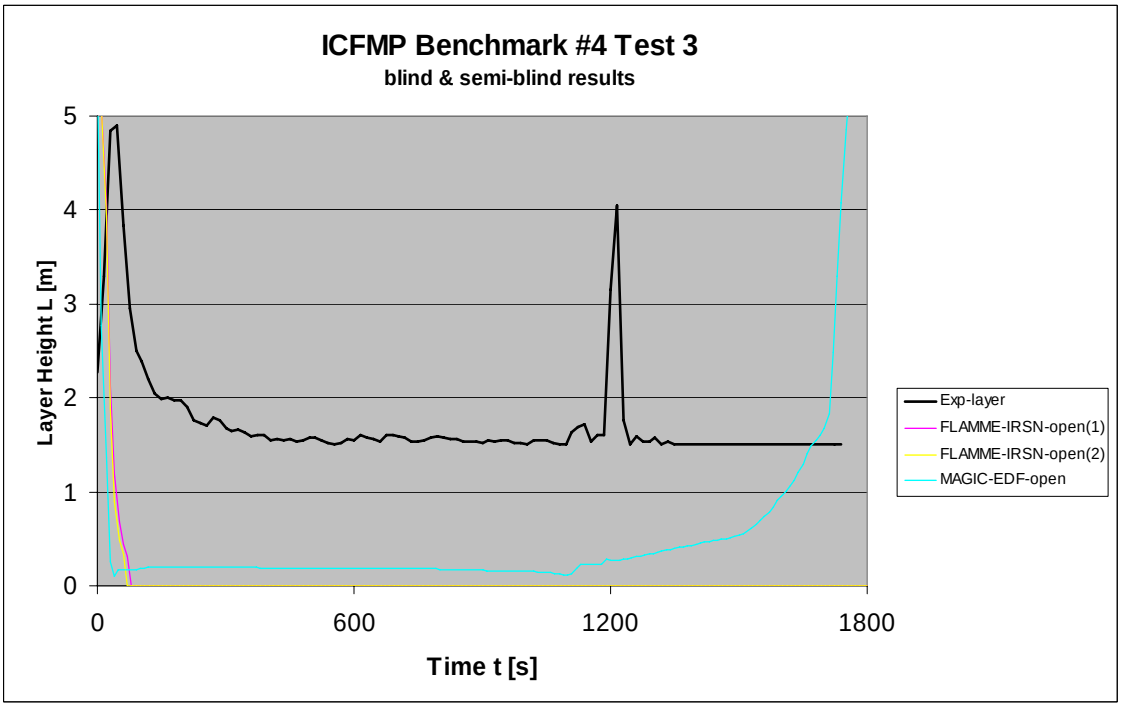

Fig. 6-25 Hot gas layer height (blind & open)

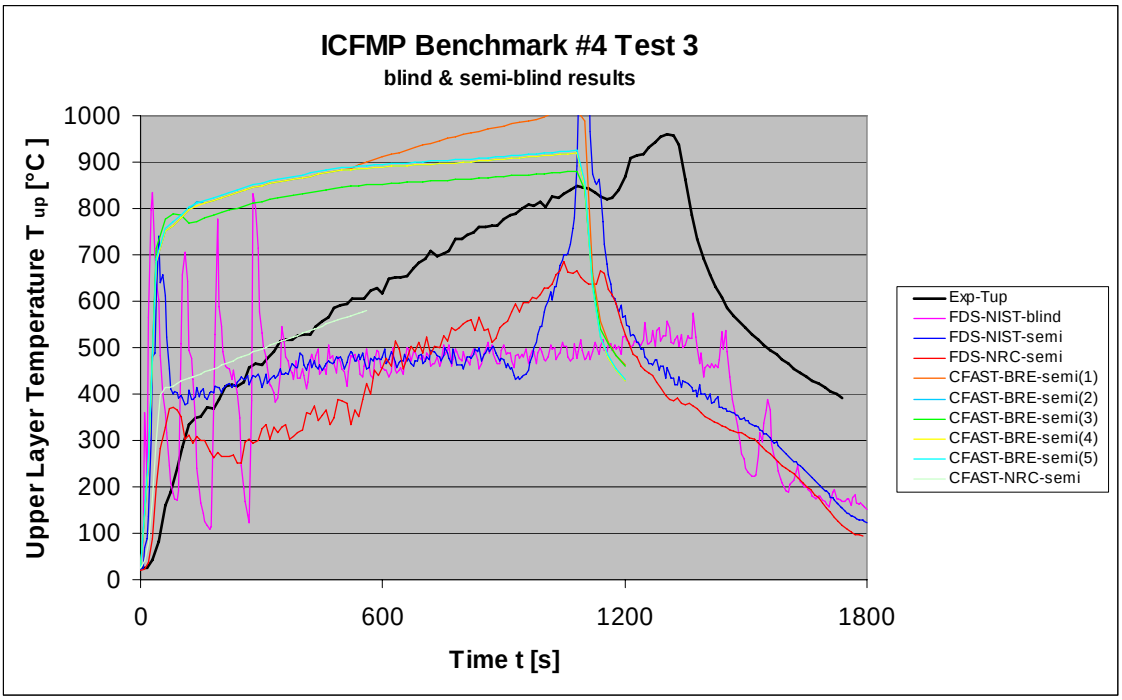

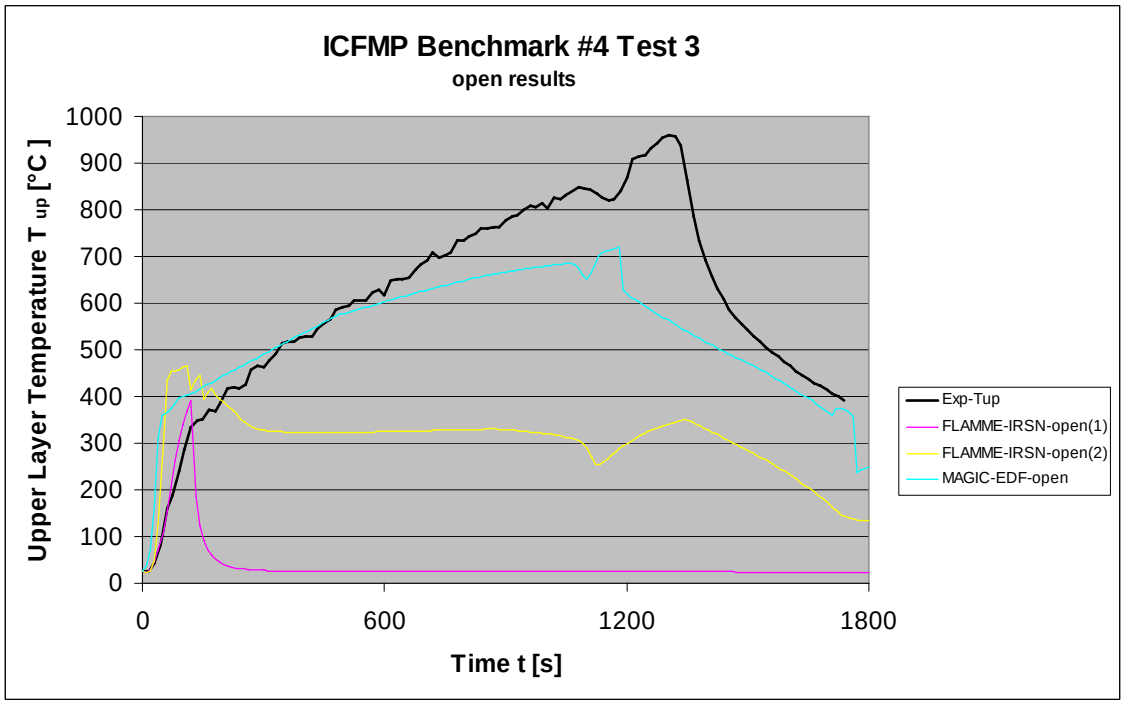

Fig. 6-26 Upper layer temperature (blind & open)

6.2.4 Gas Concentrations inside the Fire Compartment

Fig. 6-27 to Fig. 6-30 provides a comparison of the results for the gas concentrations inside and outside the fire compartment. The elevation of the inside measurement position is 3.2 m above the flame. The blind and semi-blind FDS calculations are in reasonably good agreement with measurement. The oxygen concentration is underestimated by about 2 Vol.-%. The definition of the pyrolysis rate for the semi-blind calculations leads to oxygen concentrations close to 0 Vol.-%. According to the pre-defined peak, the decrease of oxygen arises approx. 100 s too early. The semi-blind CFAST calculation performed by NRC and the open MAGIC calculation show a much too low oxygen concentration, although the calculated upper layer temperature is quite similar to the experimental data. In the open calculations, the deviation range of the results for the oxygen concentration GA1 is quite large at about 7 Vol.-% (without considering the FLAMME-S results). Except for one FDS calculation, the oxygen concentration is underestimated. The behavior of VULCAN is somewhat different compared to the other codes. The complete oxygen depletion already occurs at approx. 500 s. This could explain the different characteristics for the temperature results.

With respect to the CO_2 concentration a similar picture could be drawn. Unfortunately, no experimental data are available for the position GA1. But the variation in the open calculations is even higher compared to the blind calculations. The semi-blind calculation of FDS performed by NIST shows a strong peak in the oxygen and carbon dioxide concentrations (position GA2) at the end of the fire process. This was not been observed in the experiment. Furthermore, the other FDS simulations do not show such a peak. Similar peaks have been calculated in the open phase with CFX and FDS. This shows that the given pyrolysis rate may be somewhat questionable at the end of fire process.

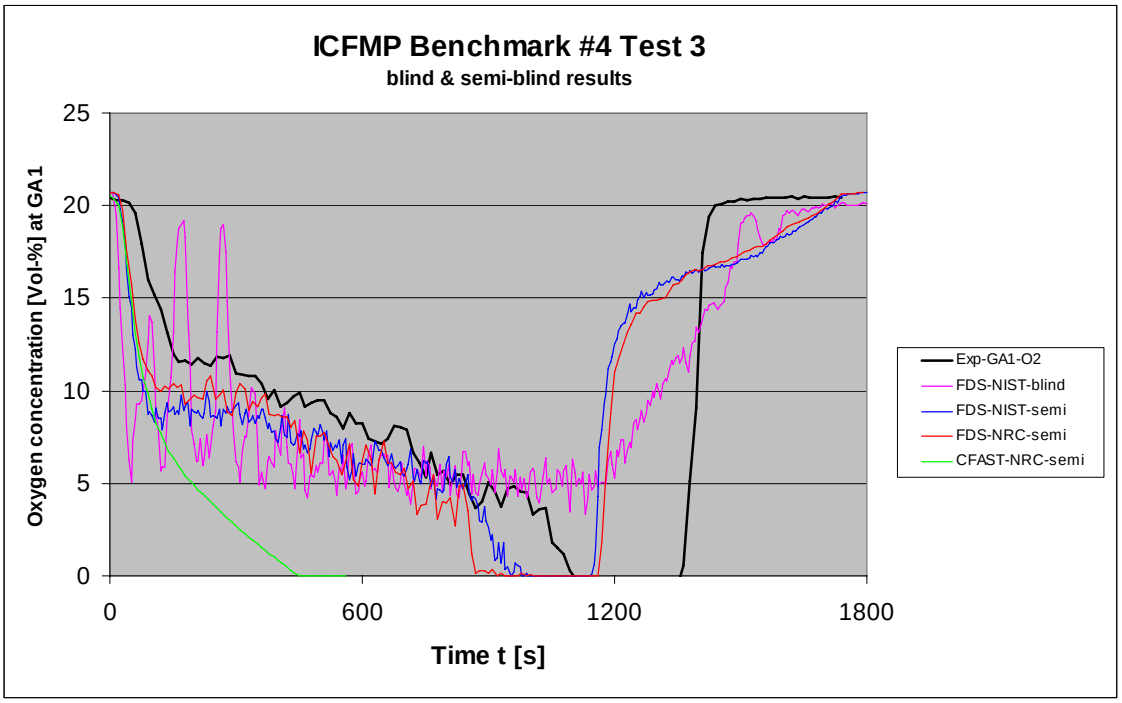

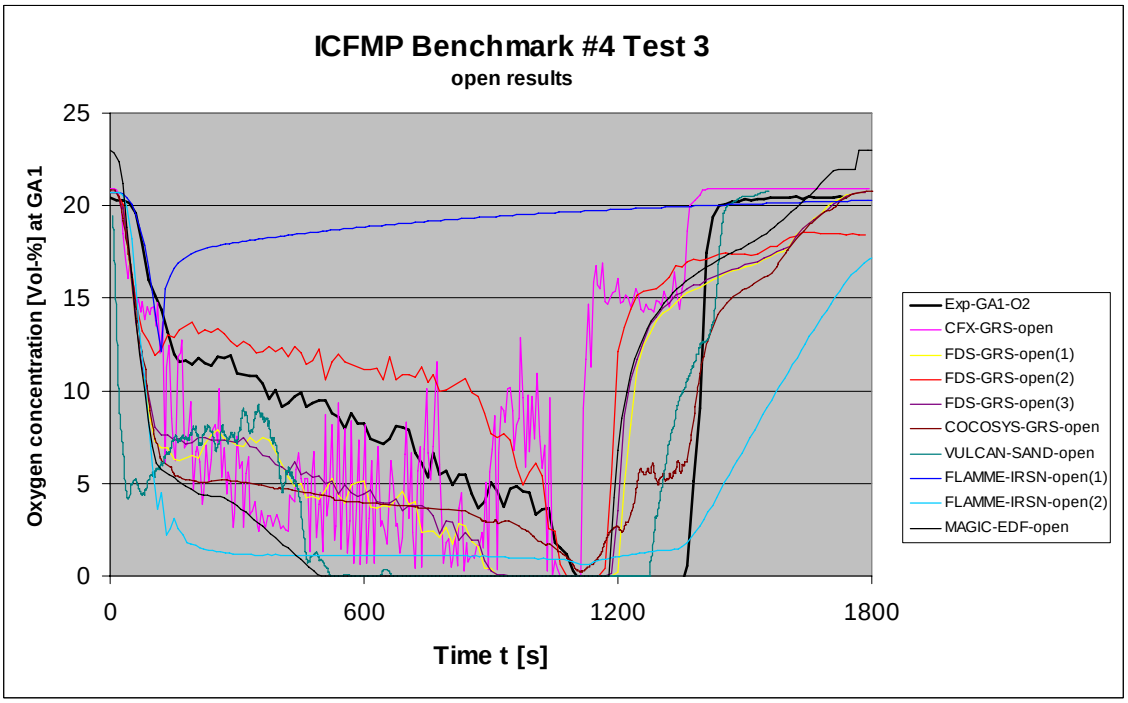

Fig. 6-27 Oxygen concentration inside fire compartment (blind & open)

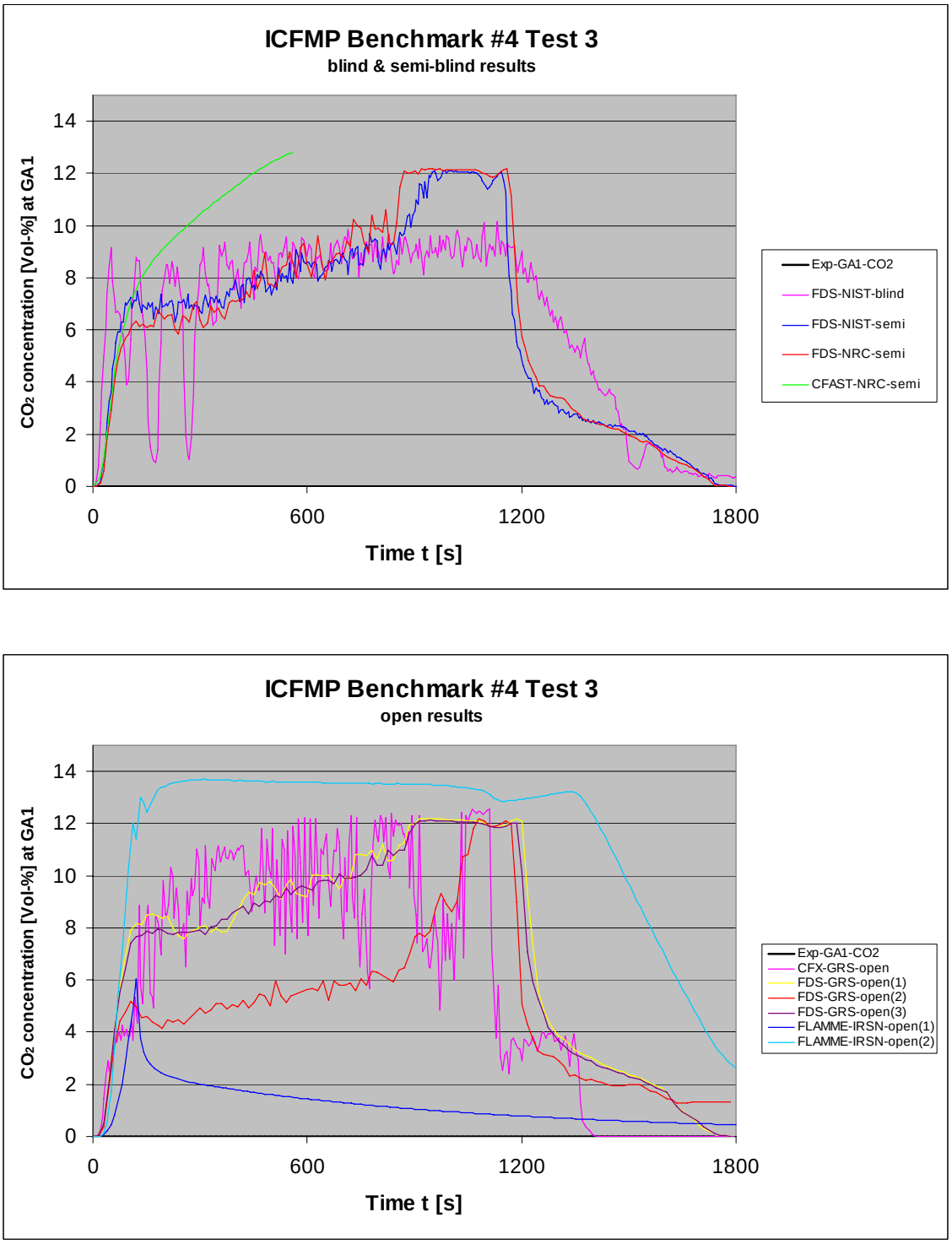

Fig. 6-28 CO_2 concentration inside fire compartment (blind & open)

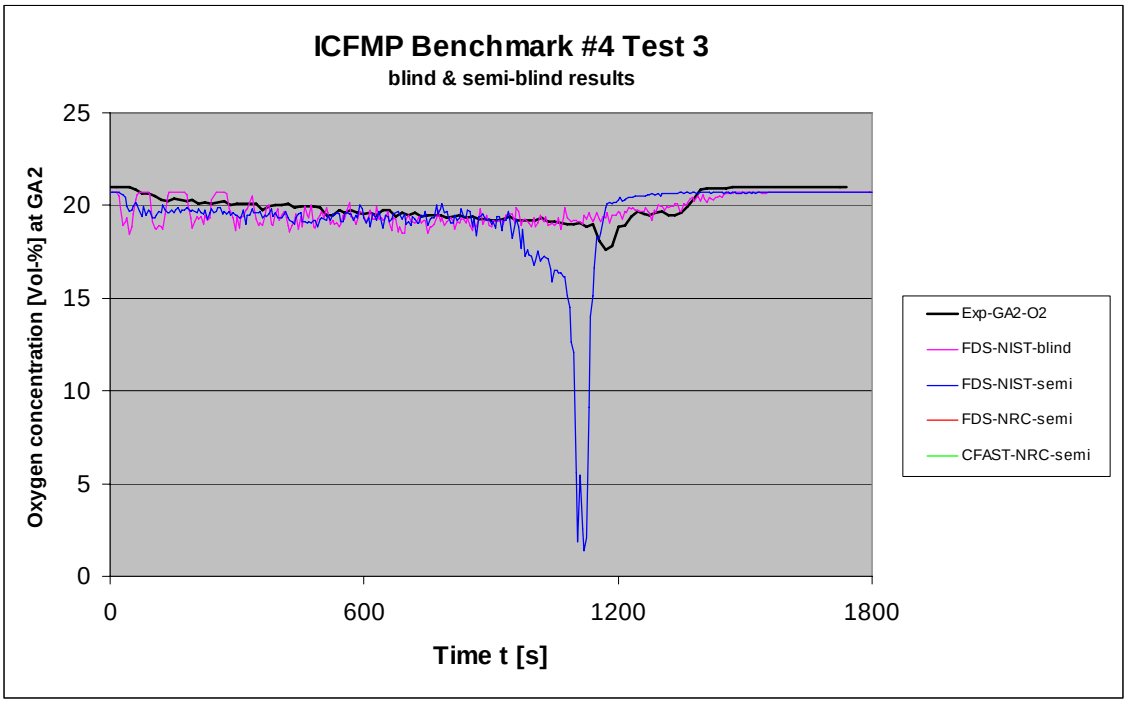

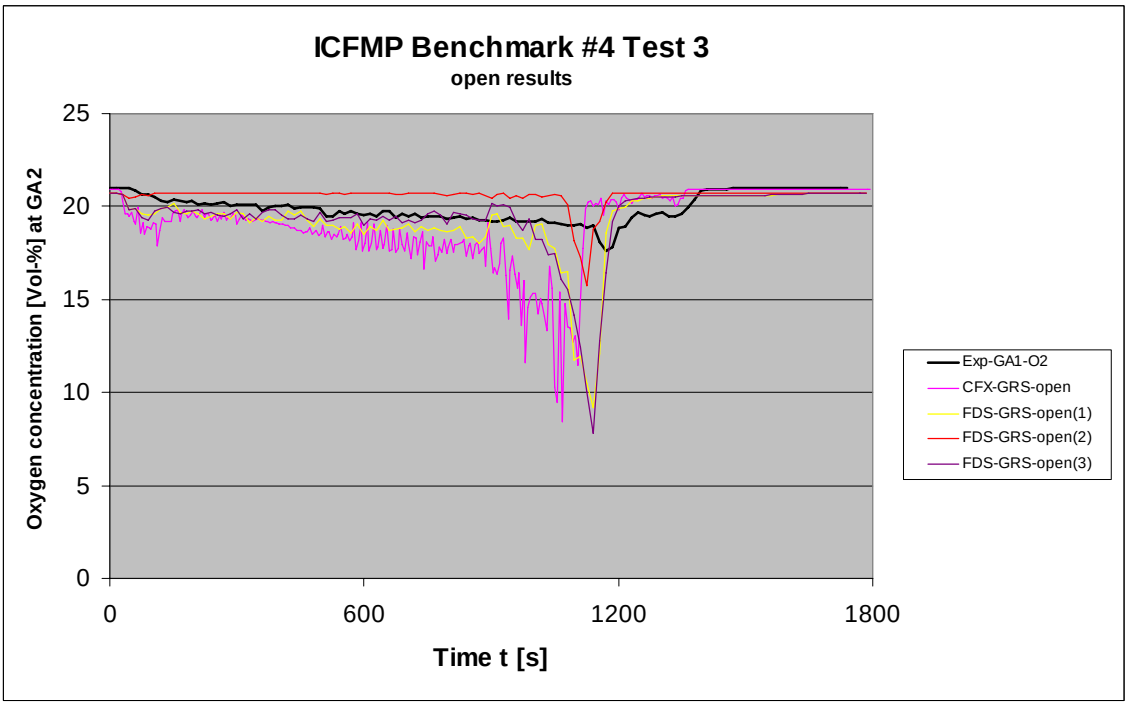

Fig. 6-29 Oxygen concentration outside fire compartment (blind & open)

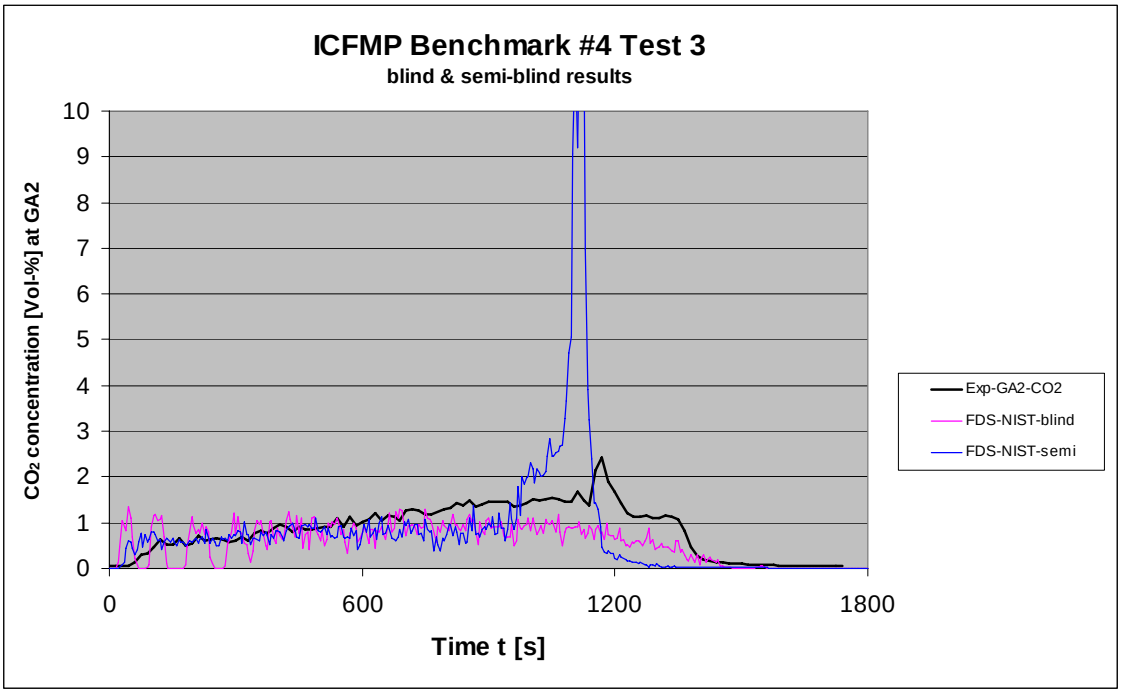

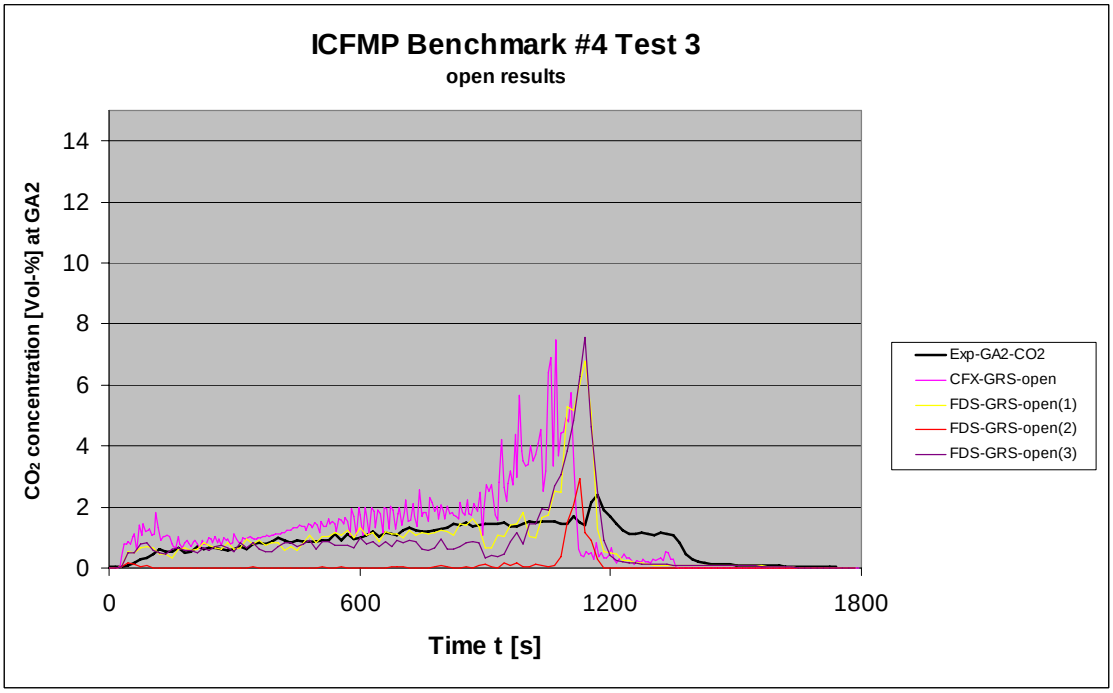

Fig. 6-30 CO_2 concentration outside the fire compartment (blind & open)

6.2.5 Probe Temperatures

One of the main objectives of fire simulations codes for NPP applications is the estimation of thermal loads on different type of targets. On the left wall of the compartment three material probes of different material types, concrete, aerated concrete and steel have been installed. Fig. 6-31 and Fig. 6-32 compare the calculated and experimental temperatures close to the material surface. The results of the blind calculations show a wide range of deviations. The semi-blind CFAST calculation performed by BRE overestimates the temperatures by about 300 K while most of the CFD codes underestimate the temperature by up to 300 K. The strong temperature peak simulated by some CFD codes as a result of the peak in the pyrolysis rate was not observed in the temperature measurements. The results of FDS for the open calculations are comparable to those for the blind simulations. The temperatures are underestimated by approx. 100 K. The results of VULCAN are on the one hand in a very good agreement with the experimental data, except the strong peak for aerated concrete. On the other hand the calculated temperature decrease at the end of the fire process is much too strong, indicating that the thermal heat conduction or heat transfer is not simulated correctly. The results of the open MAGIC calculation are reasonable and better compared to Test 1.

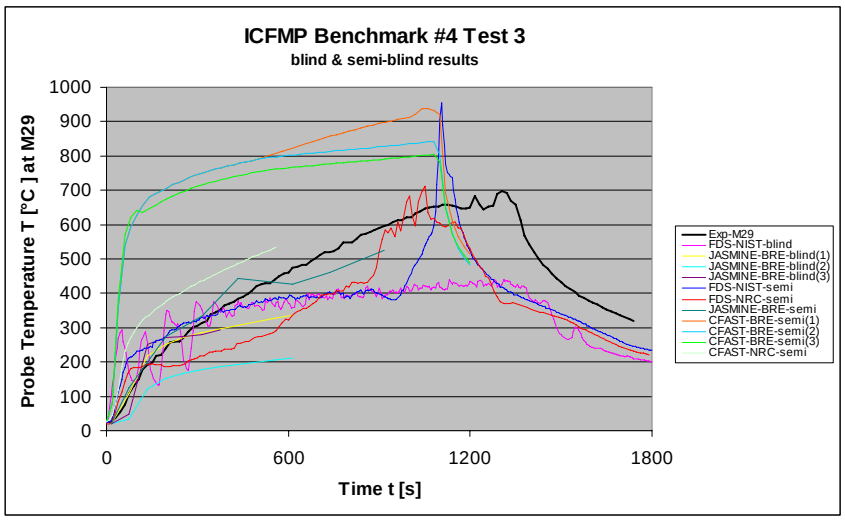

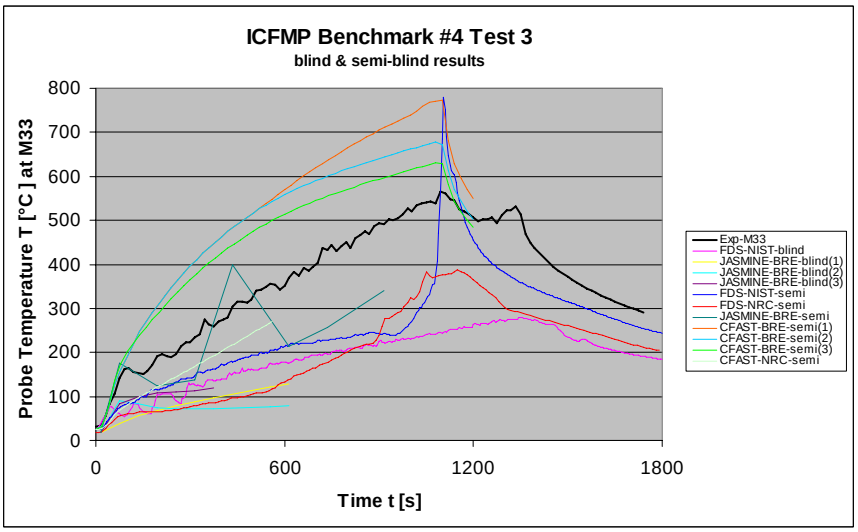

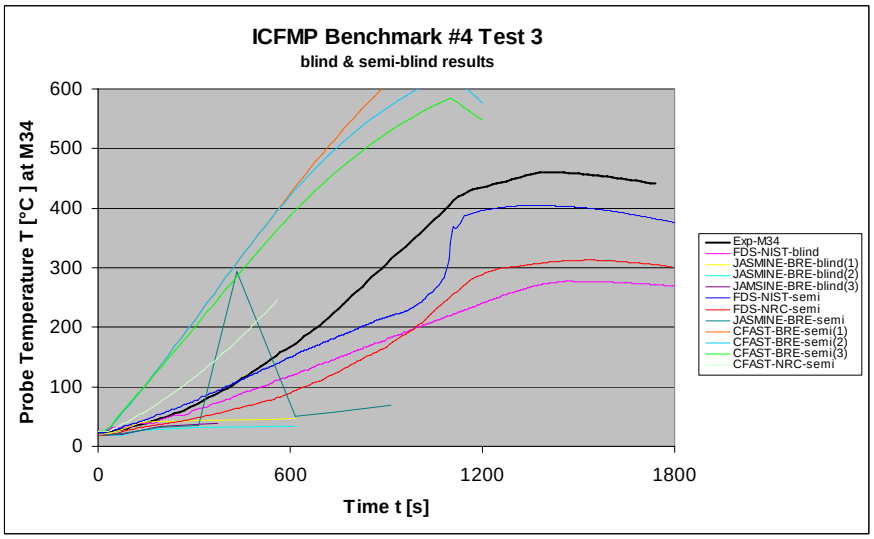

Fig. 6-31 Comparison of the probe surface temperatures (blind simulations)

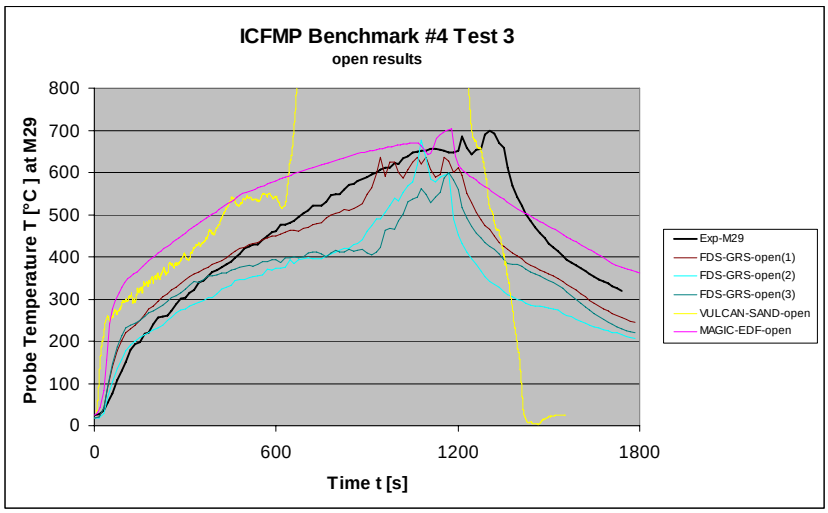

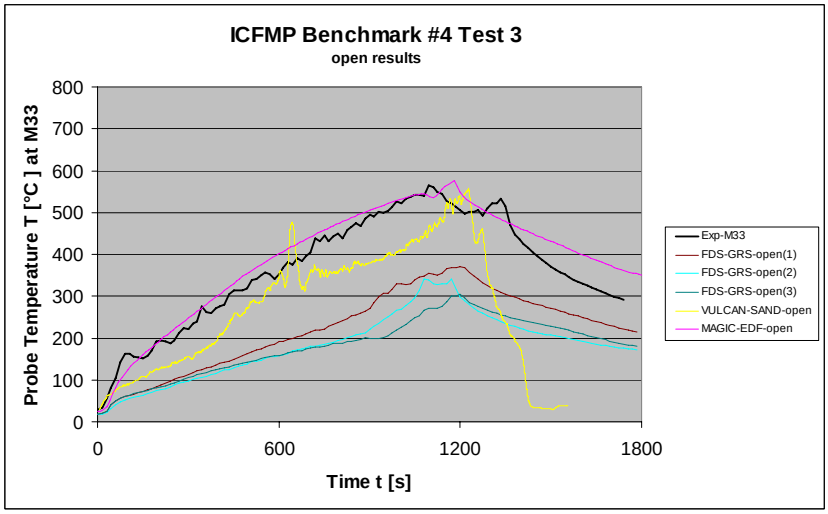

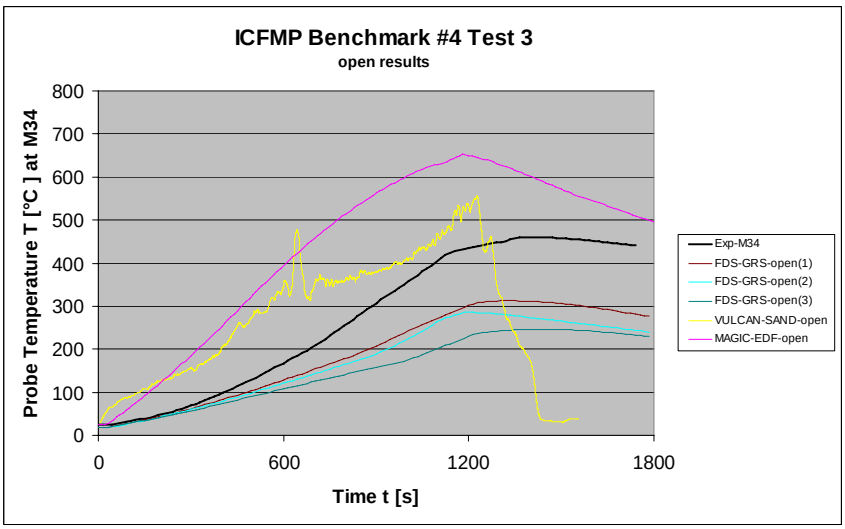

Fig. 6-32 Comparison of the probe surface temperatures (open simulations)

7 General Conclusions and Recommendations

7.1 General Conclusions

This section provides a discussion of the general conclusions derived from Benchmark Exercise No. 4.

Heat Release Rate

The pyrolysis rate and the resulting heat release rate have a great impact on the thermo-fluid conditions inside the fire compartment. The specified (measured) rate for Test 1 seems to be satisfactory, because reasonable temperatures were calculated. The rate for Test 3 is more questionable, because the temperature peak at the end of the experiment is not simulated and the calculated temperature decrease starts too early. On the other hand, due to the under-ventilated conditions, the combustion usually is incomplete and possibly under-estimated.

Blind calculations show that the models to calculate pyrolysis rates are still limited. The results of these calculations show significant deviations from the experimental results.

Gas Temperatures

The overall gas temperatures could be reasonably well simulated by zone models as well as by the more complex CFD codes, although the differences for Test 3 are larger. The CFD codes were able to simulate the drift of the flame to the rear wall due to the fresh air entrainment through the door. However, in comparing the lower temperatures at the measurement locations M8 and M10 at the rear of fire compartment, this effect seems to be over-estimated in the simulations. Particularly for targets close to the fire, these effects may be more important.

Oxygen Concentration

Key parameters for the oxygen concentration inside the fire compartment are the combustion efficiency, the ventilation conditions, and the reaction schemes modeled, particularly for CO and soot production. Here, Test 3 gives some answers for the specification of the LOL value, which should be set to 0 Vol.-%. FDS with only one single transport equation shows some principal limitations in this range.

Wall Temperatures

Wall temperatures are partly influenced by the flame shifting to the back wall. This effect could be simulated, in principle, by CFD codes only. Zone codes assume homogeneous boundary conditions.

Ventilation – Air Entrainment

For zone models the handling of the air entrainment for under-ventilated conditions is important, particularly in Test 3. Here, specific assumptions have been made in some zone model calculations.

Target Simulation

The ability to simulate the targets is restricted in the various codes. Some problems result from the cylindrical shape of the barrel target as well as from the multi-layer material configuration. Radiation has an important influence on the thermal loading, and this has to be partly specified by the user.

7.2 Recommendations

The strong differences between calculations and experiments, in particular for the blind simulations, indicates that models to predict pyrolysis rates are strongly needed. Unfortunately, there is a strong positive feedback from the thermal environment back to fuel surface which then influences the pyrolysis rate. Further local effects, such as edges to the pan, may also have an influence on the pyrolysis rate. The consequences for the estimation of uncertainties should be discussed in more detail. In this context, further blind calculations (for new experiments) will be helpful.

Scenarios with under-ventilated fires are still difficult to simulate. It has to be kept in mind that such scenarios are typical for NPPs, as most of the fire compartments in a NPP can be assumed more or less closed during a fire.

The simulation of targets should be further improved and investigated. This is highly important, because potential failures (e.g. short circuits) may occur much earlier than the ignition of the target itself.

8 Summary

The fuel pool fire Tests 1 and 3, performed in the OSKAR test facility at iBMB of Braunschweig University of Technology at the end of 2003, have been included in the benchmarking and validation exercises of the International Collaborative Fire Model Project (ICFMP) as Exercise No. 4. The objective of the collaborative project is to share the knowledge and resources of various organizations to evaluate and improve the state of the art of fire models for the use in nuclear power plant fire safety assessments, covering deterministic fire hazard analysis (FHA) as well as fire probabilistic safety assessment (PSA) studies.

The main difference between the two experiments carried out is the size of the door area. Both experiments give first indications on the effects of ventilation and fuel controlled fires as well as on the thermal loading on different types of targets. Previous benchmark exercises within the ICFMP had shown that the simulation of these two phenomena should be improved.

During the benchmark procedure, the participants performed different types of calculations. These were totally blind simulations without knowledge of the measurements, semi-blind calculations with knowledge of the pyrolysis rate only, and completely open calculations. It has been demonstrated that the pyrolysis rate has a strong influence on the calculation results. Limited information on the pyrolysis rate affects the results to some extent. This finding was supported from the comparison of the (admittedly few) blind and semi-blind simulations. The range of the results (e. g. JASMINE and FDS) is much larger for the blind simulations compared to the semi-blind ones. This overall result of Benchmark Exercise No. 4 should be somehow considered in the estimation of uncertainty parameters as an input in, for example PSA studies.

The simulation of under-ventilated fires is more difficult for the fire codes. In particular, the high transient behavior at the final phase of Test 3 leads to a wide range of simulation results. Unfortunately, the measured pyrolysis rate is no longer valid in this phase, and so the ‘specified’ pyrolysis rate may not be very reliable at this time. It should be mentioned, however, that many of the possible fire scenarios in real nuclear power plants will lead to under-ventilated conditions. Therefore, this issue should be further investigated and the models should be further improved.

Some codes have difficulties to simulate more complex targets. Most of the codes are able to simulate the material probes. The range of the results is larger compared to that for the gas temperatures. As this information is significant for estimating failures of safety related equipment, the models should be further developed and improved.

9 References

/ALL 05/ Allelein, H.-J. et al.:
Weiterentwicklung der Rechenprogramme COCOSYS und ASTEC, Abschlussbericht, GRS-A-3266, Gesellschaft für Anlagen- und Reaktorsicherheit, April 2005

/BOU 02/ Bouton, E.,
Overview of the FLAMME-S code validation matrix, Technical Note SESHP/GME/IPS/FLS/C40/NT/02.337, 2002

/CFX 04/ CFX-5.7, User Documentation, ANSYS Inc., USA, 2004

/COX 87/ Cox, G., and S. Kumar:
Field modelling of fire in forced ventilated enclosures, Combustion Science and Technology, Vol. 52, pp. 7-23, 1987

/DEY 02/ Dey M.:
Evaluation of Fire Models for Nuclear Power Plant Applications: Cable Tray Fires, NISTIR 6872, National Institute of Standard and Technology, USA, June 2002

/GAY 06/ L. GAY, B. GAUTIER
"Magic Software Version 4.1.1: Mathematical Model"
HI-82/04/024/B - March 2006

/HOL 90/ Holen, J., M. Brostrom, and B.F. Magnusson:
Finite Difference Calculation of Pool Fires, 23rd Symposium on Combustion, Combustion Institute, pp. 1677-1683, 1990

/JON 04/ Jones, W.W., et al.:
CFAST - Consolidated Model of Fire Growth and Smoke Transport , (Version 5): Technical Reference Guide. NIST Special Publication 1030, October 2004

/KLE 04/ Klein-Heßling, W.:
Website: http://techconf.llnl.gov/cgi-fire/topics

/MCG 04/ McGrattan, K.B. (ed.):
Fire Dynamics Simulator (Version 4), Technical Reference Guide, NIST Special Publication 1018, National Institute of Standards and Technology, Gaithersburg, Maryland, USA, 2004

/MCG 06/ McGrattan, K.B.:
Evaluation of Fire Models for Nuclear Power Plant Applications: Benchmark Exercise #3, International Panel Report, NISTIR 7338, to be published January 2007

/MIL 04/ Miles, S.:
International Panel Report: Benchmark Exercise # 2 - Pool Fires in Large Halls. May 2004

/PLY 04/ Plys, M.G., and J.L. Sung:
FATE^{TM} 2.0: Facility Flow, Aerosol, Thermal, and Explosion Model (Improved and Combined HANSF and HADCRT Models), FAI/04-71, SNF-23281, Two Volumes, November 2004

/RIE 06/ Riese, O., D. Hosser, M. Röwekamp:
Evaluation of Fire Models for Nuclear Power Plant Applications: Flame Spread in Cable Tray Fires, International Panel Report on Benchmark Exercise No. 5, Gesellschaft für Anlagen- und Reaktorsicherheit (GRS) Report Number GRS-214, ISBN-Nr.: 978-3-931995-81-2, in publication, 2006

/TOU 00/ Tourniaire, B., and L. Audouin:
Sensitivity analysis of a data reduction method estimating the interface height, the lower and upper temperatures in fire room, Proceedings of the International Seminar of Fire and Explosion Hazard, 2000

List of Figures

List of Tables

List of Appendices:

Gesellschaft für Anlagen- und Reaktorsicherheit (GRS) mbH

Schwertnergasse 1
50667 Köln
Telefon +49 221 2068-0
Telefax +49 221 2068-888

Forschungsinstitute
85748 Garching b. München
Telefon +49 89 32004-0
Telefax +49 89 32004-300

Kurfürstendamm 200
10719 Berlin
Telefon +49 30 88589-0
Telefax +49 30 88589-111

Theodor-Heuss-Straße 4
38122 Braunschweig
Telefon +49 531 8012-0
Telefax +49 531 8012-200

www.grs.de

ISBN 978-3-931995-80-5